Nucleosome remodelling during resection of genomic DSBs and deprotected telomeres in yeast

Dissertation

Submitted for the degree of doctor of natural sciences

(Dr. rer. nat)

To the

Faculty of Chemistry and Chemical Biology

Technical University of Dortmund

presented by

Anja Deiser

from Munich

Dortmund, 2026

Publication

The main findings of this work are published in the journal PLOS One with the title “A role for nucleosome remodellers during resection of deprotected telomeres in yeast“ (Deiser et al. 2026).

Contributions

The *cdc13-1* strain in W303 background and experimental details for QAOS analysis were kindly provided by Brian Luke (Institute of Molecular Biology (IMB), Mainz, Germany). With the help of Caitlyn Agar (Boris Pfander laboratory, Dortmund Life Science Center (DOLCE), TU Dortmund University, Germany – Current address: Department of Biomedicine, Aarhus University, Denmark), who carried out most of the lab work for QAOS experiments, I set up the experimental design and analysis in our laboratory.

Juan de Dios Barba Tena Agar (Boris Pfander laboratory, Dortmund Life Science Center (DOLCE), TU Dortmund University, Germany) came up with the idea to measure AsiSI cutting efficiency via nanopore sequencing, helped to establish the method and performed nanopore sequencing.

Otherwise, all experiments were carried out by myself.

Auxin-inducible degron strains were generated using pFA6a-IAA7 plasmids kindly provided by Sebastian Schuck (Biochemistry Center BZH, Heidelberg University, Germany).

The AsiSI double-strand break induction system and strand-specific sequencing was previously established in our laboratory (Susanne Bantele and Martina Peritore, Max Planck Institute of Biochemistry, Martinsried, Germany) using the pCL096 plasmid provided by Dr. Claudio Lademann (Department of Molecular Cell Biology, Max Planck Institute of Biochemistry, Martinsried, Germany – Current address: Merck KGaA, Darmstadt, Germany).

Next-generation sequencing was carried out by Dr. Rin Ho Kim at the NGS core facility of the Max Planck Institute of Biochemistry (Martinsried, Germany).

Content

Summary 1

Zusammenfassung 2

1. Introduction 3

1.1 Genome organisation 3

1.1.1 Genetic information is stored in chromatin 3

1.1.2 Nucleosome remodellers 4

1.1.3 Telomeres: The end of the chromosome 7

1.2 Genome integrity 10

1.2.1 Sources of DNA damage 11

1.2.2 DNA damage signalling 12

1.2.3 DNA repair pathways and double-strand breaks as major threat 13

1.2.4 Physiological roles of programmed DSBs 14

1.3 Homologous recombination and repair pathway choice 15

1.3.1 Molecular mechanism of homologous recombination 15

1.3.2 Resection is the key limiting step for repair pathway choice 18

1.3.3 Nucleosomes form a barrier for resection 19

1.4 Systems to study DSB repair 22

1.4.1 Drugs and ionising radiation induce various forms of DNA damage 23

1.4.2 Site-specific nucleases 24

1.4.3 Telomere deprotection as an alternative model for DSB induction 26

2. Aim of the study 29

3. Results 30

3.1 Nucleosome editing by INO80 is dispensable for DSB end resection 30

3.2 The telomeric long-range resection machinery involves canonical DSB enzymes 44

3.2.1 Exo1 deletion rescues lethality of telomere deprotection 44

3.2.2 Dna2 contributes to resection after telomere deprotection particularly in the absence of Exo1 52

3.3 Nucleosome remodelling influences resection of unprotected telomeres 58

3.3.1 Resection after telomere deprotection depends on nucleosome eviction remodellers 59

3.3.2 Nucleosome editing does not significantly affect resection after telomere deprotection 64

4. Discussion 69

4.1 Restriction enzyme mediated DSB induction does not support a major requirement for nucleosome editing in resection 69

4.1.1 Accurate cutting efficiency measurement is required for data interpretation using restriction enzyme based DSB induction 69

4.1.2 Dysfunction of the INO80 complex does not detectably impair resection but affects H2A.Z-associated chromatin changes 70

4.1.3 Reduced DSB generation by AsiSI limits interpretation of genotypes deficient of H2A.Z, but resection can occur without nucleosome editing 72

4.1.4 Insufficient cutting efficiency requires an alternative system to study DSB resection 73

4.2 The long-range resection machinery at deprotected telomeres resembles genomic DSB resection 74

4.3 Chromatin influences long-range resection at deprotected telomeres 76

4.3.1 Nucleosome eviction is required for resection at deprotected telomeres 76

4.3.2 Nucleosome editing does not detectably affect long-range resection at deprotected telomeres 78

4.4 Conservation in higher eukaryotes 79

5. Material and Methods 82

5.1 *S. cerevisiae* strain generation and culture 82

5.1.1 Plasmid amplification 84

5.1.2 Standard polymerase chain reaction (PCR) 85

5.1.3 Restriction digestion 85

5.1.4 Ethanol precipitation of DNA 86

5.1.5 Preparation of competent *S. cerevisiae* cells 86

5.1.6 Transformation of *S. cerevisiae* cells 86

5.1.7 Colony PCR 87

5.1.8 Agarose gel electrophoresis 87

5.1.9 Mating, sporulation and tetrad dissection 88

5.2 Growth assays 88

5.3 Flow cytometry 89

5.4 SDS-PAGE and western blot 89

5.5 Quantitative amplification of ssDNA (QAOS) 91

5.6 Analysis of DSB resection by strand-specific sequencing 93

5.7 Analysis of DSB induction by nanopore sequencing 95

5.8 Statistical analysis and coding 96

5.9 Data availability 96

5.10 AI usage 96
6. Supplementary 97
Table S1: List of slope values of mixed-effects models 97
7. References 98
Abbreviations 126
Acknowledgements 127

Summary

DNA end resection is a decisive step in the repair of DNA double-strand breaks (DSBs): degradation of the 5'-terminated strands generates 3' single-stranded DNA (ssDNA) and commits repair to homologous recombination. The core resection enzymes are well characterised, but how resection proceeds through chromatin remains incompletely understood. This thesis investigated how nucleosome remodellers influence long-range resection at AsiSI-induced DSBs and at deprotected telomeres in budding yeast.

Strand-specific sequencing was used to measure resection at AsiSI-induced DSBs in yeast strains deficient in nucleosome editing. To compare the mutant strains, cutting efficiencies need to be similar. Therefore, a nanopore-based workflow was used to quantify AsiSI cutting efficiency in parallel. The *arp8Δ* strain, in which INO80 activity is impaired, showed similar cutting efficiency compared to the control and no significant changes in resection were observed. Data of a strain deficient in SWR1 complex activity and H2A.Z remains inconclusive, as DSB induction was insufficient. Upon complete loss of nucleosome editing activity, cutting efficiency was restored and resection was found to be similar as in control cells. Therefore, nucleosome editing seems to be dispensable for resection.

To analyse resection independently of restriction-enzyme cutting, the temperature sensitive *cdc13-1* system was used. In *cdc13-1* mutants, telomeres get deprotected at restrictive temperatures, leading to activation of the DNA damage response. By quantification of single-stranded DNA (QAOS), we showed that besides Exo1 also Dna2 contributes to long-range resection at telomeres. Thus, long-range resection appeared to be similar at telomeres and DSBs and we investigated the influence of nucleosome remodeller mutants on long-range resection at deprotected telomeres. Depletion of the nucleosome-eviction complexes RSC or SWI/SNF strongly impaired resection, whereas impaired INO80 function or combined loss of SWR1 and H2A.Z had no significant effect. Together, these findings indicate that nucleosome eviction, rather than histone-variant exchange, is critical for efficient long-range resection and establish *cdc13-1* telomere deprotection as a complementary model for studying long-range resection.

Zusammenfassung

Die DNA-Endresektion ist ein entscheidender Schritt bei der Reparatur von DNA-Doppelstrangbrüchen (DSBs). Dabei entsteht durch den Abbau der 5'-terminierten Stränge 3'-einzelsträngige DNA, was die Reparatur durch homologe Rekombination einleitet und andere Mechanismen verhindert. Während die enzymatischen Aktivitäten der Resektion bekannt sind, ist der Einfluss von Chromatin auf die Regulation der Resektion bisher unzureichend erforscht. Diese Arbeit untersuchte in Bäckerhefe, wie unterschiedliche Chromatin-Remodeller-Aktivitäten die Langstreckenresektion an AsiSI generierten DSBs und an ungeschützten Telomeren beeinflussen.

Mittels strangspezifischer Sequenzierung wurde die Resektion an AsiSI generierten DSBs in verschiedenen Nucleosom-Editierungs-Mutanten verglichen. Parallel wurde eine Nanopore-basierte Methode genutzt, um die AsiSI Schnitt-Effizienz zu messen, da eine ähnliche Induktion von DSBs Voraussetzung für den Vergleich der Resektion unter unterschiedlichen experimentellen Bedingungen ist. Stämme mit eingeschränkter INO80-Aktivität zeigten eine mit der Kontrollgruppe vergleichbare Schnitteffizienz und keine signifikanten Veränderungen der Endresektion. Die Interpretation von Stämmen mit Defekten im SWR1-Komplex und ohne die Histon Variante H2A.Z war hingegen eingeschränkt, da die DSB-Induktion in diesen Stämmen reduziert war. Auch der vollständige Verlust der Nukleosom-Editierungsaktivität beeinflusste weder Schnitt-Effizienz noch Resektion. Die Ergebnisse deuten darauf hin, dass die Nukleosom-Editierung für die Langstreckenresektion entbehrlich ist.

Um die Einschränkungen des restriktionsenzymbasierten Systems zu umgehen, wurde das temperatursensitive *cdc13-1*-Modell verwendet. In *cdc13-1*-Mutanten können Telomere bei restriktiver Temperatur ungeschützt sein und Reparatur-Mechanismen werden aktiviert. Mittels quantitativer Amplifizierung von Einzelsträngiger DNA (QAOS) wurde gezeigt, dass neben Exo1 auch Dna2 zur Langstreckenresektion an Telomeren beiträgt. Da die Langstreckenresektion an Telomeren und DSBs nach vergleichbaren Mechanismen zu erfolgen scheint, wurde der Einfluss verschiedener Chromatin-Remodeller-Mutanten an ungeschützten Telomeren untersucht. Die Depletion von Nukleosom-Eviktion-Remodeller-Komplexen RSC oder SWI/SNF führte zu verringerter Resektion, während eine eingeschränkte INO80-Funktion oder der kombinierte Verlust von SWR1-Akitivität und H2A.Z keinen signifikanten Effekt zeigten. Insgesamt weisen die Ergebnisse darauf hin, dass Nukleosom-Eviktion aber nicht Nucleosom-Editierung entscheidend für effiziente Langstreckenresektion ist und etablieren das *cdc13-1*-Modell als komplementäres System zur Untersuchung der DNA-Endresektion.

1. Introduction

1.1 Genome organisation

1.1.1 Genetic information is stored in chromatin

Most of the genetic information in a eukaryotic cell is stored as deoxyribonucleic acid (DNA) in the nucleus. A human cell nucleus is typically about 10 µm in diameter, yet it contains approximately 2 m of DNA (Parmar et al. 2019). These human values illustrate the tight packaging of the genome, while remaining accessible for cellular processes. The same principle applies to other eukaryotes, including budding yeast, although genome size and nuclear architecture differ. The high level of DNA compaction is achieved by wrapping DNA around histone and non-histone proteins to form a structure known as chromatin.

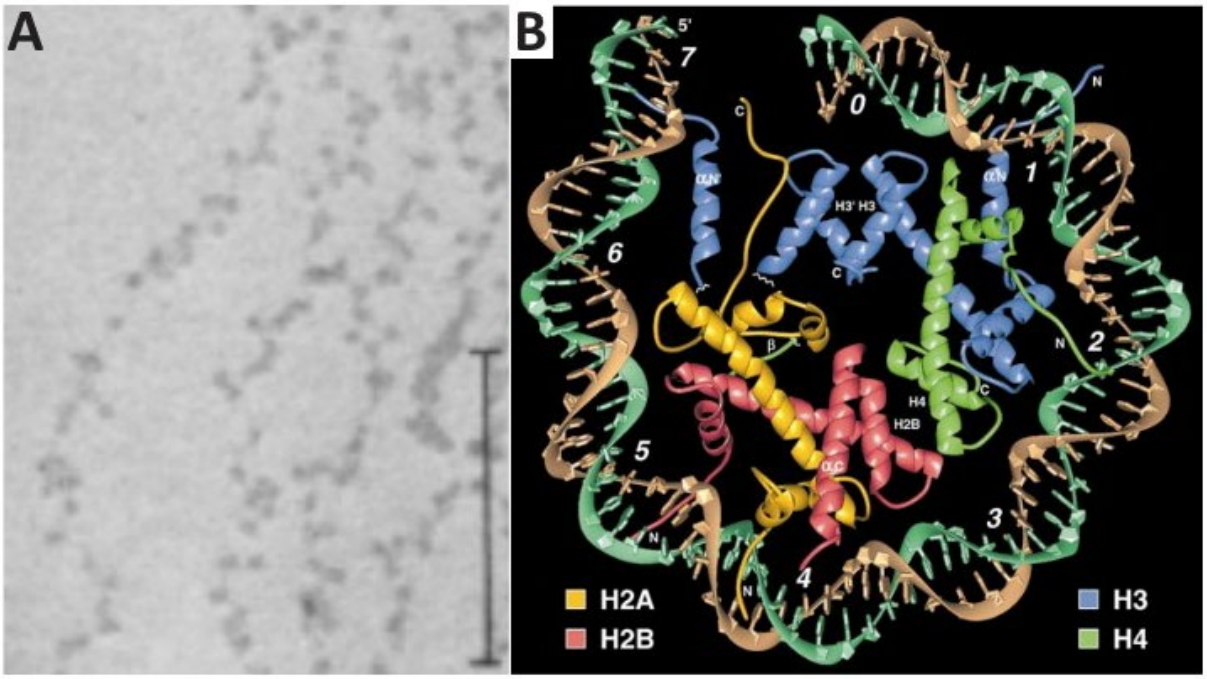


Figure 1: Structural organisation of the nucleosome.
(A) Electron micrograph of isolated rat thymus nuclei showing that chromatin fibres contain spherical particles. Scale bar: 0.2 µm. Adapted from published data (Olins and Olins 1974).
(B) Atomic model based on the electron density map of the crystal structure of a nucleosome core particle. View along the superhelix axis. H2A, H2B, H3 and H4 are shown in yellow, red, blue and light green, respectively. DNA is shown in brown and dark green. Adapted from published data (Luger et al. 1997).

The repeating organisation of chromatin was established by electron microscopy. Spherical particles connected by DNA filaments were observed and termed nucleosomes (Oudet et al. 1975; Olins and Olins 1974)(Figure 1A). X-ray crystallography of a reconstituted nucleosome core particle resolved the structure in more detail: Two copies of each of the four canonical histones H2A, H2B, H3 and H4 form a histone octamer around which approximately 146 base pairs of DNA are wrapped in a left-handed superhelix (Luger et al. 1997)(Figure 1B). This core architecture is broadly conserved across eukaryotes, whereas linker length, histone variants and post-translational modifications vary among organisms, cell types and genomic regions.

Chromatin compaction extends beyond this linear "beads-on-a-string" configuration (Oudet et al. 1975). In higher eukaryotes the linker histone H1 binds near the nucleosomal DNA entry and exit sites and promotes compaction into higher-order chromatin structures. H1 is not conserved in budding yeast but Hmo1 possesses similar functionality (M. Wang et al. 2023). The linker DNA between nucleosomes can bend, enabling folding into loops and helical arrangements (Luger et al. 1997; Widom 1989). Microscopy techniques and chromosome-conformation-capture experiments show further organisation into chromosomal domains and ultimately chromosomes (Happel and Doenecke 2009; Parmar et al. 2019). This multiscale organisation compacts the genome while still allowing regulated access. Processes such as DNA replication, transcription and repair require access to the DNA and an open chromatin conformation. Chromatin is therefore not a static entity but a highly dynamic structure and is constantly remodelled in response to cellular needs (Clapier and Cairns 2009).

1.1.2 Nucleosome remodellers

Nucleosome remodellers are ATP-dependent protein complexes which regulate DNA accessibility by altering nucleosome position, occupancy or composition. Although these complexes differ in their accessory subunits and biological functions, they all contain a conserved ATPase of the SF2 helicase superfamily. ATP hydrolysis disrupts DNA-histone interactions and drives DNA translocation relative to the histone octamer enabling nucleosome eviction, repositioning or histone-variant exchange (Clapier et al. 2017; Clapier and Cairns 2009; Eustermann et al. 2018; Yan and Chen 2020; Malik et al. 2025). Accessory subunits determine the activity and targeting of individual remodellers. For example, specific remodeller subunits recognise post-translational modifications including acetylation, methylation and phosphorylation, which predominantly occur on N-terminal histone tails

(Corona and Tamkun 2004). Based on phylogenetic and functional analyses, yeast nucleosome remodellers can be classified into four major subfamilies: Switch/sucrose non-fermentable (SWI/SNF), imitation switch (ISWI), chromodomain helicase DNA-binding (CHD) and INO80 (Clapier et al. 2017; Clapier and Cairns 2009). Their characteristic activities are summarised in Figure 2.

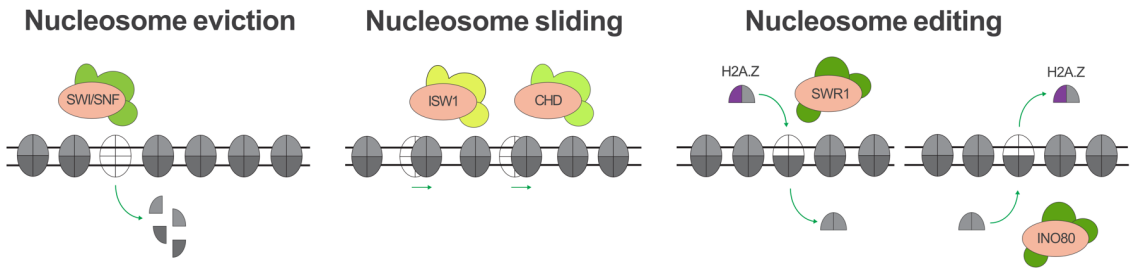


Figure 2: Characteristic activities of ATP-dependent nucleosome remodeller subfamilies in budding yeast.
The SWI/SNF subfamily is particularly associated with nucleosome eviction and the generation of open chromatin. The ISWI and CHD subfamilies primarily slide nucleosomes along DNA and can thereby generate regular arrays. The INO80 subfamily is best known for histone-variant exchange. In yeast, the SWR1 complex incorporates H2A.Z-H2B dimers into nucleosomes, whereas the INO80 complex catalyses the reverse exchange.

SWI/SNF nucleosome remodellers contain bromodomains that recognise acetylated histones and increase DNA accessibility through nucleosome eviction. In budding yeast, the SWI/SNF and RSC complexes represent the major remodellers responsible for nucleosome eviction (Clapier and Cairns 2009; Clapier et al. 2017; Karl et al. 2022). Genome-wide expression analysis showed that SWI/SNF complexes can activate or repress gene transcription but are not essential (Sudarsanam et al. 2000). In contrast, the RSC complex is required for cell viability and is highly abundant (Cairns et al. 1996). Combining chromatin immunoprecipitation with DNA microarray technology in genome-wide location analysis identified Pol III promoters as RSC targets and Pol II promoters as targets specifically in response to transcriptional activation or repression (Ng et al. 2002). Although both complexes mainly evict nucleosomes, they can also slide nucleosomes (Clapier and Cairns 2009; X. Shen et al. 2000; Eustermann et al. 2018). Nucleosome sliding is primarily mediated by the ISWI and CHD subfamilies in yeast. ISWI nucleosome remodellers interact with nucleosomes through their HAND-SANT-SLIDE (HSS) domains, which preferentially recognise unmodified histone tails. In contrast, CHD remodellers are characterised by tandem chromodomains located at the N-terminus of their catalytic ATPase subunit (Clapier and Cairns 2009). By repositioning nucleosomes along DNA,

sliding remodellers determine the spacing between neighbouring nucleosomes, referred to as the nucleosome repeat length. In budding yeast, the average nucleosome repeat length is approximately 165 bp (H. Zhang et al. 2005). *In vitro* reconstitution of chromatin using a genomic plasmid library and salt gradient dialysis for nucleosome assembly showed that different nucleosome remodellers generate distinct linker lengths between adjacent nucleosomes. The resulting nucleosome spacing patterns contribute to higher-order chromatin organisation and gene regulation. In particular, highly expressed genes are often characterised by well-positioned and regularly spaced nucleosomes downstream of the transcription start site, forming so-called phased nucleosome arrays (Baldi et al. 2020; Corona and Tamkun 2004; Oberbeckmann, Niebauer, et al. 2021; Ocampo et al. 2016; Weiner et al. 2010; Woodage et al. 1997).

Members of the INO80 family are characterised by a split ATPase domain and are best known for their ability to exchange histone variants. The yeast INO80 complex can also slide nucleosomes (Brahma et al. 2017, 2018; Knoll et al. 2018; Oberbeckmann, Krietenstein, et al. 2021; Oberbeckmann, Niebauer, et al. 2021). Nucleosome remodellers of the INO80 subfamily contain the helicase-related Rvb1/2 proteins, which form multimeric ATPase complexes and undergo conformational changes (Clapier and Cairns 2009; Nguyen et al. 2013). In budding yeast, two major nucleosome remodeller complexes belong to this subfamily: INO80 and SWR1, which act antagonistically in nucleosome editing. The INO80 complex replaces H2A.Z-H2B dimers with canonical H2A-H2B dimers, whereas the SWR1 complex catalyses the reverse reaction and incorporates H2A.Z-H2B dimers (Clapier and Cairns 2009; Mizuguchi et al. 2004; Nguyen et al. 2013; Papamichos-Chronakis et al. 2011; Singh et al. 2019). H2A.Z containing nucleosomes show reduced stability on DNA *in vivo* and *in vitro*, which may facilitate their ejection (Watanabe et al. 2013; H. Zhang et al. 2005; Adkins et al. 2013). H2A.Z incorporation contributes to chromatin organisation, transcriptional regulation and DNA repair.

Together, the coordinated activities of the SWI/SNF, ISWI, CHD and INO80 subfamilies regulate chromatin accessibility and genome organisation, thereby controlling binding of factors involved in processes such as transcription, replication and DNA repair (Barisic et al. 2019; Bennett et al. 2013; Karl et al. 2022; Längst and Manelyte 2015; Luijsterburg and Van

Attikum 2011; Peritore et al. 2021; Petty and Pillus 2013). However, functional overlap among some remodellers makes it challenging to assign specific functions to individual complexes.

1.1.3 Telomeres: The end of the chromosome

Most genomic DNA is compacted within chromatin, but chromosome ends are bound by specialised proteins. In budding yeast, telomeric DNA consists of non-protein coding heterogeneous $TG_{1\text{-}3}$ repeats. Hybridisation and primer extension assays showed that this repeat sequence ends in a short repetitive 3' single-stranded overhang of approximately 12 - 15 nucleotides (Larrivée et al. 2004; Shampay et al. 1984; Wellinger and Zakian 2012; Zakian 1996). Human telomeres likewise contain G-rich repetitive DNA, but the bound proteins differ (Blackburn et al. 2006). In general, telomeres must solve the end-replication problem and avoid recognition as DNA damage. When telomeres become unprotected, they structurally resemble one end of a DSB and are recognised by the DNA repair machinery. This can lead to extensive degradation of the 5' end or ligation to another chromosome end, resulting in end-to-end fusions (Cheung 2008; Dewar and Lydall 2012).

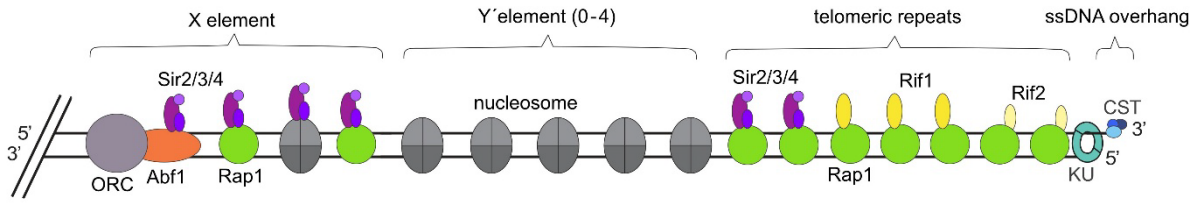


Figure 3: Structural elements of the budding yeast telomere.
Schematic representation of the chromatin structure and telomeric binding proteins at sub-telomeric X and Y' elements, the double-stranded telomeric repeat region and the 3' G-rich ssDNA overhang.

Exposed ssDNA acts as a DNA-damage signal and, when coated by RPA, can trigger checkpoint signalling and activation of the DNA repair machinery (Harrison and Haber 2006). In budding yeast, the telomeric 3' ssDNA overhang is protected by the ssDNA-binding protein Cdc13, which recruits Stn1 and Ten1 upon DNA binding to form the CST complex (Cdc13-Stn1-Ten1). Biochemical comparison of the CST complex with the major eukaryotic ssDNA-binding protein RPA revealed strong structural similarities among their components. Thus, the CST complex can be considered a telomere-specific, RPA-like complex (Anderson 2002; Dewar and Lydall

2012; Gao et al. 2007; N. Grandin 2001; N Grandin et al. 1997; Hughes et al. 2000). In addition to its role in telomere protection, the CST complex regulates telomere length. For example, Cdc13 promotes telomere elongation by recruitment of telomerase and DNA polymerase α (Qi and Zakian 2000; Y. Wu and Zakian 2011). In contrast, Stn1 works as a negative regulator. Deletion of the C-terminal domain of Stn1, which mediates Cdc13 binding, resulted in increased telomere length (Chandra et al. 2001; Grossi et al. 2004; Rice and Skordalakes 2016). The double-stranded telomeric repeats are recognised and bound by Rap1 (repressor/activator protein 1), a sequence-specific DNA-binding protein that also regulates transcription at non-telomeric loci. Rap1 binding to telomeres promotes recruitment of Rif1 and Rif2, which contribute to telomere-length regulation and end protection (Dewar and Lydall 2012). Loss of Rif1 and Rif2 led to telomere elongation, whereas their overexpression shortened telomeres (Wotton and Shore 1997). Telomere protection from degradation requires Rif2 binding to the C-terminal domain of Rap1. Increased ssDNA generation at telomeres was observed in mutants lacking Rif2 or the C-terminal domain of Rap1 (Bonetti, Clerici, Anbalagan, et al. 2010; Shi et al. 2013). In addition, Rif1 and Rif2 antagonise telomeric silencing by competing with silencing proteins for Rap1 binding (Wellinger and Zakian 2012; Shi et al. 2013; Wotton and Shore 1997). Furthermore, *in vivo* cross-linking experiments showed that the Ku complex binds repetitive telomeric DNA and contributes to telomere maintenance in addition to its established role in DNA repair (Gravel et al. 1998; Nathalie Grandin et al. 2000; Bonetti, Clerici, Anbalagan, et al. 2010; Fisher et al. 2004).

In higher eukaryotes, telomere protection differs: The repetitive TTAGGG sequence is bound by the shelterin complex, which consists of three repeat-binding subunits (TRF1, TRF2 and POT1) and three interconnecting subunits (TIN2, TPP1 and Rap1) (De Lange 2009; Palm and De Lange 2008; B. Li et al. 2000). TRF1 and TRF2 bind telomeric dsDNA and are required for the association of the shelterin complex. Their combined loss led to telomere deprotection in mouse cells (Sfeir and De Lange 2012). The scaffold protein TIN2 links TRF1 and TRF2 to TPP1 (De Lange 2009; Jones et al. 2016) and TPP1 recruits the ssDNA binding protein POT1 (Barrientos et al. 2008; Baumann and Cech 2001). TRF2 and POT1 are particularly important for telomere protection, as their loss activates the DNA damage response (Celli and De Lange 2005; Konishi and De Lange 2008; Denchi and De Lange 2007). Higher eukaryotes further protect the telomeric ssDNA overhang by a 3D structure called D-loop. The 3’ ssDNA end invades into the telomeric duplex to form a D-loop (De Lange 2009; Griffith et al. 1999). A role

for TRF2 in T-loop formation was first suggested by *in vitro* experiments and later confirmed by stochastic optical reconstruction microscopy (STORM) (Doksani et al. 2013; Stansel et al. 2001; Griffith et al. 1999; Amiard et al. 2007; Poulet et al. 2009). In budding yeast, the 3' overhang is not believed to invade the duplex DNA and form a T-loop. Instead, a fold-back structure of the telomere end mediated by protein interactions is suggested (Wellinger and Zakian 2012): Immunoprecipitation of silencing proteins from whole-cell extracts and formaldehyde cross-linking identified Rap1 as an interactor of telomeric silencing proteins (Strahl-Bolsinger et al. 1997). In addition, gene activation by an enhancer positioned downstream of a gene was shown when the gene was linked to a telomere (De Bruin et al. 2001).

In addition to protecting chromosome ends from recognition by the DNA repair machinery, telomeres must overcome the end-replication problem. Because conventional DNA polymerases synthesise DNA only in the 5'-to-3' direction and require a primer, removal of the terminal RNA primer from the lagging-strand daughter leaves a short DNA region unreplicated during each round of cell division. To counteract progressive telomere shortening, the G-rich 3' overhang is extended by telomerase through reverse transcription using its intrinsic RNA template. The complementary C-strand is subsequently synthesised by conventional polymerases. As unrestricted telomerase activity would result in excessive telomere elongation, telomerase recruitment and activity are tightly regulated. In budding yeast, the MRX complex, which also functions in the recognition of DSBs, associates with short chromosome ends and recruits the checkpoint kinase Tel1. Tel1-dependent phosphorylation of Cdc13 promotes telomerase recruitment and telomere elongation. As telomeres lengthen, increasing numbers of Rap1 molecules bind the telomeric repeats, thereby progressively inhibiting telomere extension by telomerase. This protein-counting mechanism regulates elongation and maintains telomeres at an average length of approximately 300 bp in budding yeast (Levy and Blackburn 2004; Lustig 2019; Martina et al. 2012; Yang et al. 2017). Telomere length homeostasis is further influenced by additional telomere-associated proteins and by the formation of G-quadruplex DNA structures, highlighting the complexity of telomerase regulation (Nugent et al. 1996; Wellinger and Zakian 2012; M.-L. Zhang et al. 2010).

In telomerase-positive cells of higher eukaryotes, telomere length is regulated by the shelterin complex. TPP1 mediates telomerase recruitment (Rajavel et al. 2014; Nandakumar et al.

2012), whereas TRF1 and TRF2 act as negative regulators. Overexpression of TRF1 and TRF2 resulted in telomere shortening without affecting TERT expression, the catalytic subunit of telomerase (Smogorzewska et al. 2000; Van Steensel and De Lange 1997).

The DNA adjacent to the telomeric TG_{1-3} repeat region is referred to as the sub-telomeric region and is characterised by a high number of repetitive sequences. In yeast, sub-telomeric DNA consists of two major sequence elements termed X and Y' elements. X elements are present at all chromosome ends, whereas Y' elements are optional and located between the terminal telomeric TG_{1-3} repeat region and the X element. Depending on the telomere, up to four tandem copies of Y' elements can be present (Wellinger and Zakian 2012). Although X and Y' elements both contain repetitive sequences, they differ substantially in their chromatin organisation. X elements show a heterochromatin-like structure with a high occupancy of Rap1, Sir2, Sir3 and Sir4. In contrast, Y' elements are euchromatic (Ellahi et al. 2015; Wellinger and Zakian 2012; X. Zhu and Gustafsson 2009).

In summary, specialised telomere-binding factors protect chromosome ends from recognition by the DNA repair machinery and regulate telomerase to overcome the end-replication problem. In contrast, genomic DNA is organised into chromatin, which allows a high degree of compaction. To maintain DNA accessibility for proteins involved in processes such as replication, transcription and DNA repair, nucleosome remodellers can evict, reposition or edit nucleosomes.

1.2 Genome integrity

Genome integrity refers to the preservation and faithful transmission of DNA sequence and chromosome structure throughout the lifetime of a cell and across cell divisions (Ciccia and Elledge 2010; Jackson and Bartek 2009). Failure to prevent or accurately repair DNA damage can cause genomic instability, a defining feature of many cancers. The importance of genome maintenance is further illustrated by inherited disorders caused by defects in DNA repair and damage-response pathways. Such disorders, including xeroderma pigmentosum and Fanconi anaemia, may feature developmental abnormalities, premature ageing, cancer predisposition or combinations of these phenotypes (O'Driscoll 2012).

1.2.1 Sources of DNA damage

DNA is continually exposed to endogenous and exogenous damage. Endogenous lesions arise from spontaneous chemical reactions during cell metabolism. In contrast, exogenous damage is caused by environmental, physical or chemical agents including radiation and genotoxic chemicals (Mehta and Haber 2014; Chatterjee and Walker 2017). Each human cell is estimated to experience tens of thousands of DNA lesions per day (Tubbs and Nussenzweig 2017). Thus, DNA repair mechanisms are essential for maintaining genome integrity and cell viability.

DNA replication itself presents a major endogenous challenge to genome integrity. During S phase, the genome must be duplicated once and with high fidelity. Defects in replication timing or regulation, as well as obstacles to fork progression, can cause replication stress, fork collapse, DNA lesions and under-replicated regions (Hills and Diffley 2014). Examples of endogenous sources of DNA damage are failure in the resolution of supercoiling by topoisomerases, oxidative damage or spontaneous base deamination (Mehta and Haber 2014; Chatterjee and Walker 2017).

Replication stress can also be caused by exogenous sources of DNA damage. For example, ultraviolet (UV) radiation induces covalent photoproducts, such as cyclobutane pyrimidine dimers and (6-4) photoproducts (Pfeifer 2020). If these lesions remain unrepaired, they can block replication and promote fork collapse, thereby generating double-strand breaks (DSBs) (Zeman and Cimprich 2014). Furthermore, genotoxic chemicals can perturb replication. Hydroxyurea (HU), for instance, depletes the deoxyribonucleoside triphosphate (dNTP) pool (Mehta and Haber 2014).

DNA can also directly be damaged by exogenous sources of DNA damage. For example, alkylating agents, such as methyl methanesulfonate (MMS), modify DNA bases and cisplatin forms inter-strand crosslinks. Furthermore, ionising radiation such as X-rays can induce several types of DNA damage including oxidative base lesions, single-strand breaks (SSBs) and double-strand breaks (DSBs) (J. F. Ward 1995; Little 2000; Saini and Gurung 2025; Wei et al. 2026).

1.2.2 DNA damage signalling

DNA damage checkpoints are regulatory signalling networks that respond to DNA damage and delay cell cycle progression to allow for repair (Norbury and Hickson 2001; Harrison and Haber 2006; Finn et al. 2012; Yates et al. 2025). In budding yeast, two apical checkpoint kinases sense DNA damage and activate the checkpoint: Mec1-Ddc2 (ATR-ATRIP in mammals) and Tel1 (ATM in mammals) (Falck et al. 2005; Sanchez et al. 1996). Tel1 is recruited to DSB ends through the MRX (Mre11-Rad50-Xrs2) complex (MRN (Mre11-Rad50-Nbs1) in mammals) to activate the DNA damage checkpoint (Nakada et al. 2003). In contrast, Mec1-Ddc2 is recruited to RPA-coated single-stranded DNA (ssDNA), which is generated at stalled replication forks and during the processing of most DNA lesions (Deshpande et al. 2017; Zou and Elledge 2003). During DNA double-strand break (DSB) repair by homologous recombination (HR), resection generates long tracts of ssDNA, which are covered by RPA and sensed by Mec1-Ddc2 in budding yeast or by ATR-ATRIP in mammals (Zou and Elledge 2003; Mantiero et al. 2007; Shiotani and Zou 2009; You et al. 2009; Finn et al. 2012; Bantele et al. 2019; Cejka and Symington 2021).

Mec1 and Tel1 sense different structures, but both initiate phosphorylation cascades that activate the effector kinases Rad53 and Chk1 through mediator proteins (Sanchez et al. 1996; Branzei and Foiani 2006). Analogously, the mammalian effector kinases CHK1 and CHK2 are activated by ATR- and ATM-dependent signalling (Y. Chen and Sanchez 2004; D'Andrea 2008). Effector kinases transmit damage signals throughout the cell and coordinate downstream responses including cell cycle arrest, nucleosome remodelling and activation of DNA repair pathways (Finn et al. 2012; Gardner 1999; Harrison and Haber 2006). Once the lesions have been repaired, checkpoint signalling is attenuated and cell cycle progression resumes (Finn et al. 2012; Harrison and Haber 2006).

Different stages of the signalling cascade can be monitored as readouts of DNA damage. Accumulation of RPA on ssDNA is a common marker in yeast and higher eukaryotes (Zou and Elledge 2003; Balajee and Geard 2004; Jazayeri et al. 2006; Sartori et al. 2007). Furthermore, phosphorylation of the effector kinase Rad53 indicates checkpoint activation in budding yeast (Pellicioli et al. 2001; Branzei and Foiani 2006; Bantele et al. 2019). In mammalian cells, recruitment of the mediator protein 53BP1 to DSBs, where it promotes repair by NHEJ, can be visualised (I. M. Ward et al. 2003; Panier and Boulton 2014). Phosphorylation of histone H2A in yeast and of the histone variant H2A.X in mammals promotes recruitment of DNA repair

factors (Rogakou et al. 1998; Downs et al. 2000; Paull et al. 2000) and is widely used as a DNA damage marker (Balajee and Geard 2004; Jazayeri et al. 2006; K. Li et al. 2020).

1.2.3 DNA repair pathways and double-strand breaks as major threat

Cells use specialised, partly overlapping repair pathways according to lesion type and cellular context. When only one DNA strand is affected, sequence information can be restored from the undamaged complementary strand. Nucleotide excision repair (NER), for example, removes bulky helix-distorting lesions such as UV-induced photoproducts (Pfeifer 2020), whereas base excision repair (BER) repairs small base lesions, including oxidised, deaminated and alkylated bases (Kumar et al. 2020). Mismatch repair (MMR) corrects mispaired bases that escape proofreading by replicative DNA polymerases (Kunkel and Erie 2015) and removes insertion-deletion loops, which may arise through polymerase slippage at repetitive sequences (Chatterjee and Walker 2017).

Repair of DNA double-strand breaks (DSBs) is particularly challenging because both strands are disrupted. DSBs can be repaired by end-joining pathways, among which non-homologous end joining (NHEJ) is predominant. In NHEJ, the Ku complex binds and protects the DNA ends from degradation. Re-ligation is mediated by DNA ligase IV to restore the DSB. NHEJ can be error free; however, direct re-ligation is often associated with small insertions or deletions. When ends from different DSBs are joined, large deletions or chromosomal translocations can arise. End-joining does not require a homologous repair template, can operate throughout the cell cycle and is particularly important when a sister chromatid is unavailable (Jackson and Bartek 2009; Ciccia and Elledge 2010; Chapman et al. 2012; Chiruvella et al. 2013; Chang et al. 2017; Tubbs and Nussenzweig 2017; Cejka and Symington 2021).

In the absence of NHEJ, DSBs can also be repaired by alternative error-prone end joining mechanisms (alt-NHEJ). One form is microhomology-mediated end joining (MMEJ), in which two broken ends are joined after alignment of short homologous sequences. The process involves degradation of the 5’-terminated strands, followed by removal of the non-complementary flaps, gap filling DNA synthesis and ligation. Because sequences between the aligned microhomologies are deleted, MMEJ is intrinsically error-prone (Corneo et al. 2007; Robert et al. 2009; Sfeir and Symington 2015; Pannunzio et al. 2018).

In contrast, homologous recombination (HR) can achieve high-fidelity repair by using an intact homologous template, preferentially the sister chromatid. HR is therefore favoured in S and

G2, when a sister chromatid is available as a template. HR begins with nucleolytic resection of the 5'-terminated strands of the DSB, generating 3'-single-stranded DNA (ssDNA) overhangs. Subsequently, the ssDNA regions invade homologous double-stranded DNA to search for a complementary repair template (Mimitou and Symington 2008; Lorraine S. Symington and Gautier 2011; Cejka 2015; Cejka and Symington 2021).

1.2.4 Physiological roles of programmed DSBs

Although DSBs threaten genome integrity, cells use controlled DNA cleavage for several cellular processes. One example is the relief of torsional stress during replication and transcription by topoisomerases. Type I topoisomerases form transient single-strand breaks that permit controlled strand rotation, whereas type II enzymes generate transient enzyme-bridged DSBs that allow one DNA duplex to pass through another before rapid re-ligation (J. C. Wang 2002).

Programmed DSB formation is also central to meiosis. The conserved endonuclease Spo11, which is related to type II topoisomerases, generates DSBs at defined recombination hotspots. Subsequent HR can generate crossover products, which promote accurate chromosome segregation during the first meiotic division and increase genetic diversity (Lam and Keeney 2015).

Programmed DSBs also drive site-specific genetic rearrangements. In the budding yeast *Saccharomyces cerevisiae*, the HO endonuclease initiates mating-type switching by generating a site-specific DSB at the MAT locus, which is repaired by HR. Depending on the cell´s mating type, either HMLα or HMRa is used as the donor locus resulting in gene conversion and a change of mating type (Weiffenbach and Haber 1985; X. Wu and Haber 1996; Belton et al. 2015). Another example of programmed DSBs is V(D)J recombination, which allows diversification of antigen receptors and is required for adaptive immunity. During this process, the RAG1/2 protein complex induces site-specific DSBs at recombination signal sequences that are subsequently repaired by NHEJ (Soulas-Sprauel et al. 2007).

Beyond their natural biological roles, targeted DSB formation has been harnessed for genome engineering. CRISPR-associated nucleases originate from the bacterial adaptive immune system. The Cas9 nuclease from *Streptococcus pyogenes* is most commonly used for targeted DNA cleavage and is guided to a specific genomic locus by a synthetic single-guide RNA (sgRNA) (Jinek et al. 2012). The resulting DSB is repaired by endogenous cellular pathways,

predominantly non-homologous end joining (NHEJ), often leading to insertions or deletions that can disrupt gene function. Alternatively, when a donor template is supplied, homology-directed repair can introduce precise genetic modifications, although efficiency depends strongly on cell type and cell cycle state (Xue and Greene 2021). Together, these examples demonstrate that the biological consequences of a DSB depend on both the cellular context in which it occurs and the repair pathway used.

1.3 Homologous recombination and repair pathway choice

1.3.1 Molecular mechanism of homologous recombination

Homologous recombination uses sequence homology, usually from the sister chromatid, to restore genetic information at a DSB. DNA ends are first processed by nucleolytic degradation of the 5'-terminated strands in a process termed resection. This generates long 3' single-stranded DNA overhangs which can search for homology and anneal to a complementary strand during repair (Cejka 2015; Cejka and Symington 2021)(Figure 4).

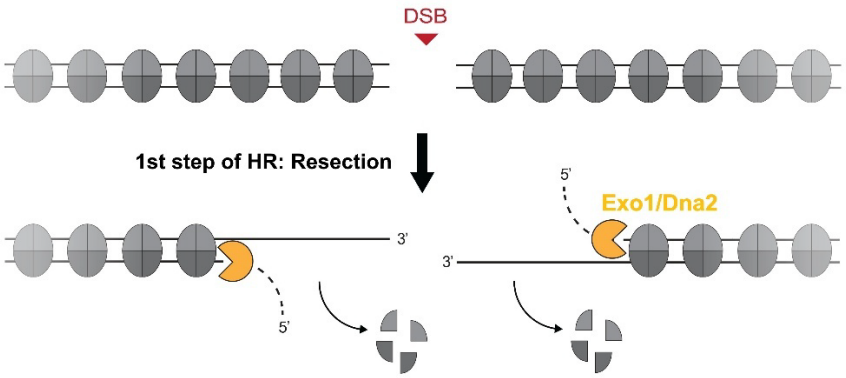


Figure 4: Schematic representation of long-range resection.
Resection is the first step of homologous recombination (HR). The 5'-terminated strands at a DSB get degraded by the nucleases Exo1 and Dna2, which generate long 3' single-stranded DNA overhangs required for homology search. Nucleosomes must be displaced as resection proceeds (further details in section 1.3.3).

Resection is initiated by the MRX (Mre11-Rad50-Xrs2) complex in budding yeast and by the orthologous MRN (Mre11-Rad50-Nbs1) complex in humans. This conserved complex recognises DNA ends, but its nuclease activity requires activation by Sae2 in budding yeast and CtIP in humans. Activated Mre11 cleaves the 5'-strand endonucleolytically near the DSB and then processes the DNA exonucleolytically towards the DNA end. This process, termed short-range resection, generates an entry point for the long-range resection machinery, which

can then extend the ssDNA overhang over several kilobases. Importantly, endonucleolytic cleavage by Mre11 and short-range resection are essential when DSB ends are chemically modified or blocked by proteins (Mimitou and Symington 2010; Ranjha et al. 2018; Reginato et al. 2017; Shim et al. 2010; Lorraine S. Symington and Gautier 2011).

Long-range resection is carried out by either of two nuclease pathways: the Exo1 exonuclease in budding yeast (EXO1 in humans) or the Dna2 flap endonuclease (DNA2 in humans) together with the STR complex (Sgs1-Top3-Rmi1) in budding yeast (the BLM-TOP3A-RMI1/2 complex in humans) (Cejka 2015; Cejka and Symington 2021; Mimitou and Symington 2008; Lorraine S. Symington and Gautier 2011; Z. Zhu et al. 2008). Mechanistically, the pathways differ: Exo1 degrades dsDNA with 5′ to 3′ directionality, thereby generating 3′ ssDNA. In contrast, Dna2 acts on ssDNA and therefore depends on the RecQ family helicase Sgs1 in yeast (BLM or WRN in humans) to unwind the DNA duplex prior to endonucleolytic cleavage (Levikova et al. 2017; Pinto et al. 2016). RPA coating of the emerging 3′ ssDNA directs Dna2 towards 5′-endonuclease activity and suppresses its 3′-nuclease activity (Cejka, Cannavo, et al. 2010; Niu et al. 2010; Lorraine S. Symington and Gautier 2011). The two long-range resection pathways are conserved from yeast to human and partially redundant. Severe defects in HR arise when both pathways are simultaneously disrupted (Cejka 2015; Gravel et al. 2008; Mimitou and Symington 2008; L. S. Symington 2014; Z. Zhu et al. 2008).

The 3′ ssDNA overhang, generated by resection, is rapidly coated by RPA (replication protein A), an ssDNA binding protein conserved from yeast to humans. RPA protects ssDNA from degradation and prevents secondary structure formation through self-annealing (Wold 1997). RPA is then replaced by the strand-exchange protein Rad51 (RAD51 in humans). Because RPA binds ssDNA with higher affinity than Rad51, this exchange requires the mediator Rad52 in budding yeast or functionally analogous proteins such as BRCA2 in humans (Benson et al. 1998; Ranjha et al. 2018). The resulting Rad51 nucleoprotein filament transiently interacts with dsDNA and searches for homology. Once a homologous sequence is found, the Rad51-coated 3′-end invades the donor duplex, displaces one strand and base-pairs with the complementary strand. The resulting joint molecule is called a displacement loop (D-loop). After the displaced strand has been stabilised by RPA and Rad51 has been removed from the invading 3′ end, DNA synthesis begins from this end as a primer (Ranjha et al. 2018). DNA synthesis restores the missing sequence information but is more error-prone than canonical replication (Hicks et al. 2010). The D-loop intermediate can then be processed by three

recombination sub-pathways: Canonical homologous recombination (HR), synthesis-dependent strand annealing (SDSA) or break-induced replication (BIR) (Ranjha et al. 2018)(Figure 5).

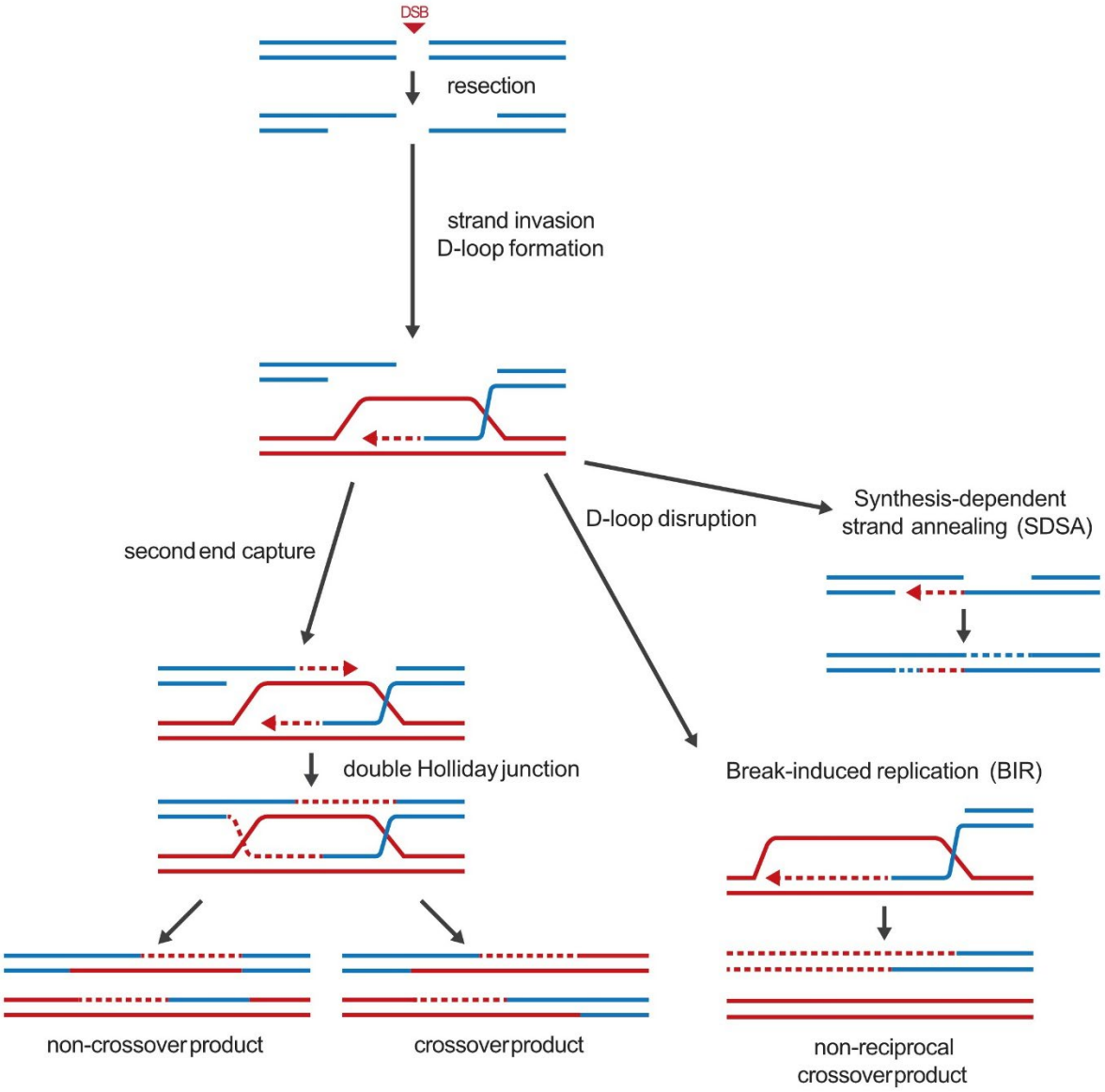


Figure 5: Schematic representation of recombination-mediated repair mechanisms.
After DSB induction, the resected end (blue) invades the repair template (red) and searches for a homologous sequence ultimately forming a D-loop. In canonical HR, the second end of the DSB is captured leading to the formation of a double Holliday junction that can be resolved into crossover or non-crossover products. In synthesis-dependent strand annealing (SDSA) and break-induced replication (BIR) the D-loop is disrupted for subsequent repair. Adapted from (Mehta and Haber 2014).

In canonical HR, the second resected DSB end is captured by the D-loop, resulting in a structure termed a double Holliday junction (dHJ). This intermediate can be processed by dissolution or resolution, which determines the genetic outcome. During dissolution, the Sgs1-Top3-Rmi1 (STR) complex in yeast (BLM, topoisomerase IIIα and RMI1-RMI2 (BTRR) complex in humans) promotes convergent branch migration of the two junctions (Cejka, Plank, et al. 2010; Ranjha et al. 2018; L. Wu and Hickson 2003). Helicase activity drives unwinding, whereas topoisomerase activity relieves torsional stress and allows the intertwined strands to separate. As a consequence, non-crossover products are generated and the two DNA duplexes are restored. Resolution, in contrast, uses structure-selective nucleases which recognise and cleave branched DNA structures. Re-ligation of the cleaved junctions can generate non-crossover or crossover products, depending on cleavage orientation (Ranjha et al. 2018; Wright et al. 2018).

In SDSA, the second end is not captured. After D-loop extension, the newly synthesised strand dissociates and anneals to the complementary ssDNA on the other resected DSB end. Subsequent DNA synthesis and re-ligation generate non-crossover products, restoring both DNA duplexes without reciprocal DNA exchange (Ranjha et al. 2018).

In BIR, DNA synthesis within the D-loop proceeds along the donor template towards the chromosome end. Because DNA synthesis during BIR is mutagenic, this pathway is largely restricted to single-ended DSBs, such as those arising from replication-fork collapse (Sakofsky and Malkova 2017).

Because these recombination sub-pathways produce different genetic outcomes, their balance is critical for maintaining genome integrity. Overall, homologous recombination including its sub-pathways is conserved from yeast to humans. Simpler organisms provide valuable models to investigate underlying principles, whereas higher eukaryotes show increasing complexity (Wright et al. 2018).

1.3.2 Resection is the key limiting step for repair pathway choice

Resection is required for homology search during HR, but simultaneously inhibits end-joining, because nucleolytic degradation of the 5’ ends prevents direct re-ligation. Therefore, resection determines repair pathway choice. Resection is cell cycle regulated and restricts HR to the S and G_2 phase of the cell cycle, when the sister chromatid is available as a repair template, whereas end joining is favoured in G_1 (Lorraine S. Symington and Gautier 2011).

Cdc28, the cyclin-dependent kinase (CDK) in budding yeast, is a major regulator of resection (Aylon et al. 2004; Ira et al. 2004). Analysis of an HO-induced DSB showed that overexpression of the CDK inhibitor Sic1 reduced ssDNA generation and prevented RPA accumulation. Consequently, Mec1 signalling and Rad53 phosphorylation were also impaired (Ira et al. 2004). CDK regulates resection initiation partly through phosphorylation of Sae2, which activates Mre11 endonuclease activity and drives short-range resection by the MRX complex (Huertas et al. 2008; Cannavo et al. 2018). Analogously, human CtIP is activated by CDK (Huertas and Jackson 2009). In budding yeast, CDK also phosphorylates Dna2 promoting its recruitment to DSBs and long-range resection (X. Chen et al. 2011). In humans, Exo1 mediated long-range resection is promoted by CDK phosphorylation (Tomimatsu et al. 2014). Furthermore, CDK may reduce binding of NHEJ factors such as the Ku complex, shifting repair pathway choice away from NHEJ (Clerici et al. 2008; Y. Zhang et al. 2009).

CDK-dependent activation of resection helps to explain why resection and HR are favoured after replication initiation rather than in the G_1 phase of the cell cycle. However, phosphorylation activity of CDK is not sufficient to fully activate resection indicating that additional cell cycle regulators activate HR (Huertas et al. 2008; X. Chen et al. 2011; Cannavo et al. 2018; Galanti et al. 2024). Recent experiments in budding yeast identified Dbf4-dependent kinase (DDK) as such an additional regulator. DDK was shown to also activate Sae2 and Dna2. Importantly, synthetic DDK activation allowed for limited resection and repair by HR even in G_1 cells, showing that DDK can provide a resection signal that is normally restricted to later cell cycle stages (Galanti et al. 2024).

1.3.3 Nucleosomes form a barrier for resection

Resection is regulated by cell cycle factors, but chromatin may provide an additional layer of control. In budding yeast, nucleosomes were lost from resected regions after DSB induction and did not detectably associate with ssDNA *in vivo* (Peritore et al. 2021). *In vitro* experiments further showed that whereas nucleosome-free DNA was digested by the resection nuclease Exo1 or by the nuclease Dna2 together with the helicase Sgs1, Exo1 activity was inhibited by nucleosomes even at low occupancy. In contrast, Dna2 in conjunction with Sgs1 could resect nucleosome-bound DNA, but only when sufficient adjacent nucleosome-free DNA was available. Consistently, the Sgs1 and its human orthologue BLM unwound nucleosome-bound dsDNA only in the presence of adjacent nucleosome-free DNA (Adkins et al. 2013). Together,

the *in vitro* and *in vivo* data suggests that nucleosomes form a barrier for the resection machinery and that cellular mechanisms must overcome this barrier for repair by HR. Nucleosome remodellers are likely candidates and their activity might contribute to resection regulation. That multiple nucleosome remodellers have been reported to be recruited to DSBs in yeast and humans supports this hypothesis (Downs et al. 2004; Morrison et al. 2004; Van Attikum et al. 2004; Chai et al. 2005; Shim et al. 2005, 2007; Park et al. 2006; Kent et al. 2007; Liang et al. 2007; Van Attikum et al. 2007; Morillo-Huesca et al. 2010; Bennett et al. 2013; Toiber et al. 2013; Bennett and Peterson 2015; Kari et al. 2016; Wiest et al. 2017; Hays et al. 2020; Casari et al. 2021; Gnugnoli et al. 2021; Karl et al. 2022). Functional studies of individual nucleosome remodeller complexes provide further insight.

In budding yeast, SWI/SNF complex dysfunction delays resection and impairs MRX recruitment to DSBs (Wiest et al. 2017). Furthermore, co-depletion of the RSC complex subunit Sth1 and the SWI/SNF complex subunit Snf2 impaired resection at restriction enzyme generated DSBs, indicating that nucleosome eviction is required for resection (Peritore et al. 2021). Because the complexes were thought to act redundantly in nucleosome eviction, only the double mutant was tested. However, the two complexes might act at different steps of the repair process, as distinct recruitment kinetics to DSBs have been reported (Chai et al. 2005). The human orthologues BAF and PBAF are less well understood, but were found to be recruited to DSBs and involved in repair, as well (Hays et al. 2020; Park et al. 2006).

The function of the INO80 complex in DSB repair remains debated. Although its contribution to DSB repair has been reported in several studies in yeast and human cells (X. Shen et al. 2000; Morrison et al. 2004; Van Attikum et al. 2004; Alatwi and Downs 2015), the specific role of the INO80 complex during HR is still unclear. Functional analysis is challenging because the INO80 complex has both nucleosome sliding and editing activities (Brahma et al. 2017; Eustermann et al. 2018; Krietenstein et al. 2016; Oberbeckmann, Krietenstein, et al. 2021; Papamichos-Chronakis et al. 2011; Xuetong Shen et al. 2003). A common approach to investigate INO80 complex dysfunction is the deletion of *ARP8*, which results in loss of the entire Arp8-module. The INO80 complex loses its ability to bind extra-nucleosomal DNA which is chemomechanically coupled to the ATPase remodelling activity of the ino80 subunit. As a result, *arp8Δ* mutants display a phenotype similar to *ino80Δ* mutants (Xuetong Shen et al. 2003; Van Attikum et al. 2004; Tosi et al. 2013; Brahma et al. 2018; Knoll et al. 2018; Kunert et al. 2022).

To investigate the function of the INO80 complex in DSB repair, the HO endonuclease was used to introduce a DSB in *arp8Δ* mutants. The minor loss of DNA around the cut site indicated reduced resection in the *arp8Δ* mutants. However, RPA levels were next to the DSB when the INO80 complex was dysfunctional. Furthermore, Rad51 filament formation was reduced, suggesting that the INO80 complex is involved in the exchange of RPA for Rad51. Additional H2A.Z loss rescued this defect in Rad51 filament formation, indicating that nucleosome editing by the INO80 complex promotes Rad51 filament formation (Lademann et al. 2017). Consistent with these results, another study showed that overexpression of Rad51 or Rad52, which mediates the exchange of RPA for Rad51, almost fully rescued the Arp8 deletion defect in allelic HR (Tsukuda et al. 2009). Therefore, the INO80 complex appears to act in HR at the step of Rad51 filament formation, which may explain the sensitivity of INO80 mutants to genotoxic agents (X. Shen et al. 2000). However, evidence for an additional function in resection remains controversial. Some studies in yeast observed resection defects in *arp8Δ* mutants at an HO-induced DSB (Lademann et al. 2017; Van Attikum et al. 2007), whereas others did not (Tsukuda et al. 2005). The nucleosome sliding function of the INO80 complex could promote resection. In contrast, its histone exchange function, which replaces H2A.Z with canonical H2A, could inhibit resection. H2A.Z containing nucleosomes are less stable on DNA and do not pose a barrier for the Exo1 resection nuclease *in vitro* (Adkins et al. 2013; Watanabe et al. 2013; H. Zhang et al. 2005). Consistent with the hypothesis that H2A.Z containing nucleosomes help to overcome the nucleosome barrier, H2A.Z deficient yeast strains show a resection defect (Adkins et al. 2013; Kalocsay et al. 2009; Lademann et al. 2017). Furthermore, H2A.Z is highly abundant at DNA damage sites in yeast and human cells (Alatwi and Downs 2015; Kalocsay et al. 2009; Nishibuchi et al. 2014; Xu et al. 2012) and the SWR1 complex is recruited to DSBs in yeast (Morillo-Huesca et al. 2010; Van Attikum et al. 2007). Therefore, the SWR1 complex might incorporate H2A.Z at DSBs and thereby eventually promote resection through nucleosome destabilisation. On the other hand, H2A.Z could also function as a signalling platform for recruitment of repair factors (Xu et al. 2012).

Nucleosome positioning is well known to be involved in gene regulation (Baldi et al. 2020; Corona and Tamkun 2004; Oberbeckmann, Niebauer, et al. 2021; Ocampo et al. 2016; Weiner et al. 2010; Woodage et al. 1997). Further studies suggest an additional role for nucleosome sliding remodellers in HR. ISW1 and CHD nucleosome remodellers were found to be recruited to DSBs and to promote resection (Casari et al. 2021; Gnugnoli et al. 2021; Kari et al. 2016;

Toiber et al. 2013). Furthermore, nucleosome arrays, which consist of regularly spaced nucleosomes relative to a reference point, form upon nucleosome sliding not only relative to a transcription factor, but also relative to a restriction enzyme induced DSB *in vitro.* (Oberbeckmann, Niebauer, et al. 2021). Therefore, nucleosome array formation might facilitate resection. However, how nucleosome array formation around a DSB might benefit HR remains unknown.

In addition to multi-subunit nucleosome remodelling complexes, the homo-dimeric remodeller Fun30 in yeast and its human orthologue SMARCAD1 promote long-range resection (Bantele et al. 2017; X. Chen et al. 2012; Costelloe et al. 2012; Eapen et al. 2012; Flaus 2006). The resection defect of *fun30Δ* mutants is rescued by co-deletion of *RAD9*, suggesting that Fun30 counteracts the inhibitory effect of Rad9 on resection (Bantele et al. 2017; X. Chen et al. 2012). Rad9 binds to nucleosomes flanking DSB through interactions with phosphorylated H2A and methylated H3K79 (Hammet et al. 2007; Lazzaro et al. 2008; Granata et al. 2013). However, the mechanism by which Fun30 antagonises Rad9-mediated inhibition of resection remains incompletely understood (X. Chen et al. 2012; Bantele et al. 2017; Bantele and Pfander 2019). Analogously, human SMARCAD1 is required to overcome the inhibitory effect of 53BP1, the functional homologue of Rad9 in budding yeast (Bothmer et al. 2011; Lottersberger et al. 2013; Densham et al. 2016; Bantele et al. 2017; Bantele and Pfander 2019). Taken together, the nucleosome barrier is likely overcome by the action of nucleosome remodellers. Several studies in yeast and higher eukaryotes reported that nucleosome remodellers promote HR. Nucleosome remodellers can evict, slide and edit nucleosomes. Why multiple remodelling activities appear to be involved in HR and in what manner they contribute to HR remains to be elucidated.

1.4 Systems to study DSB repair

DSBs arise from various sources and this diversity has enabled the development of several experimental approaches to study their repair. In addition to exogenous sources of DNA damage, such as radiation and DNA-damaging drugs, genetic systems have been established to induce DSBs in a controlled and site-specific manner. The choice of method depends on the biological question, because the approaches differ in their types, numbers and genomic locations of lesions they generate (Table 1).

Table 1: Overview of experimental systems to study DSB repair.

Induction method	Examples	Damage type and location	Reference
Ionising radiation and drugs	X-rays, ɣ-rays, radio-mimetics (phleomycin, bleomycin)	Oxidative base damage, SSBs and DSBs at various loci	(Mehta and Haber 2014)
Site-specific nucleases	HO endonuclease	Site-specific DSB induction	(S. E. Lee et al. 1998; Nicolás et al. 2000)
	Restriction enzymes (AsiSI, AscI, FseI)	Site-specific induction of multiple DSBs	(Iacovoni et al. 2010; Gnügge and Symington 2020; Peritore et al. 2021)
	Homing endonucleases (I-SceI, I-PpoI)	Site-specific induction of multiple DSBs	(Rouet et al. 1994; Berkovich et al. 2007).
	Programmable nucleases (ZFNs, TALENs, meganucleases, CRISPR/Cas)	Site-specific DSB induction at a desired genomic location	(Kim et al. 1996; Silva et al. 2011; Deng et al. 2012; Jinek et al. 2012)
Telomere deprotection	*cdc13-1*, loss of TRF1/2	Deprotected telomeres	(Garvik et al. 1995; Sfeir and De Lange 2012)

1.4.1 Drugs and ionising radiation induce various forms of DNA damage

Genome integrity is normally maintained by cellular DNA repair mechanisms, but DNA damage can experimentally be induced with ionising radiation or genotoxic drugs. Since the discovery of X-rays by Wilhelm Röntgen in 1895, ionising radiation has become widely used in medicine for diagnostic imaging and cancer treatment (Malone 2020). Whereas radiography uses comparatively low doses of ionising radiation, in radiotherapy higher doses are used to induce DNA damage with the aim to eliminate cancer cells (Baskar et al. 2014; Wei et al. 2026). Beyond its clinical applications, the ability of ionising radiation to damage DNA has also made it a powerful experimental tool for investigating DNA damage signalling and repair.

Ionising radiation (IR) damages DNA directly through ionisation of DNA molecules and indirectly through radiolysis of cellular water. Ionisation of water molecules generates reactive oxygen species (ROS), which can oxidise DNA bases and damage the phosphodiester backbone. Predominantly single-strand breaks (SSBs) are caused, but double-strand breaks (DSBs) arise as well, when two SSBs occur in close proximity on opposing DNA strands (J. F. Ward 1995; Little 2000; Mehta and Haber 2014; Saini and Gurung 2025).

Ionising radiation has been widely used to investigate DNA damage responses and repair mechanisms and contributed, for example, to the identification of DNA damage checkpoints (Ted A. Weinert and Hartwell 1988; Mehta and Haber 2014). Radio-mimetic compounds such as phleomycin and bleomycin induce similar DNA lesions while permitting more precise dosage control (Povirk 1996; Mehta and Haber 2014; Shimada et al. 2024; Shimizu et al. 2025). Because major DNA repair pathways are conserved between yeast and humans, studies in both systems advanced our understanding of the molecular responses of DNA damage. Furthermore, they contribute to the development of targeted cancer therapies and to a better understanding of genetic diseases associated with DNA repair defects (O'Connor 2015; O'Driscoll 2012).

1.4.2 Site-specific nucleases

DNA damaging drugs and ionising radiation are widely used to study damage responses and repair, but they generate lesions at largely undefined genomic locations. Conditional expression of site-specific nucleases overcomes this limitation by introducing DSBs at defined loci.

The first site-specific DSB induction system was established in budding yeast using the HO endonuclease. HO cleaves the *MAT* locus to initiate mating-type switching. Under galactose-inducible expression, sustained HO activity generates DSBs, while donor-mediated HR and mating type switching are prevented in strains lacking the *HML* and *HMR* donor sequences (S. E. Lee et al. 1998). In addition to the endogenous *MAT* locus, the HO system can be used to investigate ectopically integrated HO recognition sequences (Nickoloff et al. 1986; Berzsenyi et al. 2021). Because HO cleavage is restricted to its recognition sequence, bacterial restriction enzymes have been adapted to induce DSBs conditionally at additional loci (Berzsenyi et al. 2021). AsiSI, for example, targets 38 loci in the budding yeast genome and enabling sequence-independent analysis by averaging across multiple loci (Peritore et al. 2021). Other restriction enzymes generate different numbers of DSBs and different DNA-end structures, including sticky ends with 5' overhangs and blunt ends (Gnügge and Symington 2020). Cutting efficiencies also vary and AscI and SrfI were reported to be particularly efficient (Gnügge and Symington 2020). The LexO system provides an alternative to galactose-inducible expression by enabling conditional nuclease induction in glucose-containing medium, thereby maintaining optimal growth conditions (Gnügge and Symington 2020).

Nuclease-mediated DSB induction has also been established in mammalian cells (Berzsenyi et al. 2021). I-SceI is commonly used to generate a single DSB, whereas I-PpoI and AsiSI induce multiple DSBs (Rouet et al. 1994; Berkovich et al. 2007; Iacovoni et al. 2010). In addition, the yeast HO endonuclease has been adapted for use in mammalian cells by introducing its recognition sequence into the genome (Nicolás et al. 2000). Together, conditional expression of nucleases enables investigation of one or multiple site-specific DSBs. The nucleases do not only differ in number of genomic target sites, but also cleavage efficiency, recognition sequence length and DNA end structure which they generate (Berzsenyi et al. 2021).

Restriction enzymes induce site-specific DSBs, but are limited to their recognition sequence and cannot be directed to other genomic sequences. Programmable nucleases overcome this limitation and have become central tools for genome engineering, which requires DSB induction at a desired target sequence (Govindan and Ramalingam 2016; Maeder and Gersbach 2016). Zinc finger nucleases (ZFNs), the first widely used programmable nucleases, consist of the cleavage domain of the FokI restriction endonuclease fused to engineered zinc finger proteins, which mediate sequence-specific DNA binding (L. Li et al. 1992; Kim et al. 1996; Maeder and Gersbach 2016). TALE proteins, whose modular repeats bind to an individual base pair, enabled the design of novel DNA-binding proteins. Engineered TALE arrays were fused to the FokI cleavage domain to generate transcription activator-like effector nucleases (TALENs) (Deng et al. 2012; Maeder and Gersbach 2016). Meganucleases are homing endonucleases, such as I-CreI and I-SceI, whose binding specificity has been re-engineered to recognise novel DNA target sequences and provide an alternative to FokI-mediated DSB induction (Silva et al. 2011; Maeder and Gersbach 2016). More recently, the CRISPR/Cas system has enabled target specificity to be altered simply by modifying the guide RNA (gRNA). The gRNA, a fusion of the CRISPR RNA (crRNA) and trans-activating CRISPR RNA (tracrRNA), directs the Cas9 endonuclease to a complementary DNA sequence, where it introduces a site-specific DSB (Jinek et al. 2012; Maeder and Gersbach 2016).

Different experimental approaches can be used to analyse site-specific DSBs, depending on the biological question and the model organism. Examples include fluorescence, confocal and super-resolution microscopy, DSB-labelling approaches and chromatin immunoprecipitation (ChIP) (Berzsenyi et al. 2021). In particular, adaptase-mediated library preparation has been used to generate ssDNA sequencing libraries in which the forward and reverse strands can be

distinguished. Adaptase adds an adapter specifically to the 3’ end of an ssDNA fragment preserving fragment directionality and permitting strand-specific alignment. This method is particularly useful for analysing resection, because degradation of the 5’-terminated strands is detected as strand-specific loss of sequencing coverage around a DSB. Chromatin immunoprecipitation (ChIP) of proteins such as RPA or histones can provide complementary information about ssDNA formation and the local chromatin environment (Peritore et al. 2021).

1.4.3 Telomere deprotection as an alternative model for DSB induction

In addition to the direct investigation of DSBs, deprotected telomeres provide a complementary model. Chromosome ends structurally resemble one end of a DSB. Therefore, telomeres must be protected from recognition by the DNA repair machinery to avoid chromosomal instability, extensive telomere shortening, cancer and senescence (Cheung 2008; Meena et al. 2015). In contrast to DSBs within the genome, telomeres contain repetitive sequence motifs, which are bound by specific proteins (see section 1.1.3).

In budding yeast, telomeric ssDNA is bound by Cdc13, which recruits Stn1 and Ten1 to form the CST complex (Cdc13-Stn1-Ten1). This complex is structurally related to the ssDNA-binding protein RPA and protects the telomere end from recognition by the DNA repair machinery (Anderson 2002; Dewar and Lydall 2012; Gao et al. 2007; N. Grandin 2001; N Grandin et al. 1997; Hughes et al. 2000).

In higher eukaryotes, telomeres are protected by the shelterin complex consisting of the DNA-binding subunits TRF1, TRF2 and POT1 and the interconnecting subunits TIN2, TPP1 and Rap1 (De Lange 2009). Loss of TRF2 leads to activation of the ATM pathway (Celli and De Lange 2005; Karlseder et al. 1999) and POT1 is essential for ssDNA binding to prevent activation of the ATR pathway (Denchi and De Lange 2007). TRF2 is also required to block repair by NHEJ (Celli and De Lange 2005; Konishi and De Lange 2008). Furthermore, structural analyses of human and mouse telomeres revealed that a T-loop can form upon strand invasion of the 3’ ssDNA end into the telomere duplex. In higher eukaryotes, this configuration protects the telomeric ssDNA from degradation and blocks DNA end-binding factors (De Lange 2009; Griffith et al. 1999).

In mouse cells, telomeres became fully deprotected upon conditional deletion of TRF1 and TRF2, which indicates that the two dsDNA-binding subunits are required for association of the

shelterin complex (Sfeir and De Lange 2012). In budding yeast, temperature shift of a *cdc13-1* (P371S) mutant results in telomere deprotection. In this mutant the Cdc13 protein is misfolded at restrictive temperatures (≥ 26 °C). Structural analysis showed that at higher temperatures the dimerisation of the OB2 domain is disrupted, which compromises Stn1 binding and CST complex assembly (Mason et al. 2013). Consequently, activation of the DNA damage response, cell cycle arrest before anaphase and activation of resection, resulting in accumulation of long ssDNA stretches at telomeres, can be observed in *cdc13-1* mutants at restrictive temperatures (Booth 2001; Garvik et al. 1995; Hartwell et al. 1973; Mersaoui et al. 2018). Telomere deprotection can be used as an alternative model to study DSBs. However, because telomeric DNA has unique structural features, mechanistic conservation between telomeres and canonical DSBs cannot be assumed but must be verified.

Quantitative amplification of ssDNA (QAOS) measures ssDNA accumulation at defined sub-telomeric and telomere-proximal loci. A tagging primer anneals selectively to ssDNA at low temperature and primer extension generates a tagged DNA molecule that is subsequently detected and quantified by qPCR (Booth 2001). Using this method, it has been shown that *cdc13-1* mutants deficient in Exo1 accumulate reduced amounts of ssDNA after telomere deprotection. Therefore, Exo1 likely carries out long-range resection at telomeres, as it does at DSBs (Ngo and Lydall 2010; Schaetzlein et al. 2007; Zubko et al. 2004). Furthermore, Sgs1 appeared to contribute to resection, in particular in the absence of Rad9 (Ngo and Lydall 2010). However, whether Sgs1 acts in conjunction with the nuclease Dna2 at telomeres, as it does during DSB resection, has not yet been investigated. The current literature suggests that long-range resection is similar at telomeres and DSBs, but short-range resection differs. At DSBs, the MRX complex must generate an ssDNA entry point for long-range resection. In contrast, the MRX complex inhibits resection at telomeres (Foster et al. 2011). Because telomere deprotection already exposes a 3’ overhang, short-range resection may not be required. Instead, MRX might recruit protective telomeric proteins, such as telomerase itself (Faure et al. 2010; Vega et al. 2007).

In addition to resection, telomere deprotection has also been a valuable tool for the investigation of DSB signalling. The checkpoint proteins Mec1, Mec3, Rad17, Rad24 and Rad53 were identified in the context of telomere deprotection before their roles in DSB repair were established (T A Weinert et al. 1994; T A Weinert and Hartwell 1993).

In summary, the temperature sensitive *cdc13-1* mutant combined with QAOS provides an alternative system to DSB induction. Because telomeres have specialised structural features, mechanistic conservation between deprotected telomeres and DSBs must be verified. Available evidence supports that long-range resection pathways are similar at telomeres and canonical DSBs, but the role of Dna2 has not yet been investigated.

2. Aim of the study

DNA double-strand breaks (DSBs) represent one of the most severe forms of DNA damage and can be repaired by two major pathways: end joining and homologous recombination (HR). DNA end resection is a key limiting step in repair pathway choice and this study aimed to investigate to what extend nucleosome remodelling influences resection. *In vitro* studies have demonstrated that resection nucleases cannot efficiently degrade DNA when it is bound to nucleosomes (Adkins et al. 2013). Thus, chromatin represents a physical barrier that must be overcome to allow for resection. Nucleosome remodellers are likely candidates as they can evict, slide or edit nucleosomes (Karl et al. 2022). Although the activity of nucleosome eviction has been shown to be required for efficient resection (Peritore et al. 2021), the contribution of other nucleosome remodelling activities remains poorly understood.

The goal was to study the function of the nucleosome editing complexes INO80 and SWR1, in particular. AsiSI-mediated DSB induction in budding yeast and strand-specific sequencing were used to determine resection efficiencies of different mutants deficient in nucleosome editing. For quantitative interpretation of this strand-specific sequencing data across different yeast mutants, a nanopore-based workflow was used to measure cutting efficiencies in parallel. Furthermore, the *cdc13-1* system was aimed to be used for studying resection. *cdc13-1* mutants suffer from telomere deprotection at restrictive temperatures, which activates DNA repair and resection of the telomere ends. We first asked whether the long-range resection pathways at telomeres resemble the mechanism at canonical DSBs and quantitative amplification of ssDNA (QAOS) was used to measure the accumulation of single-stranded DNA (ssDNA) at telomere proximal regions (Booth 2001). As telomeres contain specialised chromatin features, we first asked whether nucleosome eviction is required to allow for resection at deprotected telomeres as at DSBs. We then sought to elucidate the role of nucleosome editing for resection at deprotected telomeres and compare it to our strand-specific-sequencing data.

3. Results

The budding yeast *Saccharomyces cerevisiae* provides a powerful model system to study DNA repair and nucleosome remodelling, as it combines genetic simplicity with a high degree of conservation with higher eukaryotes (Karl et al. 2022). Here, we used this model system to investigate the role of nucleosome remodelling in resection and focus on the dynamics of the histone variant H2A.Z.

3.1 Nucleosome editing by INO80 is dispensable for DSB end resection

To determine to what extend nucleosome editing is required for DNA end resection, we analysed yeast mutants deficient in INO80 activity or with combined loss of SWR1 complex activity and the histone variant H2A.Z. The restriction enzyme AsiSI can conditionally be expressed upon addition of galactose to induce multiple DSBs in these mutants. DSB induction via AsiSI has already been used to show that nucleosome eviction is required for efficient resection in budding yeast (Peritore et al. 2021). We hypothesised that also nucleosome editing affects resection. Both the INO80 and SWR1 complex, which have opposite functions in the exchange of the histone variant H2A.Z, are actively recruited to DSBs in budding yeast (Van Attikum et al. 2004).

Incorporation of histone variants can alter the stability of nucleosomes and their interaction with DNA. In yeast, nucleosomes containing the histone variant H2A.Z are less stable than those composed of canonical histones (S. Li et al. 2023). Consistently, *in vitro* studies have shown that, unlike canonical nucleosomes, H2A.Z containing nucleosomes do not present a barrier to the Exo1 nuclease (Adkins et al. 2013). Importantly, H2A.Z is highly abundant at DNA damage sites in yeast and human cells (Alatwi and Downs 2015; Kalocsay et al. 2009; Nishibuchi et al. 2014; Xu et al. 2012). Together, these findings suggest that incorporation of H2A.Z through nucleosome editing by the SWR1 complex could promote resection. However, whether this effect occurs *in vivo* remains unresolved.

Alternatively, H2A.Z may not directly facilitate resection but instead function as a signalling platform for the recruitment of DNA repair factors (Xu et al. 2012). Moreover, given its established role in transcriptional regulation, H2A.Z could indirectly influence DNA repair by promoting the expression of repair genes rather than participating directly in the resection process (Papamichos-Chronakis et al. 2011).

The INO80 complex is likely to contribute to HR. Yeast mutants with a dysfunction in INO80 complex activity are sensitive to genotoxic agents (X. Shen et al. 2000). However, its role during resection is controversial. The action of the INO80 complex would counteract H2A.Z incorporation by the SWR1 complex. Therefore, its dysfunction could facilitate resection. In contrast to this hypothesis, some studies observed a resection defect upon INO80 dysfunction (Lademann et al. 2017; Van Attikum et al. 2007). However, another study did not show any changes upon INO80 dysfunction (Tsukuda et al. 2005). Eventually, the INO80 complex is not involved in resection, but only downstream of the HR repair process in the exchange of RPA and Rad51 (Lademann et al. 2017; Tsukuda et al. 2009).

To assess the impact of the INO80 complex activity on resection, we employed an *arp8Δ* strain. While deletion of *INO80*, coding for the catalytic ATPase subunit of the INO80 complex, is lethal, loss of the Arp8 subunit is viable but results in impaired remodelling activity of the complex (Kunert et al. 2022; Xuetong Shen et al. 2003; Van Attikum et al. 2004). We further deleted the *HTZ1* gene encoding H2A.Z to directly examine the role of the histone variant. However, this deletion is associated with secondary phenotypes arising from dysfunction of the SWR1 complex. Potentially, the SWR1 complex remains bound to DNA in an attempt to incorporate H2A.Z into a nucleosome, which is not available (Halley et al. 2010; Morillo-Huesca et al. 2010). Thus, we combined *HTZ1* deletion with additional deletion of *SWR1*, thereby minimising phenotypes attributable to SWR1 complex malfunction rather than H2A.Z loss itself. Finally, we analysed the combined *arp8Δ swr1Δ htz1Δ* mutant to test whether nucleosome editing is dispensable for resection.

For all experiments, budding yeast (*Saccharomyces cerevisiae*) cultures were arrested in G2/M using nocodazole to favour repair by homologous recombination over end joining. DSBs were subsequently induced via the restriction enzyme AsiSI, fused to a nuclear localisation signal, and conditionally expressed by the galactose-inducible *pGAL1-10* promoter. Upon induction, AsiSI generates DSBs at 38 sites in the yeast genome. Samples were collected at 0 h, 2 h, 4 h, and 6 h after induction for strand-specific sequencing. In parallel, cell pellets were harvested for nanopore-based cutting efficiency analysis, western blot-based analysis of Rad53 phosphorylation and flow cytometry-based DNA content measurements to verify proper cell cycle arrest.

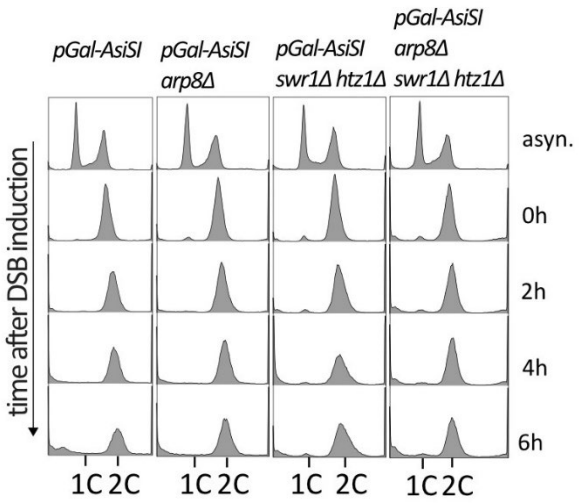


Figure 6: G2/M cell cycle arrest after DSB induction in *pGal-AsiSI* yeast mutants.
The yeast strains *pGal-AsiSI, pGal-AsiSI arp8Δ, pGal-AsiSI htz1Δ swr1Δ* and *pGal-AsiSI arp8Δ htz1Δ swr1Δ* were grown in YP-Raffinose and arrested with nocodazole. The experiment was initiated by DSB induction via addition of galactose and samples were collected at the indicated timepoints. Total DNA content was measured by flow cytometry after SYTOX green staining. Data is representative of n = 2 biological replicates.

The distribution of DNA content across the analysed yeast populations was determined by flow cytometry (Figure 6). Prior to nocodazole treatment, all strains displayed a typical asynchronous distribution, with cells containing either one or two chromosomal contents (1C/2C), as well as an intermediate population corresponding to cells undergoing DNA replication. In contrast, after nocodazole treatment, cells were almost exclusively arrested in G2/M, as indicated by a predominant population with duplicated DNA content at the 0 h timepoint. This arrest was maintained throughout the subsequent timepoints, indicating that most of the cell cycle population was in G2/M during the time course of the experiment.

During resection, 3´ single-stranded DNA (ssDNA) overhangs are generated for homology search. This process involves degradation of the 5'-terminated strands, corresponding to the forward strand on the right side of the DSB and the reverse strand on the left side. The resulting loss of DNA can be detected as a strand-specific decrease in sequencing coverage. In parallel, chromatin immunoprecipitation (ChIP) can be performed from the same chromatin extracts to assess the loss of DNA associated with proteins of interest (Peritore et al. 2021).

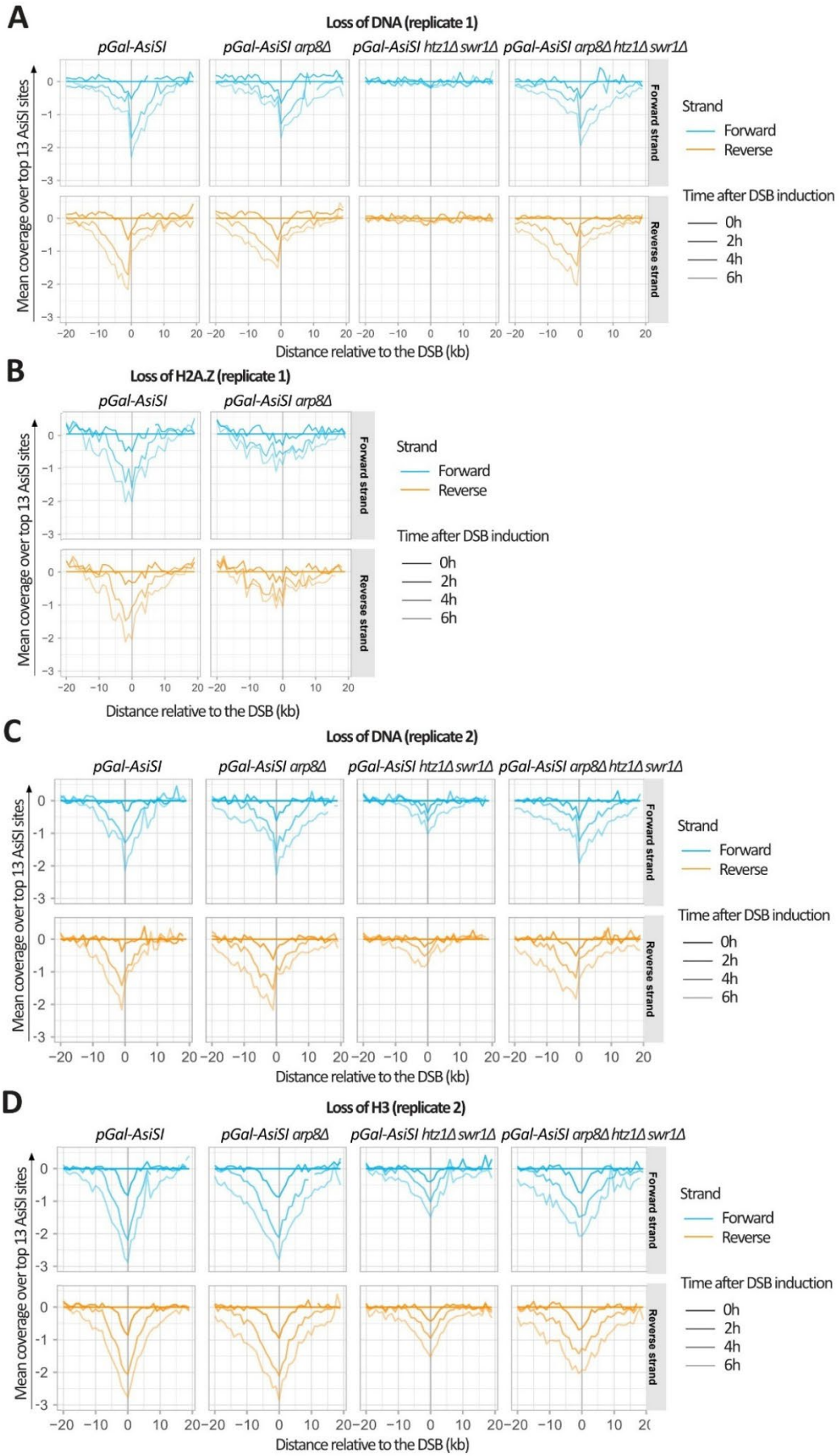

A
Loss of DNA (replicate 1)
pGal-AsiSI
pGal-AsiSI arp8Δ
pGal-AsiSI htz1Δ swr1Δ
pGal-AsiSI arp8Δ htz1Δ swr1Δ
Mean coverage over top 13 AsiSI sites
Forward strand
Reverse strand
Distance relative to the DSB (kb)
Strand
Forward
Reverse
Time after DSB induction
0h
2h
4h
6h
B
Loss of H2A.Z (replicate 1)
pGal-AsiSI
pGal-AsiSI arp8Δ
Mean coverage over top 13 AsiSI sites
Forward strand
Reverse strand
Distance relative to the DSB (kb)
Strand
Forward
Reverse
Time after DSB induction
0h
2h
4h
6h
C
Loss of DNA (replicate 2)
pGal-AsiSI
pGal-AsiSI arp8Δ
pGal-AsiSI htz1Δ swr1Δ
pGal-AsiSI arp8Δ htz1Δ swr1Δ
Mean coverage over top 13 AsiSI sites
Forward strand
Reverse strand
Distance relative to the DSB (kb)
Strand
Forward
Reverse
Time after DSB induction
0h
2h
4h
6h
D
Loss of H3 (replicate 2)
pGal-AsiSI
pGal-AsiSI arp8Δ
pGal-AsiSI htz1Δ swr1Δ
pGal-AsiSI arp8Δ htz1Δ swr1Δ
Mean coverage over top 13 AsiSI sites
Forward strand
Reverse strand
Distance relative to the DSB (kb)
Strand
Forward
Reverse
Time after DSB induction
0h
2h
4h
6h

Figure 7: Resection of yeast mutants deficient in nucleosome editing after AsiSI-induced DSB induction.
(A) Detection of DNA loss via strand-specific sequencing: AsiSI expression was induced via galactose addition to create DSBs at defined genomic loci in nocodazole arrested *pGal-AsiSI, pGal-AsiSI arp8Δ, pGal-AsiSI htz1Δ swr1Δ* and *pGal-AsiSI arp8Δ htz1Δ swr1Δ* strains. Cell pellets were collected after the indicated timepoints and library preparation for strand-specific illumina sequencing was performed from purified chromatin extracts. Normalised read coverage was divided by the 0 h timepoints coverage and log2-transformed. Mean input DNA coverage across the top 13 resected AsiSI DSB sites (Peritore et al. 2021) is shown in a 40 kb window using 1 kb bins. Data shows the first biological replicate.
(B) H2A.Z ChIP followed by strand-specific sequencing to detect loss of DNA associated with H2A.Z containing histones: Chromatin extracts from the first replicate shown in (A) were used for H2A.Z ChIP. Sequencing and data analysis was performed as in (A).
(C) Second biological replicate of the input DNA analysis shown in (A).
(D) H3 ChIP followed by strand-specific sequencing to detect loss of nucleosome-associated DNA: Chromatin extracts from the second replicate shown in (C) were used for H3 ChIP. Sequencing and data analysis were performed as in (A).

We performed strand-specific sequencing analysis for chromatin remodeller mutants deficient in nucleosome editing. For analysis, the DNA coverage was normalised to equal read numbers across the different strains and timepoints and divided by the 0 h coverage. The mean coverage around the 13 best-cut AsiSI DSB sites identified previously (Peritore et al. 2021) is shown. The overall DNA loss over time was determined by sequencing the input samples (Figure 7A and C), whereas the loss of DNA associated specifically with H2A.Z (Figure 7B) or H3 (Figure 7D) was measured by ChIP-seq from the same chromatin extracts.

In the *pGal-AsiSI* control strain, the progressive decrease in DNA coverage reflects ongoing resection following DSB induction, occurring symmetrically either on the forward or on the reverse strand (Figure 7A and C). Loss of DNA bound to H2A.Z (Figure 7B) or H3 (Figure 7D) occurred in a similar manner on both strands, indicating nucleosome loss coincides with resection, consistent with previous findings (Peritore et al. 2021). Notably, the reduction in H3-associated DNA is more pronounced than that of H2A.Z, despite comparable overall DNA loss. These observations suggest that a subset of nucleosomes that are lost upon resection contain H2A.Z. In addition, the signal for H2A.Z loss could also result from the editing function of the INO80 complex exchanging H2A.Z with H2A in a subset of nucleosomes close to the DSB site.

The *pGal-AsiSI arp8Δ* strain did not exhibit a substantial difference in overall DNA loss compared to the control, indicating that INO80 dysfunction does not strongly affect resection (Figure 7A and C). Likewise, the loss of H3-associated DNA was comparable to the control (Figure 7D). In contrast, loss of H2A.Z-associated DNA appeared to be reduced in the *pGal-AsiSI arp8Δ* strain (Figure 7B). The data suggests that the INO80 complex is involved in the removal of H2A.Z containing nucleosomes. However, we cannot differentiate if the H2A.Z containing nucleosomes are removed during the resection process or if they are removed via

nucleosome editing by the INO80 complex replacing the H2A.Z containing nucleosomes by canonical ones.

If the INO80 complex is dysfunctional, SWR1 complex activity is not counteracted. This could lead to an increase of H2A.Z containing histones. Indeed, previous studies showed that strains with a dysfunctional INO80 complex show an increased number of H2A.Z containing nucleosomes adjacent to a DSB (Lademann et al. 2017; Papamichos-Chronakis et al. 2011). Therefore, we would expect an increased loss of H2A.Z containing nucleosomes in the *pGal-AsiSI arp8Δ* strain assuming the loss of H2A.Z signal is solely related to the loss of nucleosomes to resection. In contrast, we observed a reduction in H2A.Z associated DNA loss for the *pGal-AsiSI arp8Δ* strain. The data indicates that the H2A.Z associated DNA loss arises partly because of the H2A.Z to H2A exchange function of the INO80 complex in the control strain. The signal for H2A.Z associated DNA loss in the *pGal-AsiSI arp8Δ* strain indicates that the loss of H2A.Z containing histones upon resection also contributes to the signal.

Our data elucidates resection after DSB induction at multiple sites in the yeast genome and follows up on previous data which investigated specifically one DSB site generated by the HO endonuclease. It is well known that the INO80 complex is required for repair by HR. However, a direct role for the INO80 complex in resection has been debated for the yeast model organism (Lademann et al. 2017; Papamichos-Chronakis et al. 2011; Van Attikum et al. 2004). We showed that, on average, the INO80 complex does not significantly affect resection at DSBs.

The *pGal-AsiSI htz1Δ swr1Δ* strain exhibited little to no loss of DNA (Figure 7A and C), indicating a strong impairment of resection. Correspondingly, the loss of H3-associated DNA was highly reduced, as well (Figure 7D). However, the triple mutant *pGal-AsiSI arp8Δ htz1Δ swr1Δ* displayed DNA loss profiles similar to the control (Figure 7A and C) and nucleosome eviction was likewise comparable (Figure 7D). These observations suggest that neither H2A.Z nor nucleosome editing is strictly required for resection. In contrast, the strong resection defect in the *pGal-AsiSI htz1Δ swr1Δ* strain would suggest that H2A.Z incorporation facilitates resection. This discrepancy becomes evident when considering the cutting efficiencies measured in parallel.

Previously, cutting efficiency of the *pGal-AsiSI* strain had been estimated computationally by comparing reads spanning DSB sites (uncut DNA) to average coverage (Peritore et al. 2021). However, DNA fragmentation into reads of about 350 bp during sample preparation for Illumina sequencing can introduce artefacts, because fragmentation occurring close to a site of a DSB will be misinterpreted as genuine cuts. Thus, we collected non-crosslinked samples in parallel and measured cutting efficiency by a nanopore-based approach in which very long fragments of genomic DNA are sequenced.

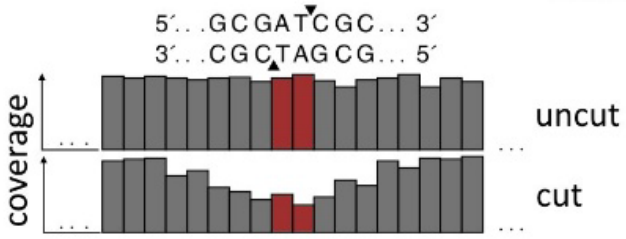


Figure 8: Principle of nanopore-based cutting efficiency analysis around an AsiSI DSB site.
AsiSI-cut DNA fragments lose the marked AT sequence during blunting in sample preparation. Coverage of this 2 bp sequence therefore represents the fraction of uncut DSB sites relative to local genomic coverage.

Because DNA ends are blunted during nanopore sample preparation, each AsiSI-cut molecule loses the "AT" sequence at the cut site (Figure 8). We calculated the fraction of uncut molecules by dividing the mean coverage of the 2 bp cut site by the mean coverage around the DSB. To normalise for local coverage while avoiding resection-associated artefacts, we used two 5 kb windows displaced by 5 kb from the cut site, covering the 5-10 kb regions on both sides of the DSB. Cutting efficiency was calculated as 1 minus the fraction of uncut DNA.

Ideally, cutting efficiency should be similar across strains so that resection phenotypes can be interpreted directly. If DSB induction is substantially reduced, apparent resection defects may instead reflect reduced break formation.

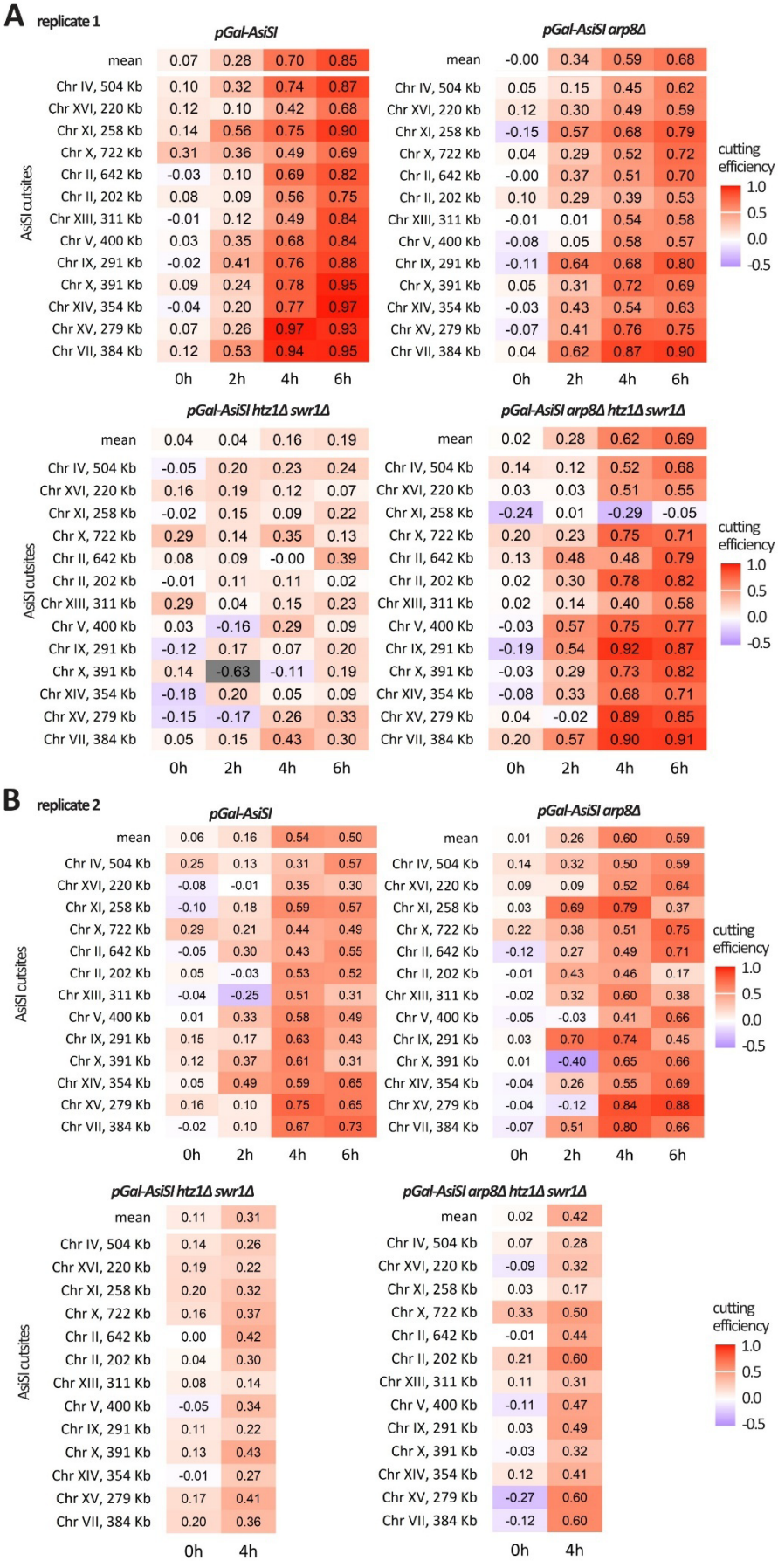

A
replicate 1
pGal-AsiSI
pGal-AsiSI arp8Δ
pGal-AsiSI htz1Δ swr1Δ
pGal-AsiSI arp8Δ htz1Δ swr1Δ
AsiSI cutsites
cutting efficiency
1.0
0.5
0.0
-0.5
0h
2h
4h
6h
B
replicate 2
pGal-AsiSI
pGal-AsiSI arp8Δ
pGal-AsiSI htz1Δ swr1Δ
pGal-AsiSI arp8Δ htz1Δ swr1Δ

Figure 9: H2A.Z-deficient mutants show reduced AsiSI cutting efficiency.
(A) Nanopore sequencing with samples collected in parallel to the first strand-specific sequencing replicate shown in Figure 7A and B for *pGal-AsiSI, pGal-AsiSI arp8Δ, pGal-AsiSI swr1Δ htz1Δ* and *pGal-AsiSI arp8Δ swr1Δ htz1Δ* strains at the indicated timepoints after DSB induction. Cutting efficiencies of the top 13 cut sites (Peritore et al. 2021) were determined from coverage of the 2 bp AsiSI cut site and averaged.
(B) Nanopore sequencing with samples collected in parallel to the second strand-specific sequencing replicate shown in Figure 7C and D. Cutting efficiencies were determined as in (A).

Within the 13 highly cut DSB sites the cutting efficiencies of the *pGal-AsiSI* control strain ranged from approximately 80 % to 97 % at 6 h after DSB induction in the first replicate (Figure 9A), consistent with previous observations (Peritore et al. 2021). In the second replicate, the mean cutting efficiency was lower with an average of 50 % at the 6 h timepoint (Figure 9B). Despite this difference, DSB induction was sufficient in both cases to yield comparable levels of resection (Figure 7).

The *pGal-AsiSI arp8Δ* strain displayed cutting efficiencies similar to the control, with a slight reduction in the first replicate, but increased efficiency in the second replicate. Likewise, the *pGal-AsiSI arp8Δ swr1Δ htz1Δ* strain showed overall comparable cutting efficiencies to the control, with only a minor reduction. Accordingly, resection levels across these strains are largely comparable. The modest decrease in resection observed in the *pGal-AsiSI arp8Δ* strain in the first replicate (Figure 7A) is likely attributable to the slightly reduced cutting efficiency in this sample (Figure 9A).

By contrast, the *pGal-AsiSI swr1Δ htz1Δ* strain exhibited markedly reduced cutting efficiencies, with only approximately 20 % cutting after 6 h in the first replicate (Figure 9A) and approximately 30 % in the second replicate (Figure 9B). This substantial reduction in DSB induction likely accounts for the pronounced phenotype observed by strand-specific sequencing (Figure 7). No resection was detected in the first replicate, whereas low levels of resection were observed in the second replicate, which had slightly higher cutting efficiency. Because the quantitative relationship between cutting efficiency and DNA loss is not fully defined, no definitive conclusion can be drawn about the contribution of H2A.Z or SWR1 to resection from these data alone. Nevertheless, the detection of residual DNA loss indicates that these factors are unlikely to be strictly essential for resection.

Strains with comparable cutting efficiencies are therefore most informative. Both the *pGal-AsiSI arp8Δ and pGal-AsiSI arp8Δ swr1Δ htz1Δ* strains showed DNA coverage profiles around DSB sites similar to the control (Figure 7), indicating that the INO80 complex does not play a major role in DSB resection. Furthermore, these data suggest that the combined

nucleosome remodelling activities of the INO80 and SWR1 complexes are largely dispensable for this process.

To assess how strongly nucleosome editing mutants respond to AsiSI-induced DNA damage, we analysed Rad53 phosphorylation by western blotting. The induction of DSBs is recognised as DNA damage by so-called apical kinases. In yeast, Tel1 detects DSBs through interaction with the MRX complex, whereas Mec1 senses RPA-coated ssDNA (Deshpande et al. 2017; Zou and Elledge 2003). During HR, resection generates extensive ssDNA and Mec1-dependent signalling becomes dominant (Sanchez et al. 1996). Apical kinases initiate a signalling cascade that phosphorylates mediator proteins and effector kinases. Rad53 is a central yeast effector kinase, and its phosphorylation can be detected by an upshift in western blotting. Rad53 phosphorylation is widely used as a readout for DNA damage response activation and correlates to the amount of ssDNA generated (Bantele et al. 2019; Branzei and Foiani 2006; Lopez-Mosqueda et al. 2010).

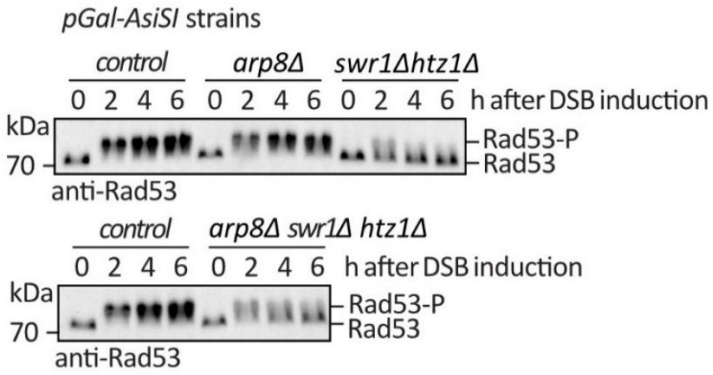


Figure 10: Reduced Rad53 activation after AsiSI-induced DSB formation in the *pGal-AsiSI swr1Δ htz1Δ* mutant.
Western blots detecting phosphorylated forms of Rad53 visible by gel shift are shown for *pGal-AsiSI, pGal-AsiSI arp8Δ, pGal-AsiSI swr1Δ htz1Δ* and *pGal-AsiSI arp8Δ swr1Δ htz1Δ* at the indicated timepoints after DSB induction. Data is representative of n = 2 biological replicates.

The *pGal-AsiSI* control strain and the *pGal-AsiSI arp8Δ* strain show a complete Rad53 upshift by 2 h after induction (Figure 10). In contrast, the *pGal-AsiSI swr1Δ htz1Δ* strain does not shift up fully even after 6 h. The *pGal-AsiSI arp8Δ swr1Δ htz1Δ* strain shows a slightly reduced upshift compared to the *pGal-AsiSI* control strain (Figure 10).

These findings are consistent with the previous observations showing lower levels of Rad53 activation in *htz1Δ* strains after HO-induced DSB formation (Kalocsay et al. 2009). Cutting efficiency was measured via qPCR in their system and lower efficiencies were detected for the *htz1Δ* strain. Therefore, the reduced Rad53 upshift observed here in the pGal-AsiSI swr1Δ htz1Δ strain is likely at least partly explained by reduced AsiSI cutting efficiency (Figure 9). Overall, the data indicate that impaired INO80 function has no or only a minor effect on DSB resection, whereas phenotypes in *HTZ1* deficient strains require cautious interpretation because DSB induction is strongly reduced.

We next asked why cutting efficiency was reduced in the *pGal-AsiSI swr1Δ htz1Δ* mutant. Two non-exclusive explanations are possible. First, chromatin structure might reduce AsiSI accessibility to its recognition sites. Efficiently cut DSB sites correlate with low nucleosome occupancy and nucleosome-depleted sites show high cutting efficiency (Oberbeckmann et al. 2019; Peritore et al. 2021). H2A.Z containing nucleosomes may constitute a weaker barrier to AsiSI than canonical nucleosomes because of their reduced DNA-binding affinity (S. Li et al. 2023). Second, loss of H2A.Z could reduce expression of the galactose-inducible AsiSI construct, as H2A.Z is involved in transcriptional regulation (Halley et al. 2010; Papamichos-Chronakis et al. 2011).

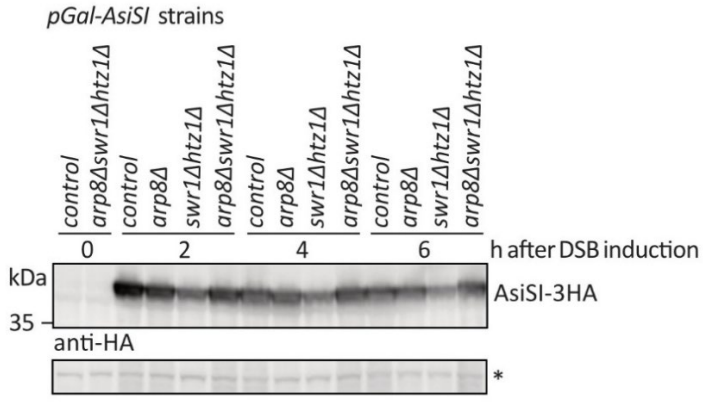


Figure 11: Reduced AsiSI expression in swr1Δ htz1Δ mutants.
Anti-HA western blot detecting levels of 3HA-tagged AsiSI in *pGal-AsiSI, pGal-AsiSI arp8Δ, pGal-AsiSI swr1Δ htz1Δ* and *pGal-AsiSI arp8Δ swr1Δ htz1Δ* at the indicated timepoints after galactose addition. The asterisk denotes a cross-reactive band. Data is representative of n = 2 biological replicates.

To test this second hypothesis and show whether AsiSI expression differs between the mutants, we performed anti-HA western blotting, as AsiSI carries a 3HA-tag. AsiSI was conditionally induced after galactose addition, with no signal detected at the 0 h timepoints (Figure 11). In the control strain, AsiSI expression reached maximal levels by 2 h and AsiSI expression was similar in the *pGal-AsiSI arp8Δ* and the *pGal-AsiSI arp8Δ swr1Δ htz1Δ* strain. In contrast, AsiSI expression appeared strongly reduced in the *pGal-AsiSI swr1Δ htz1Δ* strain. To analyse this reduced AsiSI expression more precisely, semiquantitative analysis of western blots including a 3-fold dilution series was performed (Figure 12).

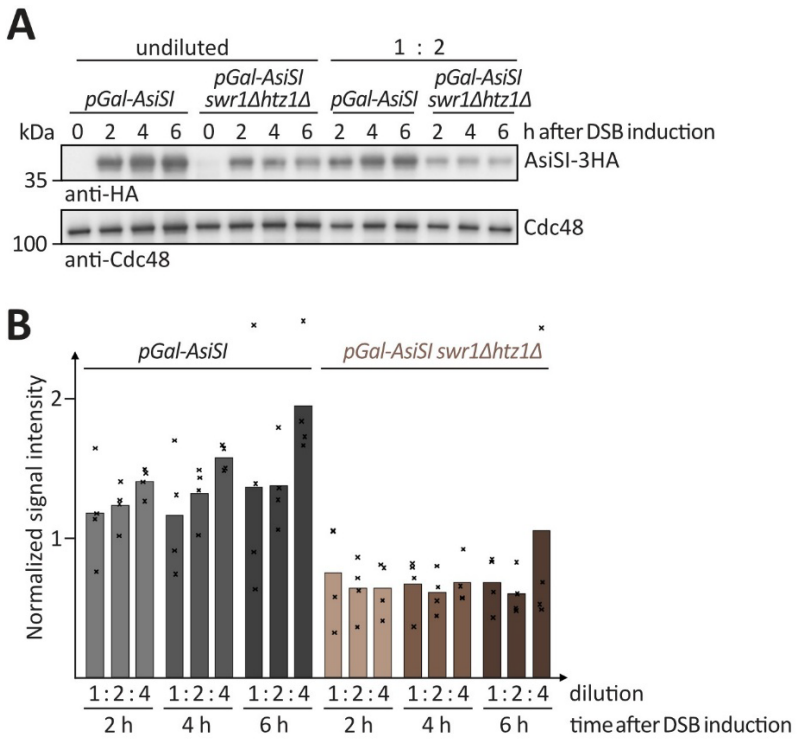


Figure 12: Semiquantitative analysis of reduced AsiSI expression in swr1Δ htz1Δ mutants.
(A) AsiSI-3HA expression in *swr1Δ htz1Δ* mutant samples compared to the *pGal-AsiSI* control strain with dilutions: Anti-HA western blot detecting levels of 3HA-tagged AsiSI after the indicated timepoints. The anti-Cdc48 western blot serves as loading control. Data is representative of n = 4 biological replicates.
(B) Semiquantitative analysis of western blot dilution series of (A) show reduced AsiSI expression in the *swr1Δ htz1Δ* mutant strain: Mean signal intensities of 3HA-tagged AsiSI expression normalised by the corresponding signal intensity of the Cdc48 loading control from 4 biological replicates are shown for a 3-fold 1:2 dilution series for *pGal-AsiSI* and *pGal-AsiSI swr1Δ htz1Δ* after the indicated timepoints.

Semiquantitative calculation of the relative signal reduction of the *pGal-AsiSI swr1Δ htz1Δ* mutant compared to the *pGal-AsiSI* control strain requires western blotting of multiple dilutions. Protein overloading can cause gel artefacts, which prevent quantification of the signal intensity. Therefore, signal intensities for AsiSI-3HA of diluted western blot samples of

four independent replicates were determined. Normalisation to the Cdc48 loading control resulted in similar signal intensities between the dilutions and timepoints (Figure 12B). On average, AsiSI expression was 50 % ± 30 % lower in the *pGal-AsiSI swr1Δ htz1Δ* strain compared to the *pGal-AsiSI* control strain. These results suggest that reduced AsiSI expression after H2A.Z loss might be at least one factor contributing to the reduced cutting efficiency. They also highlight that galactose-inducible restriction enzyme systems should be used cautiously in *HTZ1* mutant backgrounds. Besides, additional effects on restriction enzyme accessibility to chromatin may also contribute.

Reduced DSB induction efficiency may also occur in other nucleosome remodeller mutants if chromatin structure or inducible gene expression is altered. Importantly, SWI/SNF contributes to the transcription of inducible genes, including GAL10 (Peterson and Herskowitz 1992) and reduced HO cutting efficiency in *snf5Δ* cells has been attributed to reduced HO expression (Wiest et al. 2017). In previous work, strand-specific sequencing showed that SWI/SNF and RSC are essential for DSB resection, but cutting efficiency in the *pGal-AsiSI sth1-3aid* snf2-3aid** had not been measured (Peritore et al. 2021). We therefore applied our nanopore-based cutting efficiency assay to this mutant and compared it with the pGal-AsiSI control strain.

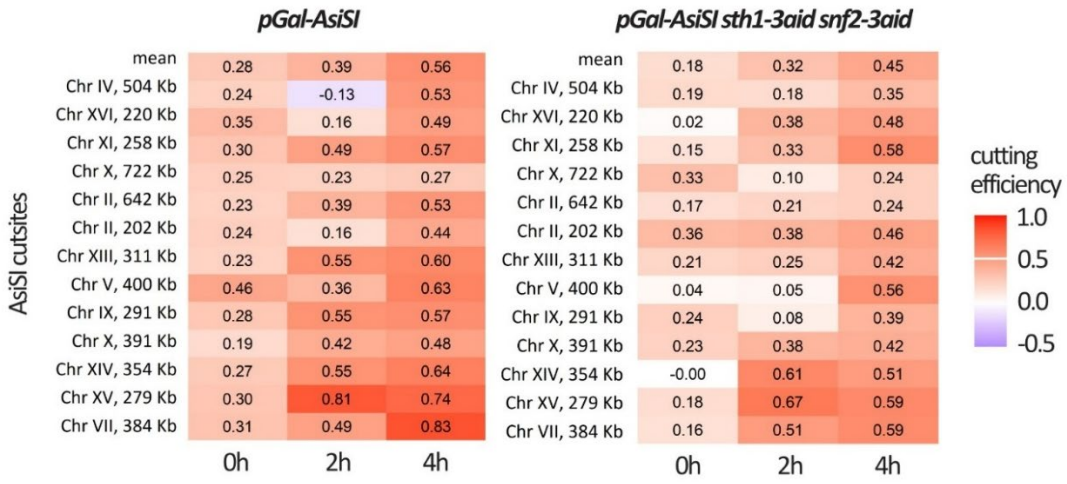


Figure 13: Nucleosome eviction deficiency does not affect AsiSI cutting efficiency.
Nanopore sequencing was performed for *pGal-AsiSI* and *pGal-AsiSI sth1-3aid* snf2-3aid** at the indicated timepoints after DSB induction. Cutting efficiencies of the top 13 AsiSI cut sites (Peritore et al. 2021) were determined from coverage of the 2 bp AsiSI cut site and averaged. Data is representative of n = 1 biological replicate.

Nanopore sequencing showed no remarkable difference in cutting efficiency between the *pGal-AsiSI* control strain and the *pGal-AsiSI sth1-3aid* snf2-3aid** strain (Figure 13). Although this experiment was performed once, efficient DSB induction across multiple AsiSI sites in the mutant indicates that impaired nucleosome eviction does not substantially affect DSB induction by galactose-induced AsiSI expression. The data supports the interpretation of the previously published strand-specific sequencing results showing that nucleosome eviction by SWI/SNF and RSC is essential for resection (Peritore et al. 2021).

Taken together, the data suggests that nucleosome editing has no or only a minor contribution to resection. The nanopore-based workflow established here allows cutting efficiency to be quantified in parallel with strand-specific sequencing. This analysis revealed that *HTZ1* mutant strains are challenging in restriction enzyme-based DSB induction systems because reduced galactose-inducible AsiSI expression leads to reduced cutting efficiency. In contrast, INO80, SWI/SNF and RSC remodeller mutants showed sufficient AsiSI cutting efficiency, supporting the conclusion that nucleosome eviction, but not nucleosome editing, is essential for resection.

Summary:

- A nanopore-based workflow was used to quantify cutting efficiency in parallel to strand-specific sequencing.
- Strand-specific sequencing revealed no major involvement of the INO80 complex in DSB resection.
- Strand-specific sequencing data for SWR1 and H2A.Z remains inconclusive because H2A.Z-deficient mutants showed markedly reduced AsiSI cutting efficiency; however, an essential role in resection is unlikely.
- Analysis of H2A.Z mutant strains requires particular caution in galactose-inducible restriction enzyme systems as AsiSI expression and cutting efficiency are reduced.
- INO80, SWI/SNF and RSC remodeller mutants showed sufficient AsiSI cutting efficiency.

3.2 The telomeric long-range resection machinery involves canonical DSB enzymes

In addition to the restriction enzyme induced DSB system, the *cdc13-1* system, which allows for conditional telomere deprotection, can serve as a model to study the DNA damage response elsewhere in the genome (Dewar and Lydall 2012). In order to be a good model to investigate long-range resection, the mechanisms must be similar at deprotected telomeres and genomic DSBs. Chromosome ends structurally resemble one end of a DSB (Dewar and Lydall 2012). To prevent recognition by the DNA repair machinery, telomeres are protected by specialised proteins. In yeast, Rap1 binds specifically to repetitive telomeric dsDNA motifs (De Lange 2009; Longtine et al. 1989; Lustig et al. 1990; Pardo and Marcand 2005). The telomeric 3' ssDNA overhang is protected by the CST complex (Cdc13-Stn1-Ten1). Temperature shift of *cdc13-1* mutants induces telomere deprotection of the ssDNA, because Cdc13 is misfolded and the CST complex does not assemble (Mason et al. 2013; Garvik et al. 1995). However, Rap1 proteins remain on the telomeric dsDNA and could affect long-range resection at telomeres compared to genomic DSBs. Besides, also other telomere specific features could affect resection. Therefore, we first asked whether the same enzymes are involved in long-range resection at deprotected telomeres and at DSBs.

3.2.1 Exo1 deletion rescues lethality of telomere deprotection

At DSBs, long-range resection is carried out by two major pathways. The DNA gets processed either by the nuclease Exo1 or by Dna2 working in conjunction with the helicase Sgs1 (Mimitou and Symington 2008; Z. Zhu et al. 2008). For long-range resection after telomere deprotection, Exo1 has been described as main nuclease and in the absence of Rad9 a contribution of Sgs1 was observed (Ngo and Lydall 2010).

Growth assays of *cdc13-1* mutants using a temperature gradient provide an indirect measure of resection after telomere deprotection. At restrictive temperatures (≥ 26 °C) telomeres become deprotected and are processed by the DNA repair machinery resulting in a growth defect. Deletion of factors required for DNA resection can partially rescue this growth defect. The analysis of a temperature gradient allows for discrimination between growth phenotypes, as at 26 °C the deprotection is minor, whereas increasing the temperature up to 30 °C leads to more effective deprotection.

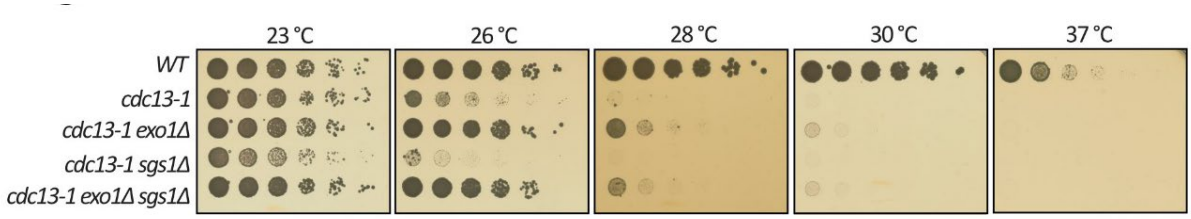


Figure 14: *EXO1* deletion rescues the *cdc13-1* growth defect at non-permissive temperatures.
Five-fold serial dilutions of *WT, cdc13-1, cdc13-1 exo1Δ, cdc13-1 sgs1Δ* and *cdc13-1 exo1Δ sgs1Δ* were spotted on YPD plates and incubated for 48 h at indicated temperatures. Data is representative of n = 2–4 biological replicates.

The *cdc13*-1 mutant showed reduced growth at elevated temperatures, whereas *WT* cells grew optimally up to 30 °C (Figure 14). Introduction of an EXO1 deletion in the *cdc13-1* mutant fully rescued the growth defect at 26 °C and partially at 28 °C, consistent with previous findings (Ngo and Lydall 2010). In contrast, deletion of the *SGS1* gene led to an additional growth defect at 23 °C and 26 °C, indicating a function of Sgs1 independent of DNA resection. This is consistent with the literature suggesting that Sgs1/BLM is involved in telomere maintenance in yeast (Ngo and Lydall 2010; Zubko et al. 2004) and mammalian cells (Crabbe et al. 2004; J. Y. Lee et al. 2007). Deletion of *SGS1* in the *cdc13-1 exo1Δ* strain did not substantially alter its growth. Interestingly, a growth rescue was observed upon *SGS1* deletion in the absence of Rad9 (Ngo and Lydall 2010). Therefore, Sgs1 might have a dual function. On the one hand, Sgs1 might protect telomeres from recognition by the DNA damage response. On the other hand, it might contribute to resection as part of the DNA repair machinery potentially working in conjunction with Dna2.

Next, we analysed Rad53 phosphorylation as an indirect readout for ssDNA accumulation after telomere deprotection. The presence of ssDNA activates the DNA damage response, leading to Rad53 phosphorylation. Thereby, the amount of phosphorylated Rad53 correlates with the amount of ssDNA generated (Bantele et al. 2019; Lopez-Mosqueda et al. 2010).

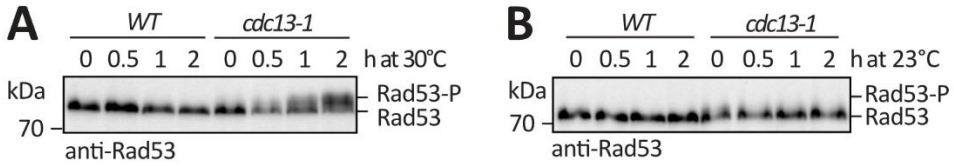


Figure 15: Telomere deprotection in *cdc13-1* mutants induces phosphorylation of Rad53.
(A) Rad53 activation after telomere deprotection in *cdc13-1* mutants: Western blots detecting phosphorylated forms of Rad53 visible by gel shift show increasing levels of phosphorylated Rad53 after temperature shift to 30 °C of the *cdc13-1* mutant, but not of *WT*. Data is representative of n = 1 biological replicate.
(B) No Rad53 activation without telomere deprotection: Western blots detecting phosphorylated forms of Rad53 visible by gel shift show no phosphorylated Rad53 for *cdc13-1* and *WT* incubated at 23 °C. Data is representative of n = 1 biological replicate.

First, we verified that the Rad53 upshift is specific for the *cdc13-1* mutation (Figure 15A) and depends on temperature shift (Figure 15B). We then compared the upshifts of *cdc13-1 exo1Δ, cdc13-1 sgs1Δ* and *cdc13-1 exo1Δ sgs1Δ* to the *cdc13-1* control strain 0.5 h, 1 h and 2 h after temperature shift to 30 °C (Figure 16A). No remarkable difference between the *cdc13-1* control strain and the *cdc13-1 sgs1Δ* strain was observed. In contrast, deletion of *EXO1* lead to a delay in Rad53 phosphorylation, which was more pronounced in the *cdc13-1 exo1Δ sgs1Δ* strain. This effect may indicate a role for Sgs1 in resection after telomere deprotection particularly in the absence of Exo1. The observed Rad53 phenotypes are consistent with previous results (Ngo and Lydall 2010).

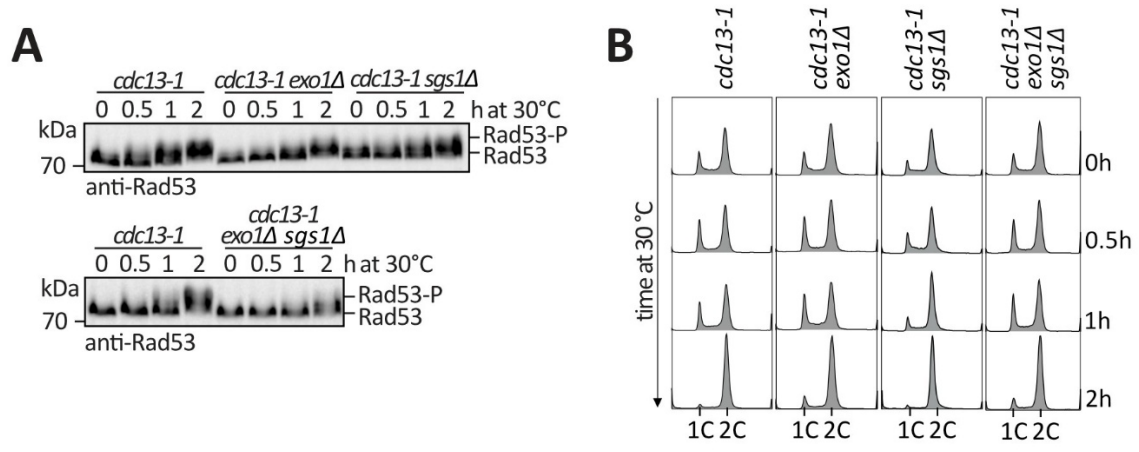


Figure 16: *Cdc13*-1 mutants show Rad53 activation and G2/M cell cycle arrest after telomere deprotection.
(A) Rad53 activation after telomere deprotection in *cdc13-1* mutants**:** Western blots detecting phosphorylated forms of Rad53 visible by gel shift show increasing levels of phosphorylated Rad53 after temperature shift to 30 °C of *cdc13-1, cdc13-1 exo1Δ, cdc13-1 sgs1Δ* and *cdc13-1 exo1Δ sgs1Δ*. Data is representative of n = 2–4 biological replicates.
(B) G2/M cell cycle arrest after telomere deprotection in *cdc13-1* mutants: *Cdc13-1, cdc13-1 exo1Δ, cdc13-1 sgs1Δ* and *cdc13-1 exo1Δ sgs1Δ* mutant strains were grown at 23°C, temperature shifted to 30 °C and samples taken at indicated timepoints. Total DNA content was measured by flow cytometry after SYTOX green staining. Data is representative of n = 2–4 biological replicates.

Activation of the DNA damage response is expected to arrest cell cycle progression (Finn et al. 2012; Gardner 1999; Harrison and Haber 2006). Consistently, we observed an almost complete G2/M arrest of all cdc13-1 strains after 2 h (Figure 16B). The strain containing a deletion of *EXO1* and the *cdc13-1 exo1Δ sgs1Δ* mutant retained a larger portion of cells in G1, indicating a delayed checkpoint-mediated cell cycle arrest and was consistent with the reduction in Rad53 phosphorylation (Figure 16A). In contrast, deletion of *SGS1* did not delay cell cycle arrest (Figure 16B), which is consistent with no change in Rad53 phosphorylation (Figure 16A).

To directly measure the amount of ssDNA generated after telomere deprotection, we used quantitative analysis of ssDNA (QAOS). The qPCR-based method specifically quantifies ssDNA at defined loci. In a first reaction at low temperature tagging primers specifically bind at a locus of interest if the DNA is single-stranded. After extension of the tagging primer, this ssDNA-dependent tagged molecule is quantified by qPCR (Booth 2001).



Figure 17: Loci used for QAOS analysis.
Distances from the right arm of chromosome V are indicated for the *PAC2*, *PDA1, YER186C* and *Y´5000* locus. PAC2 was used as an internal normalisation control.

We selected three loci (*PDA1, YER186C* and *Y´5000*) located 29.7, 14.5 and 5 kb from the right end of chromosome V for analysis (Figure 17). Importantly, all loci are outside of the telomeric region and only the *Y´5000* locus is sub-telomeric, whereas the other loci represent genomic DNA. Thus, the QAOS assay measures long-range resection at telomeres, but gives no information about short-range resection within the telomeric region. The internal *PAC2* gene was used for normalisation of input DNA.

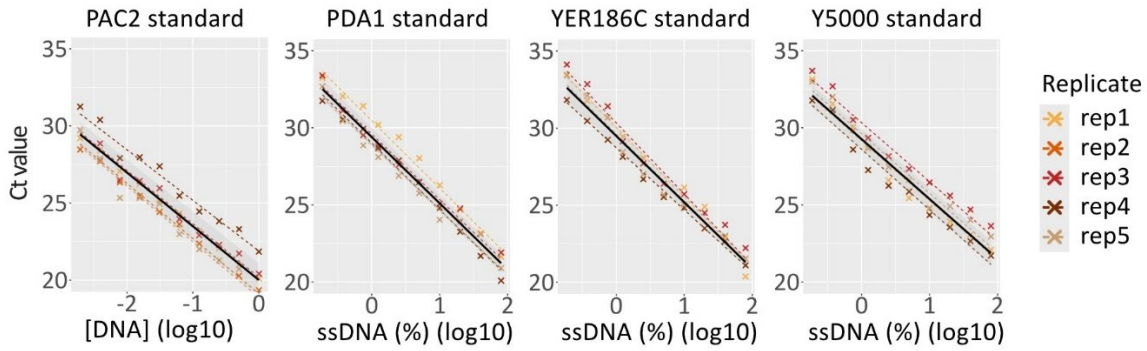


Figure 18: *PAC2* DNA dilution series and ssDNA/dsDNA standard curves for *PDA1, YER186C* and *Y´5000*.
Genomic DNA of *cdc13-1* cells grown at 23 °C was used in a 10-fold dilution series for QAOS of the PAC2 control locus. For Y´5000, YER186C and PDA1 loci, qPCR efficiency was measured by ssDNA/dsDNA standard curves generated from defined ratios of boiled and unboiled DNA. Standard curves were used for translation of the measured CT values into corresponding ssDNA percentages. Five replicates were used to calculate linear regression lines (black).

For normalisation of deviations in input DNA used for the individual QAOS samples, a DNA dilution series was generated for the internal *PAC2* locus (Figure 18). A regression line from five replicates was calculated and used for correction. For the *Y´5000, YER186C* and *PDA1* loci, qPCR efficiency was measured by ssDNA/dsDNA standard curves (Figure 18). The regression lines enabled translation of the measured Ct values into corresponding ssDNA percentages.

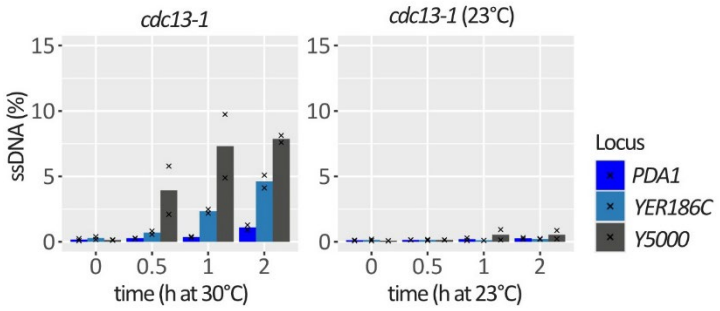


Figure 19: Quantitative amplification of ssDNA (QAOS) detects ssDNA generation at deprotected telomeres of Chr V.
One c*dc13-1* culture was shifted to 30 °C, whereas the second culture was kept at 23 °C. Samples were harvested at the indicated timepoints and ssDNA accumulation was measured at *Y´5000, YER186C* and *PDA1* loci. Data is representative of n = 2 biological replicates.

First, we validated QAOS by comparing ssDNA levels in *cdc13-1* cells growing at 23 °C to *cdc13-1* cells after temperature shift to 30 °C inducing telomere deprotection. Whereas the *cdc13-1* strain showed no ssDNA generation when incubated at 23 °C, ssDNA was generated at all loci reaching maximal levels of approximately 10 % after temperature shift to 30 °C (Figure 19). In previous studies similar ssDNA percentages were observed via QAOS after temperature shift to 36 °C (Booth 2001; Ngo and Lydall 2010; Zubko et al. 2004).

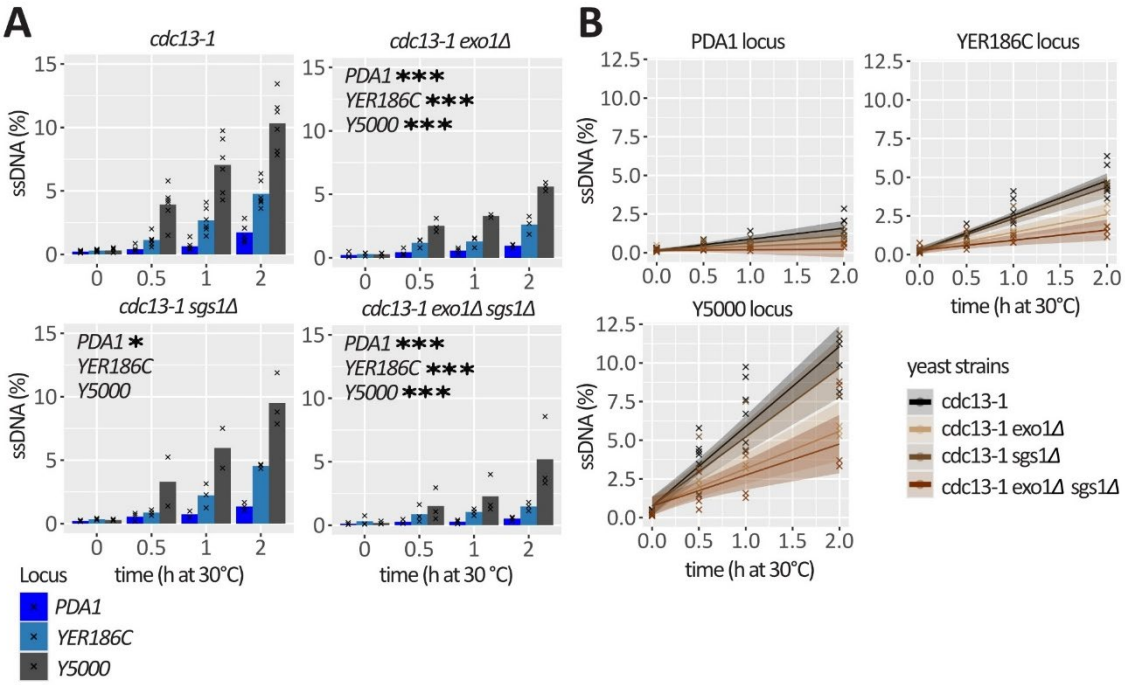


Figure 20: Exo1 is the main nuclease responsible for resection after telomere deprotection.
(A) Resection of deprotected telomeres of Chr V was measured by quantitative amplification of ssDNA (QAOS): Yeast cultures of *cdc13-1, cdc13-1 exo1Δ, cdc13-1 sgs1Δ* and *cdc13-1 exo1Δ sgs1Δ* were shifted to 30 °C and harvested at the indicated timepoints. Accumulation of ssDNA was measured at *Y´5000, YER186C* and *PDA1* loci. Data is representative of n = 3-6 biological replicates. 6 biological replicates of the *cdc13-1* control strain have been pooled and are identical to those shown in Figure 25. Statistical significance of differences in ssDNA accumulation compared to the *cdc13-1* control strain was calculated using a linear mixed-effects model.
(B) Linear mixed-effects model of QAOS experiment shown in (A): Statistical significance of the difference in ssDNA generation with time after temperature shift to 30 °C was calculated for *cdc13-1 exo1Δ, cdc13-1 sgs1Δ and cdc13-1 exo1Δ sgs1Δ* and compared to the *cdc13*-1 control strain. Slope values are given in Supplementary Table 1.

After validation of the QAOS method, we measured ssDNA amounts in *cdc13-1 exo1Δ, cdc13-1 sgs1Δ* and *cdc13-1 exo1Δ sgs1Δ* mutants compared to the *cdc13-1* control strain 0.5 h, 1 h and 2 h after temperature shift to 30 °C (Figure 20A). To test for significant differences in ssDNA accumulation a linear mixed-effects model was used (Figure 20B). We defined the different timepoints and yeast strains as fixed effects in the model and analysed the variations between biological replicates as random effects. Slope values describing the ssDNA increase over time were calculated for the individual samples and statistical analysis of the mean slope values for each mutant was performed by comparison to the *cdc13-1* control strain.
Significantly reduced ssDNA generation was detected in the *cdc13-1 exo1Δ* mutant, whereas the *cdc13-1 sgs1Δ* strain showed no significant difference to the *cdc13-1* control strain (Figure 20). Previous studies investigated the same mutants, but performed a temperature shift to 36 °C and not to 30 °C. Using this higher temperature, they could measure significantly

reduced ssDNA accumulation not only for the *cdc13-1 exo1Δ* mutant, but at some loci also for the *cdc13-1 sgs1Δ* strain (Ngo and Lydall 2010).

The *cdc13-1 exo1Δ sgs1Δ* strain showed highly reduced ssDNA levels that were even lower than in the *cdc13-1 exo1Δ* strain. To test for a significant difference, a second linear mixed-effects model directly compared the *cdc13-1 exo1Δ sgs1Δ* mutant to the *cdc13-1 exo1Δ* strain and the *cdc13-1 sgs1Δ* strain (Figure 21).

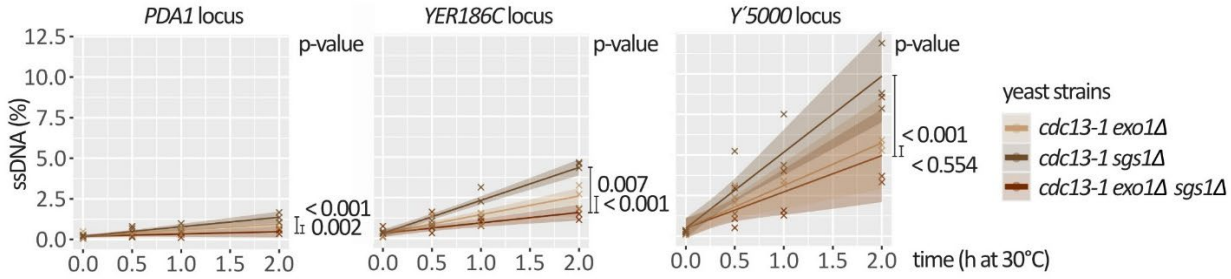


Figure 21: Additional deletion of Sgs1 further reduces ssDNA generation compared to the *cdc13-1 exo1Δ* strain.
Linear mixed-effects model of QAOS experiment shown in Figure 20: Statistical significance of the difference in ssDNA generation with time after temperature shift to 30 °C was calculated for *cdc13-1 exo1Δ sgs1Δ* and compared to the *cdc13-1 exo1Δ* and *cdc13-1 sgs1Δ* strain. The p-values indicate significant differences between the mutant strains. Slope values are given in Supplementary Table 1.

As expected, there is a clear difference between the *cdc13-1 exo1Δ sgs1Δ* mutant and the *cdc13-1 sgs1Δ* strain, which showed only slightly reduced ssDNA compared to the *cdc13-1* control strain. More interestingly, the difference between the *cdc13-1 exo1Δ sgs1Δ* mutant and the *cdc13-1 exo1Δ* strain is significant for all loci, but the *Y´5000* locus. The additional reduction in ssDNA generation in the *cdc13-1 exo1Δ sgs1Δ* mutant compared to the *cdc13-1 exo1Δ* strain indicates a role for Sgs1 in resection after telomere deprotection in particular in the absence of Exo1.

Taken together, the growth assays showed a rescue effect and Rad53 phosphorylation and cell cycle arrest were delayed when factors involved in resection were absent. Besides these indirect measurements for ssDNA generation, which triggers checkpoint activation, QAOS was performed to directly measure the amount of ssDNA generated in the resection mutants. The *cdc13-1 exo1Δ* mutant showed approximately 50 % reduced ssDNA accumulation, as well as delayed cell cycle arrest and Rad53 phosphorylation. In contrast, deletion of *SGS1* did not

significantly reduce the ssDNA generation. However, ssDNA was further reduced in the *cdc13-1 exo1Δ sgs1Δ* mutant compared to the *cdc13-1 exo1Δ* mutant and also the Rad53 response appeared to be further reduced. Previous studies observed a growth phenotype of a Rad9 deleted *cdc13-1 sgs1Δ* mutant and measured significant reduction in ssDNA accumulation in a *cdc13-1 sgs1Δ* strain when shifting the cultures to 36 °C suggesting that Sgs1 is involved in resection after telomere deprotection (Ngo and Lydall 2010). Based on these findings we speculate that Sgs1 is involved in a backup pathway in the absence of Exo1 working in conjunction with Dna2 like at DSBs (Mimitou and Symington 2008; Z. Zhu et al. 2008).

Summary:

- Growth assays, Rad53 phosphorylation, cell cycle analysis and QAOS measurements indicate that Exo1 is the major contributor to resection after telomere deprotection.
- Whereas the *cdc13-1 sgs1Δ* mutant showed no significant phenotypes in the context of resection after telomere deprotection, Sgs1 may become relevant in the absence of Exo1.
- Comparing long-range resection at telomeres to the resection machinery working at canonical DSBs, Dna2 appears to be a candidate working in conjunction with Sgs1.

3.2.2 Dna2 contributes to resection after telomere deprotection particularly in the absence of Exo1

The contribution of Exo1 and Sgs1 to resection after telomere deprotection has already been investigated (Ngo and Lydall 2010; Zubko et al. 2004), but the involvement of Dna2 remains unclear, so far. In analogy to resection at canonical DSBs, Dna2 might depend on Sgs1-mediated DNA unwinding to generate a suitable substrate (Cejka and Symington 2021; Nimonkar et al. 2011; Z. Zhu et al. 2008).

Whereas *EXO1* and *SGS1* are not essential, the deletion of *DNA2* leads to cell death due to its additional role in DNA replication. During lagging-strand synthesis, long 5' single-stranded flap structures are processed by Dna2 to avoid accumulation of toxic DNA intermediates and replication stress (Budd and Campbell 1997; Kao et al. 2004).

To test the role of Dna2 in resection of deprotected telomeres, we used an auxin-induced degradation system. In particular, we tagged Dna2 with a miniIAA7-tag and constitutively expressed *OsTIR1* (Sepers et al. 2022). The fusion of the mIAA7-tag to the protein of interest serves as a recognition motif for the plant-derived F-box protein OsTIR1. Upon addition of the synthetic auxin indole-3-acetic acid (IAA), OsTir1 binds the mIAA7 degron in an auxin-dependent manner and recruits the SCF ubiquitin ligase complex resulting in polyubiquitination of the tagged protein and subsequent proteasomal degradation (Phanindhar and Mishra 2023; Hubbe et al. 2026).

We generated three *cdc13-1* strains expressing mIAA7-tagged Dna2 and *OsTIR1* constitutively. One strain contained only mIAA7-tagged Dna2 for conditional depletion, whereas the other strains additionally carried *SGS1* or *EXO1* deletions.

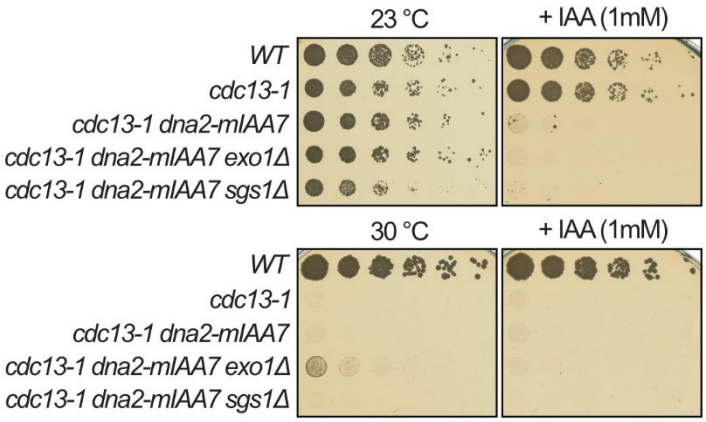


Figure 22: Growth defects of *dna2-mIAA7* strains on YPD plates supplemented with IAA indicate successful degradation. Five-fold serial dilutions of *WT, cdc13-1, cdc13-1 dna2-mIAA7, cdc13-1 dna2-mIAA7 exo1Δ* and *cdc13-1 dna2-mIAA7 sgs1Δ* were spotted on YPD and YPD + IAA (1 mM) plates and incubated for 48 h at indicated temperatures. Data is representative of n = 2-4 biological replicates.

As *DNA2* is essential, induction of widespread Dna2 degradation is expected to cause loss of viability. Growth assays showed that all mutants carrying mIAA7-tagged Dna2 die on YPD plates supplemented with auxin (Figure 22). In contrast, in the absence of auxin the *cdc13-1 dna2-mIAA7* and *cdc13-1 dna2-mIAA7 exo1Δ* strains grow similarly to the *cdc13-1* control strain at 23 °C verifying that the depletion of Dna2 is conditional. The *cdc13-1 dna2-mIAA7 sgs1Δ* strain shows a mild growth defect at 23 °C, which is consistent with the literature (Ngo and Lydall 2010; Zubko et al. 2004). At 30 °C all *cdc13-1* mutants die due to telomere deprotection and only *WT* cells can grow. Together, the observed phenotypes confirm conditional depletion of Dna2 upon auxin treatment in the *cdc13-1* background.

Furthermore, we analysed Dna2 degradation at the protein level. The mIAA7 degron was followed by a 3Flag tag, so Dna2 protein levels could be monitored by anti-Flag western blotting.

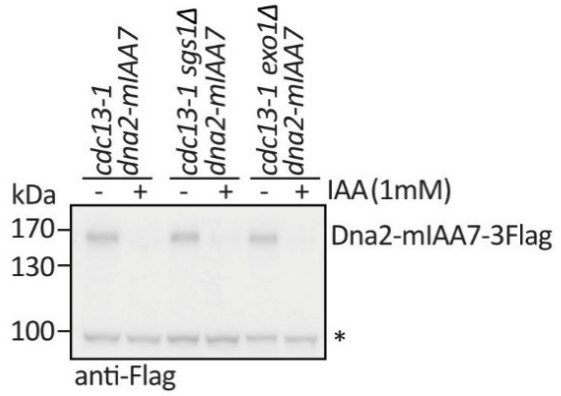


Figure 23: Dna2-mIAA7 is degraded after addition of auxin.
Anti-Flag western blot detecting levels of Dna2-mIAA7-3Flag in *cdc13-1 dna2-mIAA7, cdc13-1 dna2-mIAA7 exo1Δ* and *cdc13-1 dna2-mIAA7 sgs1Δ* strains before and after 1 h of IAA treatment (final concentration 1 mM). Asterisk denotes a cross-reactive band. Data is representative of n = 1 biological replicate.

Anti-Flag western blotting shows disappearance of the Dna2-mIAA7-3Flag band after 1 h of auxin treatment in all three generated strains (Figure 23), suggesting efficient Dna2 degradation. Thus, mIAA7-tagged strains were treated with auxin for 1 h before the start of subsequent experiments.

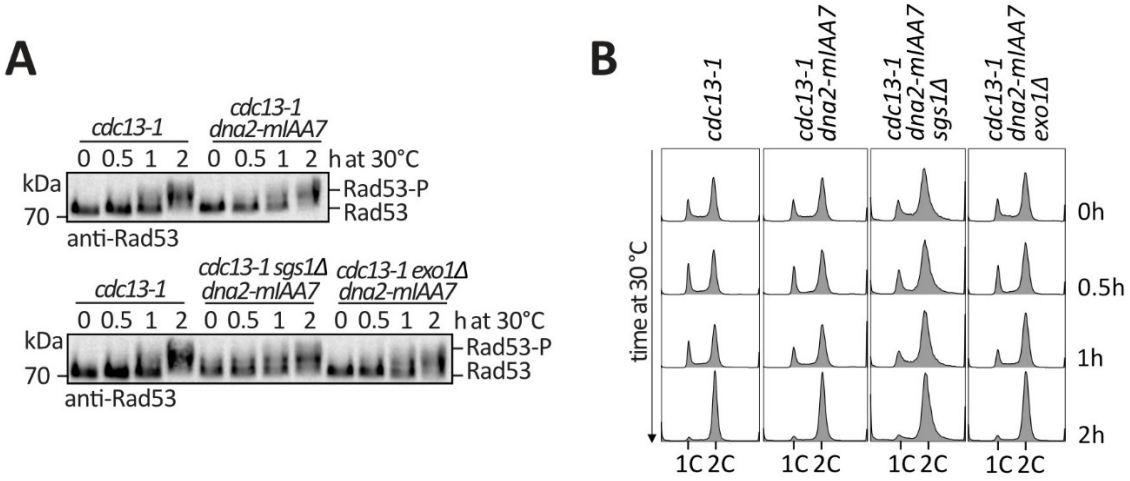


Figure 24: **Depletion of Dna2 does not strongly impair Rad53 activation or G2/M cell cycle arrest in c*dc13*-1 mutants.**
(A) Rad53 activation after telomere deprotection in *cdc13-1* mutants**:** Western blots detecting phosphorylated forms of Rad53 visible by gel shift show increasing levels of phosphorylated Rad53 after 1 h of auxin treatment followed by temperature shift to 30 °C of *cdc13-1, cdc13-1 dna2-mIAA7, cdc13-1 sgs1Δ dna2-mIAA7 and cdc13-1 exo1Δ dna2-mIAA7*. Data is representative of n = 2–3 biological replicates.
(B) G2/M cell cycle arrest after telomere deprotection in *cdc13-1* mutants: *Cdc13-1, cdc13-1 dna2-mIAA7, cdc13-1 sgs1Δ dna2-mIAA7 and cdc13-1 exo1Δ dna2-mIAA7* mutant strains were grown at 23 °C and after 1 h of auxin treatment followed by temperature shift to 30 °C samples were taken at the indicated timepoints. Total DNA content was measured by flow cytometry after SYTOX green staining. Data is representative of n = 2 biological replicates.

After we verified conditional Dna2 degradation phenotypically and at the protein level, we aimed to elucidate the function of Dna2 in resection after telomere deprotection. As the level of Rad53 phosphorylation correlates with the amount of ssDNA (Bantele et al. 2019; Lopez-Mosqueda et al. 2010), we performed a Rad53 upshift assay of the generated *cdc13-1 dna2-mIAA7* strains. We depleted Dna2 with auxin for 1 h before shifting the cultures to 30 °C to induce telomere deprotection. Samples were collected over a 2 h time course after temperature shift.

The *cdc13-1* control strain showed high Rad53 phosphorylation within 2 h after temperature shift (Figure 24A). In contrast, all *cdc13-1* strains harbouring the *dna2-mIAA7* mutation exhibit a slight Rad53 upshift already after 0.5 h, whereas no such early activation is observed in the control strain. The *cdc13-1 dna2-mIAA7 sgs1Δ* mutant displays a weak Rad53 phosphorylation signal at 0 h. However, this was likely a loading artefact, as it was not reproducible in a second replicate.

Despite earlier onset of Rad53 phosphorylation in the Dna2-depleted strains, the overall Rad53 phosphorylation after 2 h is lower compared to the control. Whereas the control strain shows complete Rad53 phosphorylation after 2 h, a fraction of Rad53 remains unphosphorylated in all Dna2 depleted mutants. The strains with an additional deletion of *SGS1* or *EXO1* show no major differences compared to the *cdc13-1 dna2-mIAA7* strain.

Reduced Rad53 phosphorylation after Dna2 depletion may have several explanations. Impaired resection could limit ssDNA generation and reduce checkpoint activation. Alternatively, Dna2 has been shown to be involved in checkpoint signalling during DNA replication. As a nuclease-helicase essential for Okazaki fragment processing, Dna2 functions during S phase to stimulate the Mec1 kinase and promote activation of the replication checkpoint (Kumar et al. 2020). Both hypotheses would explain the reduction in Rad53 phosphorylation in Dna2 depleted strains.

Activation of the checkpoint results in almost complete G2/M cell cycle arrest in *cdc13-1* strains 2 h after telomere deprotection (Figure 24B). A similar arrest phenotype was observed in all Dna2-depleted strains. This lack of an effect on cell cycle progression is consistent with the minor changes observed in Rad53 phosphorylation (Figure 24A). Notably, the *cdc13-1 dna2-mIAA7 exo1Δ* mutant did not display the delayed cell cycle arrest observed for the

cdc13-1 exo1Δ strain (Figure 16B), which may be explained by earlier Rad53 activation in Dna2-depleted cells.

Overall, Rad53 phosphorylation and cell cycle analysis showed minor or no effects associated with Dna2 depletion in contrast to Exo1 deletion. The data suggest that whereas Exo1 has a major contribution to checkpoint activation likely through ssDNA generation, Dna2 is less involved. Because Dna2 works in conjunction with Sgs1 at DSBs and the combined deletion of *SGS1* and *EXO1* resulted in a strong reduction of ssDNA formation after telomere deprotection (Figure 20), Dna2 might function in a backup pathway in the absence of Exo1. To test this hypothesis, QAOS was performed with the *cdc13-1* strains depleted of Dna2 to directly measure ssDNA accumulation at the right arm of chromosome V after deprotection as described above.

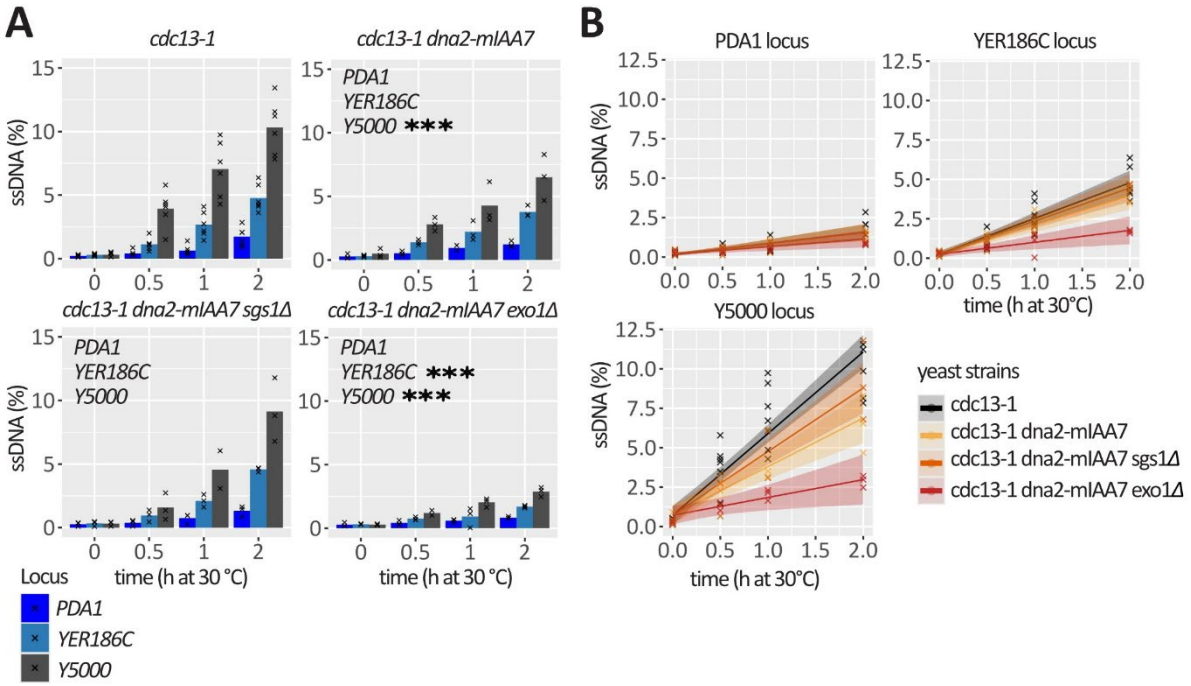


Figure 25: Dna2 is involved in a backup pathway for resection after telomere deprotection.
(A) Resection of deprotected telomeres of Chr V in mutants after auxin treatment was measured by quantitative amplification of ssDNA (QAOS): Yeast cultures of *cdc13-1, cdc13-1 dna2-mlAA7, cdc13-1 sgs1Δ dna2-mlAA7* and *cdc13-1 exo1Δ dna2-mlAA7* were shifted to 30 °C after 1 h of auxin treatment and harvested at indicated timepoints. Accumulation of ssDNA was measured at *Y´5000, YER186C* and *PDA1* loci. Data is representative of n = 3-6 biological replicates. 6 biological replicates of the *cdc13-1* control strain have been pooled and are identical to those shown in Figure 20. Statistical significance of differences in ssDNA accumulation compared to the *cdc13-1* control strain was calculated using a linear mixed-effects model. **(B)** Linear mixed-effects model of QAOS experiment shown in (A): Statistical significance of the difference in ssDNA generation with time after temperature shift to 30 °C was calculated for *cdc13-1 dna2-mlAA7, cdc13-1 dna2-mlAA7 sgs1Δ* and *cdc13-1 exo1Δ dna2-mlAA7* and compared to the *cdc13-1* control strain. Slope values are given in Supplementary Table 1.

The *cdc13-1 dna2-mIAA7* mutant showed decreased ssDNA generation compared to the control strain (Figure 25). However, whereas the *cdc13-1 exo1Δ* mutant generated significantly less ssDNA within the 2 h time course at all loci, the *cdc13-1 dna2-mIAA7* mutant showed significantly decreased ssDNA accumulation only at the *Y´5000* locus which is closest to the telomere end. The *cdc13-1 sgs1Δ dna2-mIAA7* showed non-significant reduction in ssDNA generation. In contrast, strongly reduced levels of ssDNA were measured in the *cdc13-1 exo1Δ dna2-mIAA7* mutant.

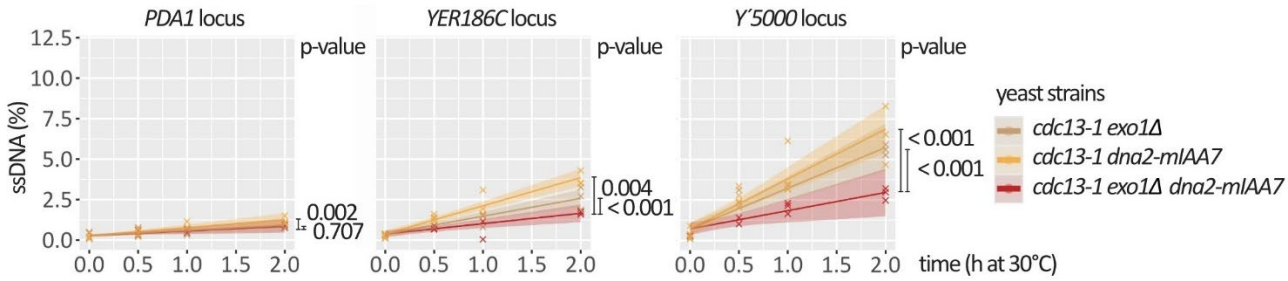


Figure 26: Dna2 seems to work in conjunction with Sgs1 but in a separate pathway from Exo1.
Linear mixed-effects model of QAOS experiment shown in Figure 25: Statistical significance of the difference in ssDNA generation with time after temperature shift to 30 °C was calculated for the *cdc13-1 exo1Δ dna2-mIAA7* strain and compared with the *cdc13-1 exo1Δ* and *cdc13-1 dna2-mIAA7* strain. The p-values indicate significant differences between the mutant strains. Slope values are given in Supplementary Table 1.

To compare the reduction in ssDNA generation between the *cdc13-1 exo1Δ dna2-mIAA7* mutant to the previously measured *cdc13-1 exo1Δ* strain, the mixed-effect model was applied to the *cdc13-1 exo1Δ dna2-mIAA7* mutant testing for significant differences to the *cdc13-1 exo1Δ* and *cdc13-1 dna2-mIAA7* strain. This direct comparison shows a significant reduction when both nucleases are absent compared to the deficiency of only one resection nuclease (Figure 26) suggesting that Exo1 and Dna2 process telomeric DNA through distinct pathways. In contrast to the additive effects upon loss of Exo1 and Dna2, the *cdc13-1 sgs1Δ dna2-mIAA7* mutant did not show significantly reduced ssDNA generation. Because the phenotype of the combined enzyme deficiencies was similar to the single deletions, we hypothesise that Dna2 works in conjunction with Sgs1. However, we can only speculate, as the effects were mostly not significant. In fact, the reduction of ssDNA generation in the *cdc13-1 sgs1Δ dna2-mIAA7* strain was minor compared to the *cdc13-1 dna2-mIAA7* mutant, which might be explained by epistasis and a second function of Sgs1.

Taken together, resection after telomere deprotection is carried out by the same nucleases as long-range resection at canonical DSBs. We found evidence that Dna2 contributes to resection after telomere deprotection in addition to Exo1. Whereas Exo1 is the dominant nuclease at telomeres, a second pathway most likely mediated by Dna2 together with Sgs1 gains importance in the absence of Exo1. These findings support the use of the *cdc13-1* system as a model to study DNA resection more broadly.

Summary:

- Efficient degradation of Dna2 after auxin treatment using the miniIAA7 system (Sepers et al. 2022) was confirmed at the protein level and by phenotypical analysis.
- Rad53 phosphorylation and cell cycle analysis did not reveal a strong phenotype associated with Dna2 depletion.
- Deficiency of both resection nucleases led to further reduction in ssDNA generation compared to the *cdc13-1 exo1Δ* mutant or the *cdc13-1 dna2-mIAA7* mutant. In contrast, the *cdc13-1 sgs1Δ dna2-mIAA7* mutant did not show significantly reduced ssDNA levels. Thus, we hypothesise that Exo1 works in a pathway separate from Dna2 and Sgs1.
- The parallels between long-range resection after telomere deprotection and DSB induction support that the *cdc13-1* system can serve as a model for DNA resection.

3.3 Nucleosome remodelling influences resection of unprotected telomeres

We found evidence that long-range resection after telomere deprotection is similar to DSBs. Therefore, the *cdc13-1* system could serve as an alternative to study long-range resection in a broader context, independent of DSB induction efficiencies. In the following we used the *cdc13-1* system to investigate how nucleosome remodelling influences long-range resection after telomere deprotection.

The question of how the nucleosome barrier is overcome *in vivo* was raised based on *in vitro* data, which showed that DNA fully occupied by nucleosomes is processed by neither Exo1 nor Dna2 together with Sgs1 (Adkins et al. 2013). The two resection nucleases differ in their activities: Whereas Exo1 degrades dsDNA in 5´ to 3´ direction, Dna2 can process DNA

independent of its directionality, but requires the helicase activity of Sgs1 for DNA unwinding (Nimonkar et al. 2011). *In vitro*, Exo1 activity was shown to be inhibited by nucleosomes, whereas Dna2 together with Sgs1 processed nucleosome-bound DNA, when a nucleosome-free region of approximately 300 bp was present (Adkins et al. 2013). However, such long nucleosome-free regions are uncommon *in* vivo suggesting that also Dna2 and Sgs1 require a mechanism to overcome the nucleosome barrier.

Nucleosome remodellers are likely candidates and we investigated nucleosome eviction and editing mutants in the *cdc13-1* background. We measured the differences in ssDNA accumulation via QAOS at three loci outside of the telomeric region. These regions, in particular the *YER186C* and *PDA1* loci resemble conventional chromatin. Solely the *Y´5000* locus might be influenced by its repetitive nature. Initial processing of deprotected telomeres might differ due to specialised telomeric features, but the chromatin environment affecting long-range resection is similar at deprotected telomeres and DSBs within the genome.

3.3.1 Resection after telomere deprotection depends on nucleosome eviction remodellers

We first asked whether nucleosome eviction is required for long-range resection after telomere deprotection. SWI/SNF and RSC have been implicated in DSB repair in multiple studies (Hughes et al. 2000; Kapoor et al. 2015; Kent et al. 2007; Liang et al. 2007; Park et al. 2006; Peritore et al. 2021; Shim et al. 2005, 2007; Wiest et al. 2017). Both complexes were found to be recruited to DSBs (Chai et al. 2005; Shim et al. 2005, 2007; Kent et al. 2007; Liang et al. 2007; Bennett et al. 2013; Bennett and Peterson 2015; Wiest et al. 2017) and involved in recruitment of the MRX complex (Shim et al. 2007; Wiest et al. 2017). Furthermore, dysfunction of either complex reduced activation of the DNA damage checkpoint (Shim et al. 2007; Wiest et al. 2017). After induction of a DSB in the yeast genome by the HO endonuclease, reduced ssDNA generation was observed in a strain depleted of the RSC complex subunit Sth1 (Shim et al. 2007) and also in a strain lacking the SWI/SNF complex subunit *SNF5* (Wiest et al. 2017). However, these effects may be site-specific, as only a single DSB locus was investigated. This limitation can be overcome by using the restriction enzyme AsiSI which induces multiple DSBs throughout the yeast genome. Strand-specific sequencing of mutants depleted of Sth1 and Snf2, resulting in the loss of both RSC and SWI/SNF activity, showed abolished resection at several DSB sites (Peritore et al. 2021). However, individual contributions of RSC or SWI/SNF were not examined.

To test if SWI/SNF and RSC remodelling activity is required for resection after telomere deprotection, we generated *cdc13-1* mutants depleted of Sth1 or Snf2 or both. Depletion via the mIAA7 auxin-inducible degradation system was used, as *STH1* is essential (Sepers et al. 2022).

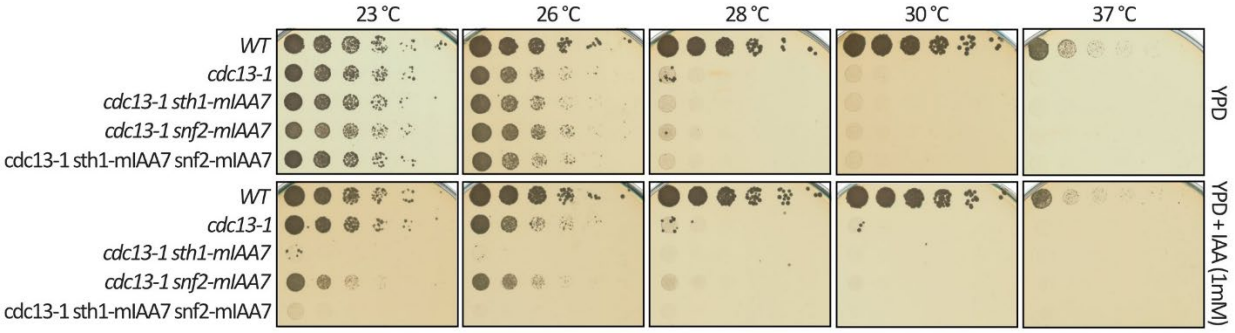


Figure 27: Growth defects of *cdc13-1 sth1-mIAA7, cdc13-1 snf2-mIAA7* and *cdc13-1 sth1-mIAA7 snf2-mIAA7* strains on YPD plates supplemented with IAA indicate successful degradation.
Five-fold serial dilutions of *WT, cdc13-1, cdc13-1 sth1-mIAA7, cdc13-1 snf2-mIAA7* and *cdc13-1 sth1-mIAA7 snf2-mIAA7* were spotted on YPD and YPD + IAA (1 mM) plates and incubated for 48 h at indicated temperatures. Data is representative of n = 2 biological replicates.

The *cdc13-1 sth1-mIAA7, cdc13-1 snf2-mIAA7* and *cdc13-1 sth1-mIAA7 snf2-mIAA7* grow similarly to the *cdc13*-1 control strain at 23 °C on YPD, indicating that the tagged proteins were functional in the absence of auxin (Figure 27). In contrast, on plates supplemented with auxin the *cdc13-1 sth1-mIAA7* and *cdc13-1 sth1-mIAA7 snf2-mIAA7* mutant lost viability. As *STH1* is essential, this phenotype suggests efficient degradation of the RSC subunit. The *cdc13-1 snf2-mIAA7* strain showed reduced growth specifically for plates supplemented with auxin. As loss of Snf2 is known to reduce cell growth (Weider et al. 2011), the observed effect suggests conditional depletion of Snf2. Furthermore, higher temperatures reduced growth of all *cdc13-1* mutants, consistent with telomere deprotection. Together, the observed phenotypes support efficient conditional depletion of Sth1 and Snf2 in a background which allows for telomere deprotection.

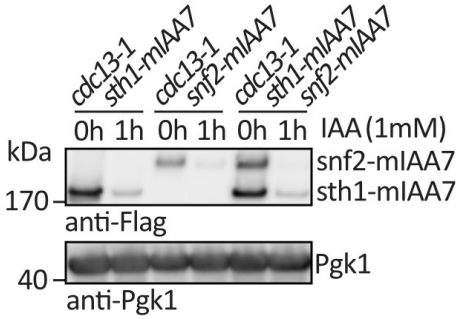


Figure 28: *Sth1-mIAA7 and Snf2-mIAA7* are degraded after addition of auxin.
Anti-Flag western blot detecting levels of Sth1-mIAA7-3Flag and Snf2-mIAA7-3Flag in *cdc13-1 sth1-mIAA7, cdc13-1 snf2-mIAA7* and *cdc13-1 sth1-mIAA7 snf2-mIAA7* before and after 1 h of IAA treatment (final concentration 1 mM). The anti-Pgk1 western blot serves as loading control. Data is representative of n = 2 biological replicates.

In addition to the phenotypical analysis, we confirmed efficient degradation of Sth1 and Snf2 at the protein level. Anti-Flag western blotting (Figure 28) allowed for detection of Sth1 or Snf2 because the mIAA7-tag is followed by a 3Flag-tag in the tested strains. The signal against Pgk1 served as a loading control and showed equal loading of all samples. After 1 h of auxin treatment, residual signal for Sth1-mIAA7-3Flag remained in the *cdc13-1 sth1-mIAA7* strain and in the *cdc13-1 sth1-mIAA7 snf2-mIAA7* mutant. However, all Sth1-depleted cells died on auxin plates (Figure 27), which indicates that the remaining levels of Sth1 were insufficient to promote cellular proliferation. The signal for Snf2-mIAA7-3Flag was not detectable after 1 h of auxin treatment, indicating successful degradation. Therefore, the strains were treated with auxin for 1 h before the start of an experiment.

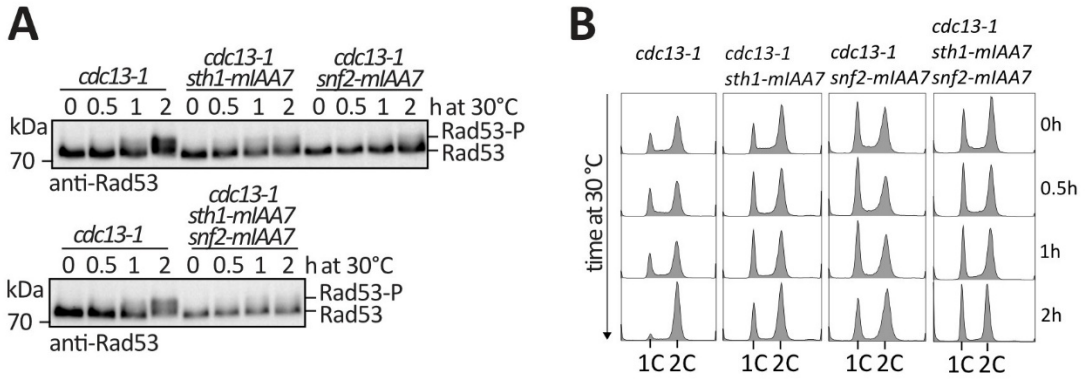


Figure 29: *Cdc13-1* mutants lacking nucleosome eviction activity show reduced Rad53 activation and fail to arrest in G2/M after telomere deprotection.
(A) Dysfunctional nucleosome eviction leads to reduced Rad53 activation after telomere deprotection in *cdc13-1* mutants: Western blots detecting phosphorylated forms of Rad53 visible by gel shift show reduced levels of phosphorylated Rad53 after 1 h of auxin treatment followed by temperature shift to 30 °C in *cdc13-1 sth1-mIAA7, cdc13-1 snf2-mIAA7* and *cdc13-1 sth1-mIAA7 snf2-mIAA7* compared to the *cdc13-1* strain. Data is representative of n = 2–3 biological replicates.
(B) No G2/M cell cycle arrest of *cdc13-1* mutants deficient in nucleosome eviction after telomere deprotection: *Cdc13-1 sth1-mIAA7, cdc13-1 snf2-mIAA7* and *cdc13-1 sth1-mIAA7 snf2-mIAA7* mutant strains were grown at 23 °C and after 1 h of auxin treatment followed by temperature shift to 30 °C samples were taken at the indicated timepoints. Total DNA content was measured by flow cytometry after SYTOX green staining. Data is representative of n = 2 biological replicates.

After verification of auxin-dependent depletion of Sth1 and Snf2 in *cdc13-1* background, we performed a Rad53 upshift assay in order to indirectly measure the presence of ssDNA (Bantele et al. 2019). Whereas the *cdc13-1* control strain showed high levels of Rad53 phosphorylation 2 h after temperature shift, the mutants depleted in either Sth1 or Snf2 and their combined depletion resulted only in a minor Rad53 upshift (Figure 29A). The reduced checkpoint activation indicates that in mutants deficient in nucleosome eviction less ssDNA is generated after telomere deprotection.

Checkpoint activation normally causes cell cycle arrest in order to allow for repair of the damage before the cell cycle progresses to the next phase. As expected, the *cdc13-1* strain showed a G2/M arrest after 2 h at 30 °C (Figure 29B). In contrast, the mutants depleted of Sth1, Snf2 or both showed no arrest. This is consistent with the reduced Rad53 phosphorylation (Figure 29A), as activation of the effector kinase Rad53 results in cell cycle arrest (Finn et al., 2012; Harrison and Haber, 2006).

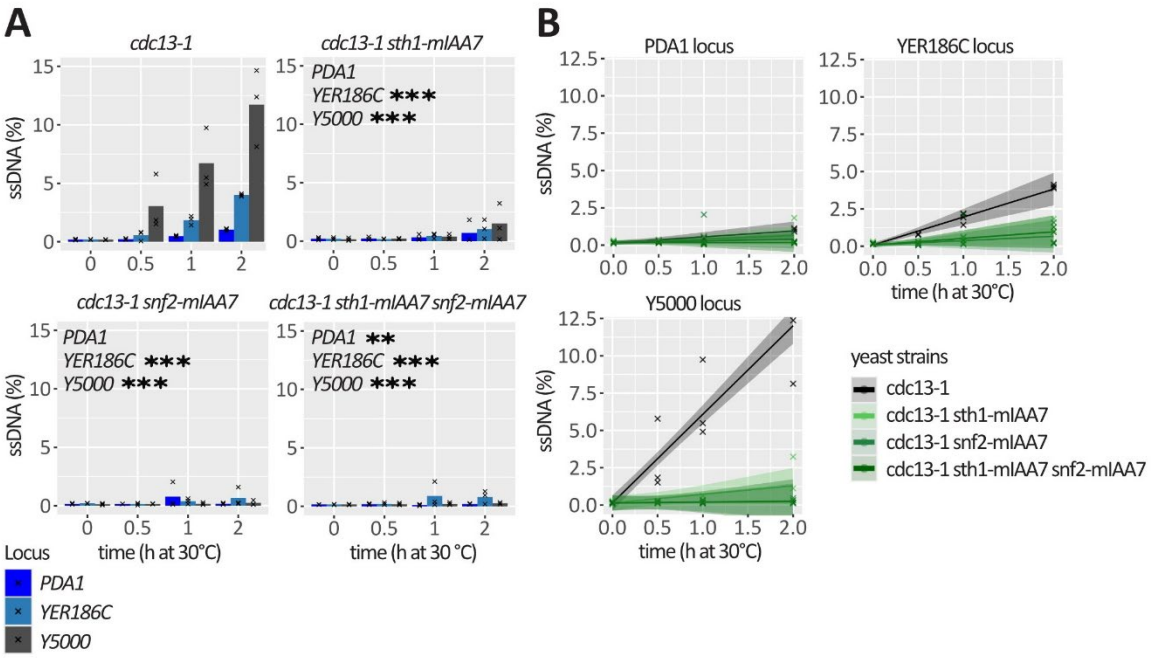


Figure 30: Nucleosome eviction is essential for resection after telomere deprotection.
(A) No extensive resection of deprotected telomeres of Chr V was measured by quantitative amplification of ssDNA (QAOS) for mutants deficient in nucleosome eviction: Yeast cultures of *cdc13-1, cdc13-1 sth1-mIAA7, cdc13-1 snf2-mIAA7* and *cdc13-1 sth1-mIAA7 snf2-mIAA7* were shifted to 30 °C after 1 h of auxin treatment and harvested at indicated timepoints. Accumulation of ssDNA was measured at *Y´5000, YER186C* and *PDA1* loci. Data is representative of n = 3 biological replicates. One biological replicate of the *cdc13-1* control strain is identical to that shown in Figure 20. Statistical significance of differences in ssDNA accumulation compared to the cdc13-1 control strain was calculated using a linear mixed-effects model. **(B)** Linear mixed-effects model of the QAOS experiment shown in (A): Statistical significance of the difference in ssDNA generation with time after temperature shift to 30 °C was calculated for *cdc13-1 sth1-mIAA7, cdc13-1 snf2-mIAA7* and *cdc13-1 sth1-mIAA7 snf2-mIAA7* and compared to the *cdc13*-1 control strain. Slope values are given in Supplementary Table 1.

Rad53 and cell cycle analysis (Figure 29) already indicated that loss of nucleosome eviction activity impairs resection after telomere deprotection. To directly measure ssDNA generation, we performed QAOS analysis in *cdc13-1 sth1-mIAA7, cdc13-1 snf2-mIAA7* and *cdc13-1 sth1-mIAA7 snf2-mIAA7* mutants after 1 h of auxin treatment; all strains showed almost no ssDNA accumulation at *Y´5000, YER186C* and *PDA1* loci after temperature shift to 30 °C in contrast to the *cdc13-1* control strain (Figure 30). Not only the depletion of both, but also depletion of either individual remodeller subunit was sufficient to strongly suppress ssDNA generation. This suggests that both the SWI/SNF and RSC complex are required for resection after telomere deprotection.

Generation of ssDNA after telomere deprotection was dependent on SWI/SNF and RSC complex remodelling as observed for resection at DSBs. However, the mechanism by which SWI/SNF and RSC support resection after telomere deprotection remains unclear.

Importantly, the QAOS assay does not allow us to determine whether the resection defect occurs already at the telomeric regions (short-range resection) or at the nucleosome barrier (long-range resection). Furthermore, depletion of the SWI/SNF or RSC complex might cause side effects and therefore protect telomeres from degradation.

3.3.2 Nucleosome editing does not significantly affect resection after telomere deprotection

Nucleosome eviction had similar effects on long-range resection at DSBs and deprotected telomeres. Therefore, we investigated how nucleosome editing affects long-range resection at deprotected telomeres. For this purpose, the *cdc13-1* system is a particularly valuable tool, as reduced cutting efficiency of AsiSI-mediated DSB induction limited data analysis for the *pGal-AsiSI swr1Δ htz1Δ* mutant (Figure 9).

Growth assays with DNA damaging drugs suggest an involvement of the INO80 complex in DNA repair (Brahma et al. 2018), but the underlying mechanism remains unclear. *In vivo* studies indicate that the INO80 complex acts downstream of resection (Horigome et al. 2014; Lademann et al. 2017). In contrast, the INO80 complex might counteract resection by exchanging H2A.Z containing nucleosomes with canonical ones, as *in vitro* data suggests that H2A.Z containing nucleosomes could facilitate resection and resolve the nucleosome barrier (Adkins et al. 2013). Besides, H2A.Z could have other functions, such as serving as signalling platform for other DNA repair factors (Xu et al. 2012).

To elucidate how nucleosome editing affects long-range resection, we generated a *cdc13-1 arp8Δ* strain with impaired INO80 complex activity. Furthermore, a *cdc13-1 swr1Δ htz1Δ* strain was constructed lacking H2A.Z and a functional SWR1 complex. Both *SWR1* and *HTZ1*, which encodes H2A.Z, were deleted, because deletion of *HTZ1* alone results in SWR1 complex malfunction (Halley et al. 2010; Morillo-Huesca et al. 2010). Analysis of the *cdc13-1 arp8Δ swr1Δ htz1Δ* strain allowed us to examine consequences of a complete loss of nucleosome editing activity.

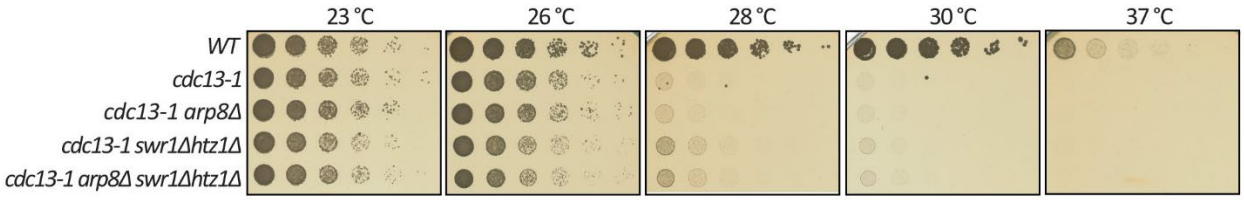


Figure 31: Strains dysfunctional in nucleosome editing show reduced growth under permissive conditions.
Five-fold serial dilutions of *WT, cdc13-1, cdc13-1 arp8Δ, cdc13-1 swr1Δ htz1Δ* and *cdc13-1 arp8Δ swr1Δ htz1Δ* were spotted on YPD and incubated for 48 h at indicated temperatures. Data is representative of n = 2 biological replicates.

The *cdc13-1 arp8Δ, cdc13-1 swr1Δ htz1Δ* and *cdc13-1 arp8Δ swr1Δ htz1Δ* strains showed mild growth defects already at 23 °C (Figure 31). Such reduced growth independent of telomere deprotection is consistent with known functions of H2A.Z in transcription, replication and cell cycle progression (Dhillon et al. 2006) and the various cellular functions of the INO80 complex (Brahma et al. 2018). In the *cdc13-1* background, none of the introduced mutations rescued temperature sensitivity, suggesting that nucleosome editing is not essential for resection after telomere deprotection.

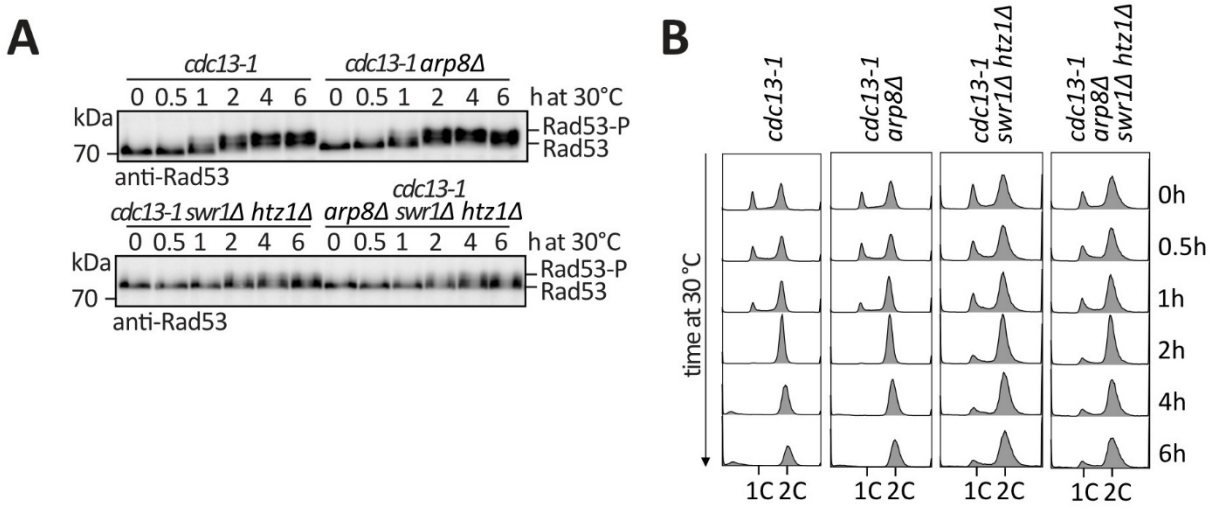


Figure 32: Reduced Rad53 activation and incomplete cell cycle arrest in G2/M after telomere deprotection in *cdc13*-1 mutants with H2A.Z deficiency.
(A) Rad53 activation after telomere deprotection in *cdc13-1* mutants: Western blots detecting phosphorylated forms of Rad53 visible by gel shift show increasing levels of phosphorylated Rad53 after temperature shift to 30 °C in *cdc13-1, cdc13-1 arp8Δ, cdc13-1 swr1Δ htz1Δ* and *cdc13-1 arp8Δ swr1Δ htz1Δ* strains. Data is representative of n = 2–3 biological replicates.
(B) G2/M cell cycle arrest of *cdc13-1* mutants after telomere deprotection: Mutant strains were grown at 23 °C, temperature shifted to 30 °C and samples were taken at the indicated timepoints. Total DNA content was measured by flow cytometry after SYTOX green staining. Data is representative of n = 1–3 biological replicates.

We next analysed Rad53 phosphorylation, as checkpoint activation correlates with the amount of ssDNA (Bantele et al. 2019). The *cdc13-1 arp8Δ* mutant behaved similarly to the *cdc13-1* control strain (Figure 32A). In contrast, strains lacking *SWR1* and *HTZ1* showed delayed Rad53 phosphorylation, with a clear upshift visible only after 2 h rather than after 1 h as in the *cdc13-1* control strain. These results contrast with the previous observations that *htz1Δ* cells show earlier Rad53 phosphorylation after hydroxyurea treatment (Dhillon et al. 2006) and increased levels of phosphorylated H2A.X upon CPT treatment (Papamichos-Chronakis et al. 2006). MMS treatment also increased H2A.X phosphorylation in *swr1Δ* cells (Papamichos-Chronakis et al. 2006). This discrepancy may reflect differences in damage type or severity. In the *cdc13-1* strains, the reduced Rad53 phosphorylation of the *cdc13-1 swr1Δ htz1Δ* strain could result from impaired resection after telomere deprotection. However, further possible explanations are altered telomeric chromatin structure or heterochromatin spreading after H2A.Z loss, which might stabilise the telomeres and prevent ssDNA generation (Martins-Taylor et al. 2011). Furthermore, the reduced growth of *htz1Δ* cells might delay Rad53 phosphorylation (Figure 31)(Dhillon et al. 2006).

Cell cycle analysis was consistent with the observed effects in Rad53 phosphorylation. *cdc13-1 swr1Δ htz1Δ* cells showed delayed and incomplete checkpoint activation and did not undergo complete G2/M arrest even after 6 h (Figure 32B). In contrast, the *cdc13-1 arp8Δ* strain behaved similarly to the control, indicating that the INO80 complex does not affect checkpoint activation after telomere deprotection.

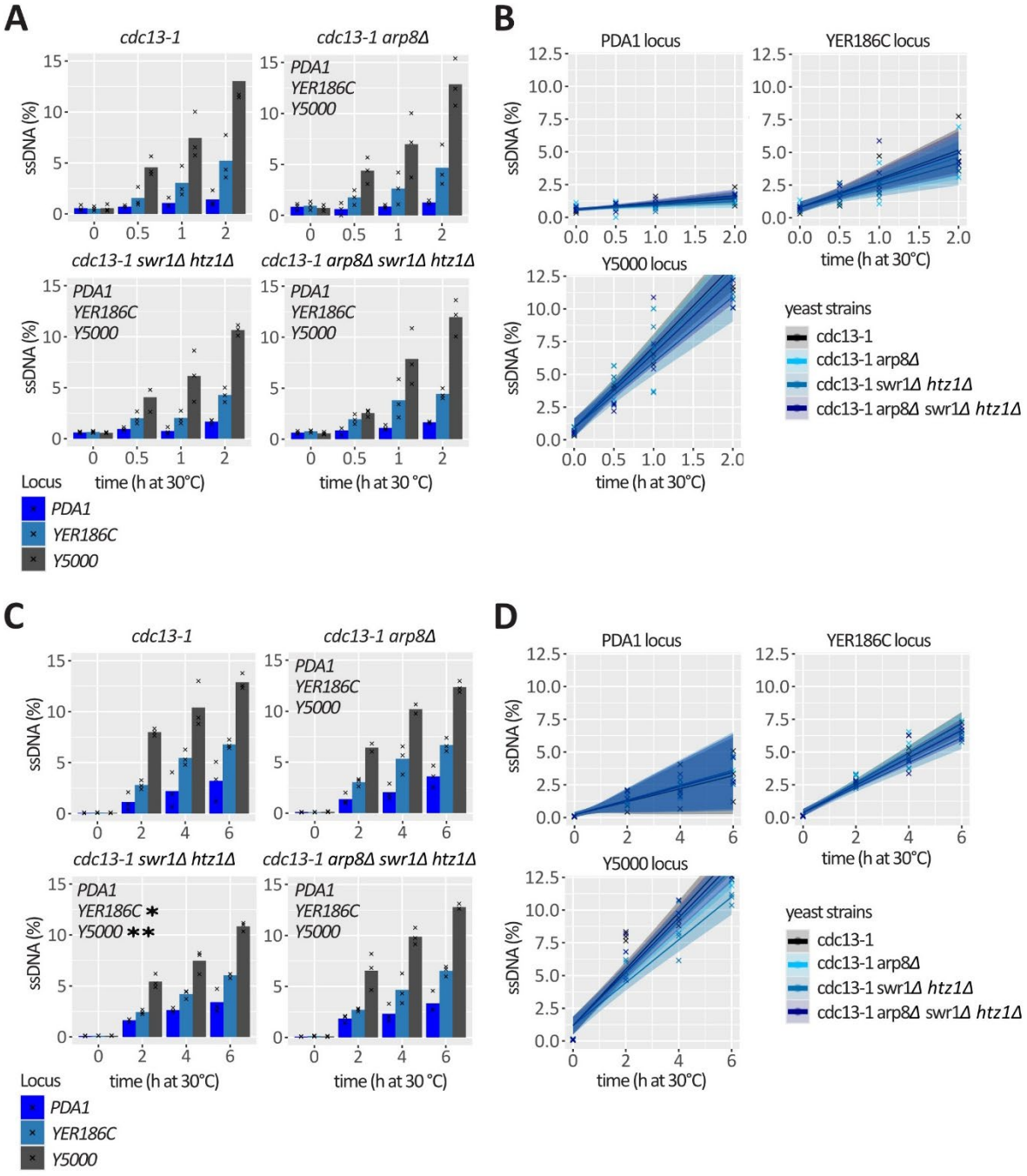


Figure 33: Nucleosome editing does not significantly affect resection after telomere deprotection.
(A) Resection of deprotected telomeres of Chr V was measured by quantitative amplification of ssDNA (QAOS) for mutants deficient in nucleosome editing: Yeast cultures of *cdc13-1, cdc13-1 arp8Δ, cdc13-1 swr1Δ htz1Δ* and *cdc13-1 arp8Δ swr1Δ htz1Δ* were shifted to 30 °C and harvested at indicated timepoints. Accumulation of ssDNA was measured at *Y´5000, YER186C* and *PDA1* loci. Data is representative of n = 3 biological replicates. 1 biological replicate of the *cdc13-1* control strain is the same as in Figure 20 and Figure 25. Statistical significance of differences in ssDNA accumulation compared to the cdc13-1 control strain was calculated using a linear mixed-effects model.
(B) Linear mixed-effects model of the QAOS experiment shown in (A): Statistical significance of the difference in ssDNA generation with time after temperature shift to 30 °C was calculated for *cdc13-1 arp8Δ, cdc13-1 swr1Δ htz1Δ* and *cdc13-1 arp8Δ swr1Δ htz1Δ* compared to the *cdc13*-1 control strain. Slope values are given in Supplementary Table 1.
(C) Resection of deprotected telomeres was measured by QAOS as in (A), but for 0, 2, 4 and 6 h. Data is representative of n = 3 biological replicates.
(D) Linear mixed-effects model of the QAOS experiment shown in (C): Analysis was performed as in (B) but for 0, 2, 4 and 6 h. Slope values are given in Supplementary Table 1.

To determine whether incomplete Rad53 phosphorylation and cell cycle arrest of the *cdc13-1* mutants lacking *HTZ1* and *SWR1* arise from a defect in resection after telomere deprotection, we quantified ssDNA generation by QAOS as described above. No significant differences in ssDNA accumulation were detected for *cdc13-1 arp8Δ, cdc13-1 swr1Δ htz1Δ* or *cdc13-1 arp8Δ swr1Δ htz1Δ* compared to the *cdc13-1* control (Figure 33A and B). To test whether significant differences might become apparent at the distal *PDA1* locus, located 29.7 kb from the telomere, we extended the time course to 6 h (Figure 33C). However, no significant decrease in ssDNA generation was observed (Figure 33D).

Taken together, we conclude that nucleosome editing does not substantially affect ssDNA generation after telomere deprotection. The incomplete Rad53 phosphorylation and cell cycle arrest observed in *HTZ1*-deficient strains (Figure 32) likely do not result from reduced ssDNA accumulation, but may instead reflect indirect roles of H2A.Z in cell cycle progression, checkpoint signalling or chromatin organisation (Dhillon et al. 2006).

Taken together, we showed that nucleosome eviction is essential not only for resection at DSBs (Peritore et al. 2021), but also for long-range resection at telomeres. Therefore, the *cdc13-1* system is a useful alternative for studying long-range resection, in particular when restriction enzyme-based DSB induction is inefficient. We observed no significant effect on long-range resection after telomere deprotection in the absence of INO80 complex function or SWR1 complex function combined with H2A.Z deficiency.

Summary:

- Nucleosome eviction by the RSC or SWI/SNF complex is essential for resection after telomere deprotection.
- The observed requirement for RSC and SWI/SNF activity for resection at deprotected telomeres is consistent with resection at DSBs within the genome (Peritore et al. 2021) and supports the use of the *cdc13-1* system as a model to study resection in the context of chromatin.
- Nucleosome editing does not significantly affect long-range resection after telomere deprotection.

4. Discussion

In this study, we investigated DNA end resection with a particular focus on chromatin and how nucleosome remodelling influences long-range resection. Resection is the first step of homologous recombination (HR) and the key limiting step of repair pathway choice. Knowing about resection regulation is relevant for our understanding of genome stability and may help improve genome editing.

Previous work showed that nucleosome eviction by the SWI/SNF and RSC complexes is required to overcome the nucleosome barrier and allow for resection (Peritore et al. 2021). However, the contribution of some other nucleosome remodellers to this process remains unclear. We therefore asked to what extent the INO80 complex and the SWR1 complex, which act antagonistically in H2A.Z exchange, contribute to resection. We investigated resection at DSB sites induced by the restriction enzyme AsiSI. Furthermore, we used telomere deprotection via the *cdc13-1* system as an alternative model. First, we showed that the same resection nucleases are involved in long-range resection after telomere deprotection as at DSBs. Then we verified that nucleosome eviction is also required for long-range resection at deprotected telomeres and analysed nucleosome editing mutants.

4.1 Restriction enzyme mediated DSB induction does not support a major requirement for nucleosome editing in resection

4.1.1 Accurate cutting efficiency measurement is required for data interpretation using restriction enzyme based DSB induction

Strand-specific sequencing enables the quantification of DNA end resection at restriction enzyme-induced DSBs. By averaging DNA loss across multiple break sites, the influence of sequence-dependent effects can be reduced. Nevertheless, meaningful comparisons of resection between mutant strains require not only reproducible cutting efficiencies across biological replicates, but also comparable cutting efficiencies between strains, because differences in DSB induction can influence the apparent extent of resection.

Cutting efficiency can be quantified by qPCR using primer pairs flanking the DSB site. After DSB induction, only uncut DNA molecules generate a PCR product, whereas cleaved molecules do not contribute to the signal. This approach is informative, but not scalable for systems that induce many genomic cuts at different loci. Furthermore, the exponential nature of PCR

amplification can introduce experimental variability. Alternatively, cutting efficiency can be estimated directly from strand-specific sequencing data by determining the fraction of sequencing reads that span a DSB site. However, this method also has limitations. During library preparation, the genomic DNA is randomly fragmented into fragments of approximately 350 bp. Deep sequencing is required to quantify reads spanning the DSBs and is associated with high costs.

To address these limitations in measuring cutting efficiency at restriction enzyme-induced DSBs, we used a nanopore-based approach that sequences long genomic DNA fragments. A restriction enzyme that generates sticky ends is required, because the method relies on the loss of coverage of these ends. When the restriction enzyme generates a DSB, blunting during library preparation leads to reduced coverage of the sticky ends. Comparing this local coverage reduction with the mean coverage around the DSB site provides a precise measurement of cutting efficiency for the individual DSB sites (Figure 8).

When we applied this method to our *pGal-AsiSI* strain, we observed cutting efficiencies similar to those determined by quantifying DSB-spanning reads in strand-specific sequencing. Therefore, we used the same cut sites for plotting mean DNA loss in the strand-specific sequencing as in our previous study (Peritore et al. 2021).

In previously published data about the RSC and SWI/SNF complex (Peritore et al. 2021) similar cutting efficiencies between the control and the mutant strain were assumed. We measured cutting efficiency of the *pGal-AsiSI sth1-3aid* snf2-3aid** strain via nanopore and could confirm sufficiently similar cutting efficiencies (Figure 13). This validated the interpretation of the results, which had previously relied on the assumption of comparable cutting efficiency.

4.1.2 Dysfunction of the INO80 complex does not detectably impair resection but affects H2A.Z-associated chromatin changes

To extend the knowledge about the INO80 complex and how it contributes to resection, we generated a *pGal-AsiSI arp8Δ* strain and aimed to compare resection at AsiSI-induced DSBs to the *pGal-AsiSI* control strain. As cutting efficiencies were similar between the strains, we could directly compare the strand-specific sequencing data. We did not observe detectable differences in input DNA loss or H3 loss, indicating that the INO80 complex does not detectably affect resection. In contrast, the signal indicating loss of H2A.Z containing nucleosomes was reduced compared to loss of H3 and lower in the *pGal-AsiSI arp8Δ* mutant than in the control

strain (Figure 7). In the *pGal-AsiSI* control strain the signal for H2A.Z loss could result from removal of H2A.Z containing nucleosomes as a consequence of resection, but also from DSB-induced and INO80-dependent editing replacing H2A.Z containing nucleosomes with canonical nucleosomes. In the *pGal-AsiSI arp8Δ* mutant H2A.Z removal by the INO80 complex is impaired, so loss of H2A.Z is likely associated with resection. However, additional effects of the mutant might contribute. The additional loss of H2A.Z in the *pGal-AsiSI* control compared to the *pGal-AsiSI arp8Δ* mutant likely results from INO80-dependent nucleosome remodelling. However, this nucleosome editing activity does not detectably affect resection, because the signal for loss of DNA input and H3 was comparable between the control strain and the *pGal-AsiSI arp8Δ* mutant. Furthermore, our ChIP data indicates that only a subset of nucleosomes removed upon resection contain H2A.Z, because the reduction of H3-associated DNA was more pronounced than for H2A.Z (Figure 7B and D).

Consistent with these results, another study observed resection levels comparable to the control in an *ino80Δ* strain using the HO system for DSB induction (Papamichos-Chronakis et al. 2006). Furthermore, decreased levels of H2A.X and increased levels of H2A.Z were detected when the INO80 complex was dysfunctional. This imbalance could be restored by additional deletion of the SWR1 complex or by removal of H2A.Z. Therefore, the authors proposed that the INO80 complex is required to remove H2A.Z in order to allow for H2A.X phosphorylation and proper checkpoint activation (Papamichos-Chronakis et al. 2006).

Our data is consistent with the hypothesis that both H2A.Z containing and canonical nucleosomes are present at DSBs and that canonical nucleosomes mediate γH2A.X spreading. Thus, the INO80 complex might be required to maintain sufficient amounts of canonical nucleosomes and to prevent excessive SWR1-dependent nucleosome editing (Papamichos-Chronakis et al. 2006, 2011; Lademann et al. 2017).

Some studies reported a resection defect at an HO-induced cut site when the function of the INO80 complex was impaired (Lademann et al. 2017; Van Attikum et al. 2004). However, the reduction of resection was minor and significant only 4 h after DSB induction (Lademann et al. 2017). Site-specific effects may contribute to this discrepancy, because the HO endonuclease was targeted to different genomic locations. By generating multiple DSBs in the yeast genome and averaging ssDNA generation over the most efficiently cut DSBs, our approach reduces the influence of cut-site-specific effects.

Overall, our data does not support a direct role for the INO80 complex in resection. However, it is essential for other processes in HR. For example, *arp8Δ* mutants displayed elevated levels of RPA but were deficient in Rad51 accumulation, indicating that the INO80 complex contributes to Rad51 filament formation downstream of resection (Lademann et al. 2017). In addition, reduced growth upon exposure to DNA damage (Van Attikum et al. 2004) and decreased recombination rates in *arp8Δ* mutants (Lademann et al. 2017) indicate that the INO80 complex is required for HR.

4.1.3 Reduced DSB generation by AsiSI limits interpretation of genotypes deficient of H2A.Z, but resection can occur without nucleosome editing

To gain further insight into nucleosome editing around DSBs, we also analysed a *pGal-AsiSI htz1Δ swr1Δ* strain (Figure 7). As the absence of H2A.Z is associated with secondary phenotypes arising from dysfunction of the SWR1 complex, we additionally deleted *SWR1* (Halley et al. 2010; Morillo-Huesca et al. 2010). Cutting efficiency was highly reduced in this mutant (Figure 9), preventing a direct quantitative comparison of the apparent resection defect with the *pGal-AsiSI* control strain. Nevertheless, the two available replicates allow qualitative interpretation. In the first replicate, DSB generation was almost completely absent and no significant DNA loss was observed. In the second replicate, cutting efficiency was higher, although still low, reaching approximately 30 % 4 h after DSB induction. In this replicate, resection was detectable 4 h and 6 h after DSB induction. Thus, loss of H2A.Z and SWR1 does not appear to fully abolish resection. Because a linear relationship between cutting efficiency and DNA loss cannot be assumed, minor effects on resection cannot be assessed from these data.

A study using the HO endonuclease for DSB induction reported reduced resection in an H2A.Z-deficient strain (Lademann et al. 2017). Because cutting efficiency was not measured in that study, reduced DSB generation could have contributed to the observed defect, highlighting the importance of determining cutting efficiency for data interpretation. Another study that did take cutting efficiency into account using qPCR detected lower levels of ssDNA and RPA around the HO cut site in an *htz1Δ* strain compared to the control (Kalocsay et al. 2009). However, the *htz1Δ* strain could be affected by malfunction of the SWR1 complex in the absence of its substrate H2A.Z. Importantly, no resection defect at an HO cut site was observed in a strain lacking the SWR1 complex (Van Attikum et al. 2007). Overall, a major

direct contribution of the SWR1 complex and H2A.Z to resection appears unlikely based on the available data, although minor effects cannot be excluded.

Analysis of the *pGal-AsiSI arp8Δ htz1Δ swr1Δ* strain showed no difference in DNA loss compared to the *pGal-AsiSI* control strain (Figure 7). That cutting efficiencies were sufficiently similar between the control strain and the mutant allowed for their comparison. Resection was not inhibited through the complete absence of nucleosome editing activity. Incorporation of H2A.Z was not required to allow for resection in the absence of a functional INO80 complex. Therefore, nucleosome editing seems to be dispensable for resection.

4.1.4 Insufficient cutting efficiency requires an alternative system to study DSB resection

In most mutant backgrounds, cutting efficiency was similar to that in the control strain. However, the strong reduction in DSB generation in the *pGal-AsiSI htz1Δ swr1Δ* strain prevented interpretation of the sequencing data and an alternative system to galactose-inducible AsiSI expression is required to study resection in the *htz1Δ swr1Δ* background.

The reduced cutting efficiency in the *pGal-AsiSI htz1Δ swr1Δ* strain could arise from reduced accessibility of AsiSI to its recognition sequence. This possibility is supported by the observation that cut sites occupied by a nucleosome are associated with reduced cutting efficiency compared to nucleosome-free cut sites (Oberbeckmann et al. 2019; Peritore et al. 2021). H2A.Z containing nucleosomes may represent a weaker barrier for the restriction enzyme than canonical nucleosomes, because they show weaker DNA interactions (Adkins et al. 2013). In addition, AsiSI expression could influence the number of generated DSBs. Consistent with this possibility, we measured reduced AsiSI abundance of about 50 % +/- 30 % in the *pGal-AsiSI htz1Δ swr1Δ* strain. Importantly, AsiSI expression was similar to the control in the *pGal-AsiSI arp8Δ htz1Δ swr1Δ* strain showing efficient cutting. Thus, reduced AsiSI expression might at least in part be responsible for the reduced cutting efficiency in the *pGal-AsiSI htz1Δ swr1Δ* strain.

To overcome inefficient AsiSI cutting from the *pGAL* promoter, the system could in principle be redesigned so that AsiSI is expressed from a different promoter. The *pGAL* promoter has been reported to be affected by H2A.Z (Halley et al. 2010). However, expression from other promoters might also be affected in an *htz1Δ* background. Therefore, we turned to the

cdc13-1 system to investigate the function of the SWR1 complex and H2A.Z in long-range resection independent of AsiSI-mediated DSB induction efficiency.

4.2 The long-range resection machinery at deprotected telomeres resembles genomic DSB resection

Telomeres structurally resemble one end of a DSB and can become resected upon removal of protecting protein complexes. Therefore, they can provide an alternative system to investigate resection without inducing DSBs. In budding yeast, temperature shift of *cdc13-1* mutants results in telomere deprotection. To serve as a useful model to study long-range resection, the involved resection enzymes should be the same as at genomic DSBs.

Roles for Exo1 and Sgs1 in resection at deprotected telomeres have already been described. Quantitative analysis of ssDNA (QAOS) of *cdc13-1* mutants showed reduced resection upon Exo1 deletion, and Sgs1 also affected resection, particularly in the absence of Rad9 (Booth 2001; Dewar and Lydall 2012; Ngo and Lydall 2010; Zubko et al. 2004). At DSBs, the Sgs1 helicase functions together with Dna2, and it has been proposed that the same may be true at telomeres (Ngo and Lydall, 2010). To test whether Dna2 affects resection after telomere deprotection, we used an auxin-mediated degron system to deplete Dna2. We adopted the QAOS protocol and in contrast to *cdc13-1 exo1Δ* (Figure 20) did not observe a significant effect on resection in the *cdc13-1 dna2-mIAA7* mutant (Figure 25). However, ssDNA was further reduced in the *cdc13-1 exo1Δ dna2-mIAA7* mutant compared to the *cdc13-1 exo1Δ* and *cdc13-1 dna2-mIAA7 mutants* (Figure 26). Therefore, combined loss of the two resection nucleases, which are known to act at DSBs, reduced ssDNA generation after telomere deprotection more strongly than loss of either nuclease alone. These results indicate that both Exo1 and Dna2 contribute to resection at deprotected telomeres. However, depletion of Dna2 alone had no significant effect on resection, suggesting that Exo1 acts as the major nuclease during resection of deprotected telomeres, whereas Dna2 likely works in a backup pathway, which becomes important when Exo1 is absent.

We further analysed *sgs1Δ* mutants to test whether Dna2 works in conjunction with the STR complex (Sgs1-Top3-Rmi1). Analogous to Dna2, no significant defect in ssDNA accumulation was observed in a strain carrying only a Sgs1 deletion (Figure 20). However, combined loss of Exo1 and Sgs1 resulted in almost no ssDNA generation (Figure 20) and was significantly

reduced compared to the *cdc13-1 exo1Δ* strain (Figure 21). This data is consistent with the hypothesis that Exo1 works in a pathway separate from Sgs1, analogous to Dna2. Furthermore, combined absence of Sgs1 and Dna2 did not increase the resection defect of the single mutants. The *cdc13-1 sgs1Δ dna2-mIAA7* mutant behaved similarly to the *cdc13-1* control strain (Figure 25). Because no clear effect was observed when Sgs1 or Dna2 or both were absent, epistasis cannot be claimed from the data. Nevertheless, the results are consistent with Sgs1 and Dna2 acting in the same pathway, whereas Exo1 represents the major nuclease for resection after telomere deprotection.

In general, we measured ssDNA generation within 2 h after telomere deprotection. The *Y´5000* and *YER186C* loci are relatively close to the telomere end and in the *cdc13-1* control strain, we observed an increase in ssDNA of about 12 % and 5 %, respectively. The *PDA1* locus is located 29.7 kb from the telomere. Assuming a resection speed of approximately 4 kb/h (Z. Zhu et al. 2008; Eapen et al. 2012), resection cannot easily reach this locus. This explains the minor increase in ssDNA observed at the *PDA1* locus.

Overall, the results suggest that long-range resection after telomere deprotection relies on the same major nuclease pathways as resection at genomic DSBs (Mimitou and Symington 2008; Z. Zhu et al. 2008). However, short-range resection differs at deprotected telomeres. At DSBs, MRX activity is required to generate a starting point for long-range resection (Cejka 2015; Cejka and Symington 2021), but deprotected telomeres already contain 3' ssDNA. Therefore, the MRX complex is not required to initiate long-range resection at deprotected telomeres. In contrast, the MRX complex has been reported to have a protective role at telomeres (Foster et al. 2006). Telomeric binding proteins such as Rap1, together with Rif2, inhibit the nuclease activity of MRX (Casari et al. 2022; Marsella et al. 2021; Bonetti, Clerici, Manfrini, et al. 2010; Mattarocci et al. 2026). Binding of this inactive form of the MRX complex could hinder processing by other nucleases or promote recruitment of telomerase or other protective proteins (Foster et al. 2006; Faure et al. 2010; Dewar and Lydall 2012)

4.3 Chromatin influences long-range resection at deprotected telomeres

Having established that the long-range resection pathways acting at deprotected telomeres resemble DSB resection, we used the *cdc13-1* system to investigate how chromatin influences long-range resection. This system is particularly useful when DSB induction by restriction enzymes is limiting and we aimed to investigate the effect of H2A.Z deficiency on resection in particular.

Telomeres contain a specialised chromatin structure. Adjacent to the telomeric ssDNA, Rap1 binds repetitive telomeric dsDNA sequences (De Lange 2009; Lustig et al. 1990). Rap1 is essential for telomere maintenance and counteracts telomere fusion (Conrad et al. 1990; Pardo and Marcand 2005). In addition, Sir proteins are associated with telomeric silencing (Bourns et al. 1998).

Upon telomere deprotection in the *cdc13-1* system, telomeric ssDNA is exposed and can serve as a starting point for resection. Because of the specialised chromatin structure of telomeric DNA, resection might initially differ from resection at genomic DSBs. QAOS does not measure ssDNA within the telomeric repeat region, but detects ssDNA generation at loci located 5 kb, 14 kb and 29 kb from the telomere end. The *Y´5000* locus, located 5 kb from the chromosome end, may still be influenced by repetitive sub-telomeric sequence features, whereas the other two loci represent euchromatic regions. Thus, the chromatin measured by QAOS should reflect genomic DNA. However, the approach does not provide information about preceding short-range resection.

To investigate how resection overcomes the nucleosome barrier after telomere deprotection, we generated nucleosome-remodeller mutants carrying the *cdc13-1* allele. First, we tested whether nucleosome eviction contributes to resection after telomere deprotection, because it was previously shown to be required for efficient resection at DSBs (Peritore et al. 2021). Then we examined nucleosome editing to extend the findings from the DSB induction system.

4.3.1 Nucleosome eviction is required for resection at deprotected telomeres

The SWI/SNF and RSC nucleosome-remodelling complexes evict nucleosomes from DNA. Both complexes function in transcriptional regulation, and RSC remodelling activity is essential for cell proliferation. Therefore, we used conditional depletion of Sth1, the catalytic ATPase of RSC, and Snf2, the catalytic ATPase of SWI/SNF, individually and in combination in a *cdc13-1* background. QAOS analysis showed a strong resection defect in all depletion mutants. In

addition, the Rad53 response was reduced and no cell cycle arrest was observed (Figure 29 and Figure 30). These results indicate that nucleosome eviction is required for ssDNA accumulation after telomere deprotection, consistent with the requirement for nucleosome eviction at DSBs. After restriction enzyme-induced DSB formation, a strong resection defect was observed when Sth1 and Snf2 were depleted together (Peritore et al. 2021). Single mutants were not tested in that system because functional redundancy between SWI/SNF and RSC was expected (Rawal et al. 2018; Sahu et al. 2021; Schlichter et al. 2020). However, our data suggests that at least after telomere deprotection both complexes are required.

Several non-mutually exclusive explanations could account for this non-redundant function of the SWI/SNF and RSC complex. First, transcriptional dysregulation in the nucleosome remodeller mutants could indirectly affect resection. However, conditional depletion was induced only shortly before telomere deprotection and transcriptional changes in telomeric binding proteins after SWI/SNF or RSC complex dysfunction have not been reported so far (Dutta et al. 2017; Klein-Brill et al. 2019). Nevertheless, indirect effects cannot be fully excluded.

Second, one of the remodeller complexes might be involved in telomere resection prior to long-range resection. By QAOS we detect ssDNA generated by long-range resection. However, inhibition of short-range processing or of resection through the telomeric region would also prevent long-range resection downstream. SWI/SNF or RSC might be involved in removing telomeric binding proteins. Consistently, the SWI/SNF complex can evict Sir proteins (Manning and Peterson 2014; Sinha et al. 2009) and influences Rap1 binding at promoters (Lieb et al. 2001).

Third, SWI/SNF and RSC may both act in promoting resection through nucleosomes and could be partially redundant in their enzymatic activity. However, their recruitment to the DSB sites or substrate specificity might differ. One complex could be particularly important for removing nucleosomes within sub-telomeric chromatin, whereas the other might act more efficiently within genomic euchromatin.

Overall, we hypothesise that nucleosome eviction remodellers are required to remove nucleosomes so that resection nucleases can degrade DNA. Our results suggest that nucleosome eviction is required for both, long-range resection at genomic DSBs and deprotected telomeres, although QAOS cannot distinguish whether the defect arises during long-range resection or prior during telomere resection.

4.3.2 Nucleosome editing does not detectably affect long-range resection at deprotected telomeres

Nucleosome editing could provide an alternative to nucleosome eviction to overcome the nucleosome barrier. We first tested this hypothesis by AsiSI-mediated DSB induction. However, we did not detect a significant change in DNA loss when the INO80 complex was dysfunctional nor in the *pGal-AsiSI arp8Δ htz1Δ swr1Δ* strain where nucleosome editing is fully abolished (Figure 7). This data suggests that nucleosome editing is not required for resection. Due to insufficient cutting efficiency, we were unable to analyse the effect of H2A.Z deficiency on resection with the *pGal-AsiSI htz1Δ swr1Δ* strain. This limitation was overcome by using the *cdc13-1* system and telomere deprotection. QAOS analysis of a *cdc13-1 swr1Δ htz1Δ* strain indicates that loss of H2A.Z and SWR1 does not detectably affect resection (Figure 33). Consistent with our findings from the DSB induction system also dysfunction of the INO80 complex nor complete loss of nucleosome editing activity did not significantly affect resection after telomere deprotection (Figure 33). We also did not observe any changes in resection in the nucleosome editing mutants after extending the time course to 6 h, which allowed resection to proceed to the more distal *PDA1* locus (Figure 33C and D).

Our QAOS data verifies the previous results from the DSB induction system and suggests that neither INO80 nor H2A.Z incorporation is required for long-range resection. Instead, the INO80 complex might promote HR downstream of resection (Lademann et al. 2017) and H2A.Z incorporation at DSB sites might function as a signalling platform for recruitment of repair factors (Xu et al. 2012). By investigating multiple DSB sites induced by the restriction enzyme AsiSI and complementary analysis of long-range resection after telomere deprotection we expanded previous studies that were limited to a single DSB site and therefore susceptible to sequence-specific effects (Van Attikum et al. 2004; Papamichos-Chronakis et al. 2006; Lademann et al. 2017).

Taken together, the DSB induction system and the *cdc13-1* system provide complementary evidence that nucleosome editing is not detectably required for long-range resection. The restriction enzyme-based DSB system showed that dysfunction of the INO80 complex and complete loss of the nucleosome editing function did not impair DNA loss when cutting efficiency was comparable. However, inefficient DSB generation limited direct interpretation of the *pGal-AsiSI swr1Δ htz1Δ* strain. Investigation of long-range resection after telomere

deprotection bypassed this limitation and showed that loss of SWR1 complex function and H2A.Z did not detectably impair long-range resection.

In contrast, depletion of the nucleosome eviction remodeller complexes SWI/SNF and RSC strongly reduced resection after telomere deprotection as previously shown at DSBs. The data does not support a model in which nucleosome editing provides an alternative mechanism to overcome the nucleosome barrier during long-range resection. Instead, efficient long-range resection appears to depend primarily on nucleosome eviction, whereas the INO80 complex is more likely to contribute to DNA damage signalling and to HR processes downstream of resection in budding yeast.

We showed complementary resection phenotypes upon resection nuclease deficiency and nucleosome remodelling dysfunction within the DSB induction system and the *cdc13-1* system. Thus, we highlight the value of the *cdc13-1* system as an alternative approach for investigating long-range resection, particularly in genetic backgrounds in which restriction enzyme-based DSB induction is inefficient.

4.4 Conservation in higher eukaryotes

We aimed to elucidate to what extend nucleosome remodelling contributes to resection and DSB repair using budding yeast as a model organism. Homologous recombination and the major long-range resection enzymes are conserved across eukaryotes (Cejka 2015; Cejka and Symington 2021; Mimitou and Symington 2008; Lorraine S. Symington and Gautier 2011; Z. Zhu et al. 2008) and several studies indicate that also nucleosome remodelling in response to DNA damage is conserved: The mammalian homologues of the SWI/SNF and RSC complex, BAF and PBAF, were found to be recruited to DSBs and promote resection (Park et al. 2006; Hays et al. 2020). Moreover, an accumulation of H2A.Z has been observed around DSBs in mammals (Nishibuchi et al. 2014; Alatwi and Downs 2015; Gursoy-Yuzugullu et al. 2015). Besides, detection of BrdU-labelled ssDNA and immunofluorescent staining of RPA showed that the INO80 complex promotes resection and RPA accumulation (Gospodinov et al. 2011; Alatwi and Downs 2015). Importantly, Rad51 foci formation was impaired in the absence of a functional INO80 complex. This defect was rescued in the absence of H2A.Z analogous to budding yeast (Alatwi and Downs 2015; Lademann et al. 2017). Furthermore, p400, which is considered the mammalian equivalent of the SWR1 complex, was shown to contribute to DSB

repair: p400 is required for Rad51 and 53BP1 recruitment to DSBs and NaCl fractionation indicated that it can reduce histone-DNA interactions (Xu et al. 2010; Courilleau et al. 2012). These findings support the utility of budding yeast as a simple model organism to investigate mechanisms conserved in higher eukaryotes. However, the majority of the *S. cerevisiae* genome is euchromatic, whereas higher eukaryotes contain large heterochromatic regions and might require additional regulatory mechanisms.

Telomere deprotection has provided insights in DSB signalling, processing and repair also in higher eukaryotes (Lazzerini-Denchi and Sfeir 2016). Cdc13 is not conserved, but telomeres can be deprotected by deletion of components of the shelterin complex. Combined loss of the dsDNA-binding proteins TRF1 and TRF2 prevents shelterin complex assembly and results in full telomere deprotection (Sfeir and De Lange 2012). Importantly, loss of TRF2 specifically activates the ATM pathway (Celli and De Lange 2005; Karlseder et al. 1999) and upon loss of the ssDNA binding protein POT1 the ATR pathway is activated (Denchi and De Lange 2007; Palm et al. 2009). In S phase the ATR kinase is also activated in the absence of TRF1 due to replication fork stalling during telomere replication (Sfeir et al. 2009).

Not only DSB repair signalling pathways but also downstream factors were investigated after telomere deprotection. In the G1 phase TRF2 deficiency leads to NHEJ and results in telomere fusions, which can be observed by in-gel hybridisation (Dimitrova et al. 2008; Lottersberger et al. 2013). Furthermore, time-lapse microscopy showed that DNA damage foci formation through the dynamic behaviour of chromatin depends on 53BP1 and that NHEJ is inhibited in the absence of 53BP1 (Dimitrova et al. 2008). In addition, TRF2 depletion revealed that 53BP1 counteracts resection by inhibiting CtIP (Lottersberger et al. 2013). The specialised structure of telomeres enables their selective investigation for example by immunofluorescence, a quantitative telomeric chromatin isolation protocol (QTIP) or proteomics of isolated chromatin segments (PICh) (Grolimund et al. 2013; Lottersberger et al. 2013; Bartocci et al. 2014). However, conservation between deprotected telomeres and DSB repair needs to be verified.

A better understanding of resection at deprotected telomeres is valuable for elucidating DSB repair mechanism but may also provide insights into carcinogenesis. Cancer cells must activate a telomere maintenance mechanism to gain replicative immortality and the potential for unlimited proliferation. Most cancer types maintain telomeres through reactivation of

telomerase, but approximately 10-15 % rely on the alternative lengthening of telomeres (ALT) pathway (Dilley and Greenberg 2015) which is based on HR and requires resection (Iskandar et al. 2025; Muoio and Fouquerel 2025). Identifying regulators of resection at telomeres may therefore improve mechanistic understanding of ALT and potentially contribute to the development of therapeutic strategies.

5. Material and Methods

5.1 *S. cerevisiae* strain generation and culture

All budding yeast strains used in this study are derived from the W303 background. Gene deletions and tags were introduced using a PCR-based protocol (Janke et al. 2004). Integrative plasmids were linearised before transformation. The temperature sensitive *cdc13-1* in W303 background was obtained from Brian Luke and corresponds to the allele *cdc13-P371S* (Pires et al. 2023).

For short-term storage, *S. cerevisiae* cells were cultivated on YPD plates (1 % yeast extract, 2 % bacto-peptone, 2 % glucose, 2 % agar) and stored at 4 °C. For long-term storage, overnight cultures were supplemented with 15 % glycerol (v/v) and kept at -80 °C.

For an experiment, cells were streaked on YPD plates from glycerol stocks using a sterile toothpick to inoculate overnight liquid cultures (5 mL). Overnight cultures were diluted into the appropriate volume of medium and grown to exponential phase (OD600 = 0.5-0.7) before the start of an experiment. All *cdc13-1* yeast strains were grown at 23 °C unless indicated otherwise, whilst all other strains were grown at 30 °C. In general, YP-medium (1 % yeast extract, 2 % bacto-peptone) supplemented with 2 % glucose (YPD) was used for cultivation. For experiments using *pGAL1-10-AsiSI*, YP-medium supplemented with 2 % raffinose (YPR) was used for cultivation and conditional expression was achieved by addition of galactose (2 % final concentration). For M-phase arrest, cultures were treated with 5 µg/mL nocodazole (Sigma, M1404) for 3 h before the start of the experiment. Degradation of mIAA7-tagged proteins (Dna2, Sth1, Snf2) was achieved by treatment with 1 mM IAA (Sigma, I3750) for 1 h before starting the experiment.

Table 2: List of *S. cerevisiae* strains used in this study.

Number	Description	Full genotype
#6940	*WT*	*MATa leu2-3,112 trp1-1 can1-100 ura3-1 ade2-1 his3-11,15 RAD5*
#6941	*cdc13-1*	*MATa leu2-3,112 trp1-1 can1-100 ura3-1 ade2-1 his3-11,15 RAD5 cdc13-1*
#6963 (6964)	*cdc13-1 exo1Δ*	*MATa leu2-3,112 trp1-1 can1-100 ura3-1 ade2-1 his3-11,15 RAD5 cdc13-1 exo1Δ::his3MX6*
#7408	*cdc13-1 sgs1Δ*	*MATa leu2-3,112 trp1-1 can1-100 ura3-1 ade2-1 his3-11,15 RAD5 cdc13-1 TIR1-9myc::URA3 sgs1::HphNT1*
#6998 (7385)	*cdc13-1 exo1Δ sgs1Δ*	*MATa leu2-3,112 trp1-1 can1-100 ura3-1 ade2-1 his3-11,15 cdc13-1 exo1Δ::natNT2 sgs1Δ::kanMX4*
#7350	*cdc13-1 dna2-mIAA7*	*MATa leu2-3,112 trp1-1 can1-100 ura3-1 ade2-1 his3-11,15 RAD5 cdc13-1 TIR1-9myc::URA3 dna2-mIAA7-3Flag-his3MX6*
#7409 (7410)	*cdc13-1 dna2-mIAA7 sgs1Δ*	*MATa leu2-3,112 trp1-1 can1-100 ura3-1 ade2-1 his3-11,15 RAD5 cdc13-1 TIR1-9myc::URA3 dna2-mIAA7-3Flag-his3MX6 sgs1::HphNT1*
#7367	*cdc13-1 dna2-mIAA7 exo1Δ*	*MATa leu2-3,112 trp1-1 can1-100 ura3-1 ade2-1 his3-11,15 RAD5 cdc13-1 TIR1-9myc::URA3 dna2-mIAA7-3Flag-his3MX6 exo1Δ::TRP1*
#7166	*cdc13-1 arp8Δ*	*MATa leu2-3,112 trp1-1 can1-100 ura3-1 ade2-1 his3-11,15 RAD5 cdc13-1 arp8Δ::URA3*
#6990	*cdc13-1 swr1Δ htz1Δ*	*MATa leu2-3,112 trp1-1 can1-100 ura3-1 ade2-1 his3-11,15 RAD5 cdc13-1 swr1Δ::his3MX6 htz1Δ::TRP1*
#7168	*cdc13-1 arp8Δ swr1Δ htz1Δ*	*MATa leu2-3,112 trp1-1 can1-100 ura3-1 ade2-1 his3-11,15 RAD5 cdc13-1 swr1Δ::his3MX6 htz1Δ::TRP1 arp8Δ::URA3*
#7353 (7354)	*cdc13-1 sth1-mIAA7*	*MATa leu2-3,112 trp1-1 can1-100 ade2-1 his3-11,15 RAD5 cdc13-1 TIR1-9myc::URA3 sth1-mIAA7-3Flag-his3MX6*
#7399 (7398)	*cdc13-1 snf2-mIAA7*	*MATa leu2-3,112 trp1-1 can1-100 ade2-1 his3-11,15 RAD5 cdc13-1 TIR1-9myc::URA3 snf2-mIAA7-3Flag-kanMX*
#7400	*cdc13-1 sth1-mIAA7 snf2-mIAA7*	*MATa leu2-3,112 trp1-1 can1-100 ade2-1 his3-11,15 RAD5 cdc13-1 TIR1-9myc::URA3 sth1-mIAA7-3Flag-his3MX6 snf2-mIAA7-3Flag-kanMX*
#6870	*AsiSI*	*MATa pGal-AsiSI::URA3*
#4079	*AsiSI arp8Δ*	*MATa pGal-AsiSI::URA3 arp8Δ::natNT2*
#6986	*AsiSI swr1Δ htz1Δ*	*MATa pGal-AsiSI::URA3 htz1Δ::hphNT1 swr1Δ::his3MX6*
#7055	*AsiSI arp8Δ swr1Δ htz1Δ*	*MATa pGal-AsiSI::URA3 arp8Δ::natNT2 htz1Δ::hphNT1 swr1Δ::his3MX6*

5.1.1 Plasmid amplification

Chemically competent *E. coli* cells were prepared according to the Inoue protocol (Inoue et al. 1990). In brief, cells were grown at 18 °C to an OD600 of approximately 0.55 and cooled to 4 °C. After washing and resuspension in ice-cold Inoue transformation buffer (10 mM PIPES, pH 6.7, 250 mM KCl, 55 mM $MnCl_2$, 15 mM $CaCl_2$) supplemented with 7.5 % (v/v) DMSO, aliquots (50 µL) were snap-frozen in liquid nitrogen and stored at -80°C.

For bacterial transformation, 50 µL of competent XL-1 blue (Stratagene) cells were thawed on ice and mixed with 1 µL of plasmid (approximately 10 ng/µL). After incubation for 15 min on ice, cells were heat-shocked at 42 °C for 45 s. The cells were incubated on ice for 5 min and recovered in 1 mL LB medium (1 % tryptone, 0.5 % yeast extract, 1 % NaCl) at 37 °C for 1 h. Afterwards, cells were plated on selective LB-plates (1 % tryptone, 0.5 % yeast extract, 1 % NaCl, 1.5 % agar) supplemented with the appropriate antibiotic (100 µg/mL ampicillin, 30 µg/mL kanamycin, 34 µg/mL chloramphenicol).

For plasmid DNA extraction, *E. coli* cells were inoculated in 5 mL LB medium supplemented with the appropriate antibiotic (100 µg/mL ampicillin, 30 µg/mL kanamycin, 34 µg/mL chloramphenicol) overnight at 37 °C with shaking (220 rpm) and the Monarch Spin Plasmid Miniprep Kit (NEB) was used according to the manufacturer´s instructions.

Table 3: *E. coli* plasmids used in this study.

Number	Description	Reference/Source
ev53	pFA6a-His3	(Janke et al. 2004)
ev54	pFA6a-hphNT	(Janke et al. 2004)
ev55	pFA6a-natNT2	(Janke et al. 2004)
ev56	pFA6a-kanMX6	(Janke et al. 2004)
ev155	pFA6a-IAA7-3xFLAG-kanMX6	Schuck lab
ev156	pFA6a-IAA7-3xFlag-His3	Schuck lab
pNHK53	OsTir1-9myc	Pfander lab

5.1.2 Standard polymerase chain reaction (PCR)

Cassettes for introducing deletions or tags into competent yeast cells were amplified using a standard PCR-based strategy (Janke et al. 2004). Primers for cassette amplification contained a sequence annealing to the cassette and a flanking sequence which was homologous to the desired chromosomal locus in order to allow for chromosomal integration by homologous recombination. For gene deletions, the selective marker cassette replaced part of the coding sequence of the target gene. For C-terminal tagging, the tag was integrated immediately upstream of the native stop codon to generate an in-frame fusion with the protein of interest. PCR amplification was performed using the following components and the CASTORP PCR program:

Components of a standard PCR reaction:

2 µL template
3.2 µL primer 1 (10 µM)
3.2 µL primer 2 (10 µM)
1.75 µL dNTPs (10 mM, NEB-N0447L)
10 µL HF-buffer (NEB-B0518S)
1 µL DMSO (NEB-B0518S)
0.5 µL Phusion polymerase
28.35 µL water

CASTORP PCR program:

(1) 95 °C for 4 min
(2) 95 °C for 1 min
(3) 45 °C for 35 s
(4) 72 °C for 1:40 min
repeat steps (2)-(4) for 10 cycles
(5) 95 °C for 1 min
(6) 54 °C for 30 s
(7) 72 °C for 1:40 min
repeat steps (5)-(7) for 20 cycles and increase extension time by 20 s each cycle
(8) hold at 4 °C

5.1.3 Restriction digestion

For plasmid linearisation 2 µg of DNA were digested in a 30 µL reaction with 5 U of the respective restriction enzyme(s) (NEB) according to the manufacturer's instructions for 1 h at 37 °C.

5.1.4 Ethanol precipitation of DNA

Ethanol precipitation was performed to purify DNA containing solutions obtained from restriction digestion or cassette amplification prior to transformation. DNA was precipitated by adding 0.1 volumes 3 M sodium acetate pH 4.8 and 2.5 volumes absolute ethanol, followed by incubation for at least 30 min at -20 °C. The precipitated DNA was pelleted by centrifugation (15 min, max speed) and dried for at least 30 min at room temperature. Dried DNA was resuspended in an appropriate amount of water.

5.1.5 Preparation of competent *S. cerevisiae* cells

Yeast cells were inoculated in YPD and grown to exponential phase at an OD600 between 0.6 and 0.9 (corresponding to approximately 1.8×10^7 yeast cells). After pelleting (3 min, 3500 rpm), cells were washed with sterile H_2O and SORB buffer (100 mM lithium acetate, 10 mM Tris-HCl pH 8.0, 1 mM EDTA pH 8.0, 1 M sorbitol). The pellet was resuspended in SORB buffer (8 µL buffer per 1 mL yeast culture) and supplemented with denatured herring sperm DNA (10 mg/mL, Invitrogen) in a 10:1 ratio. Competent yeast cells were aliquoted (100 µL) and stored at -80 °C.

5.1.6 Transformation of *S. cerevisiae* cells

10 µl of precipitated PCR product or 1 µg of linearised plasmid was added to 100 µl of competent yeast cells (corresponding to 19×10^7 cells) and mixed with 6 volumes of PEG buffer (100 mM lithium acetate, 10 mM Tris-HCl pH 8.0, 1 mM EDTA pH 8.0, 40 % (w/v) PEG-3350). After incubation for 30 min with shaking at room temperature, DMSO was added to a final concentration of 10 %. Cells were heat-shocked at 42 °C for 15 min. Cells were pelleted (3 min, 3500 rpm) and recovered in YPD for 3 h at 30 °C or in case of a strain containing a *cdc13-1* mutation for 5 h at 23 °C. When an auxotrophic marker was introduced, cells were not recovered but washed with H_2O and directly plated on selective plates lacking the corresponding amino acid. For antibiotic selection, YPD plates supplemented with 200 mg/L geneticin G418 or 500 mg/L hygromycin B or 100 mg/L nourseothricin were used. Genotyping of the single colonies was verified via colony PCR.

5.1.7 Colony PCR

Cassette integration was verified by colony PCR using a forward primer annealing to a genomic sequence upstream of the insertion site and a reverse primer annealing within the inserted sequence. This primer combination allows amplification only when the cassette has been correctly integrated at the target locus. Single colonies obtained after transformation were tested by transferring a small amount of yeast cells from each colony into separate PCR tubes. 40 µL of PCR reaction mix was added to each tube and the cell suspension was mixed before running the following PCR program:

Reaction recipe (40 µL reaction):

4 µL 10x colony PCR buffer (200 mM Tris pH 8.8, 100 mM $(NH4)_2SO_4$, 100 mM KCl, 25 mM $MgCl_2$)
1.5 µL dNTPs (each 10 mM stock, 0.38 mM final concentration)
4 µL betaine (5 M stock containing 0.5 % orange G, filtered)
2 µL forward primer (10 µM stock, 0.5 µM final concentration)
2 µL reverse primer (10 µM stock, 0.5 µM final concentration)
26 µL water
0.5 µL Taq Polymerase (Sigma)

PCR program:

(1) 97 °C for 7 min
(2) 95 °C for 30 s
(3) 50 °C for 30 s
(4) 72 °C, 1 min/kb
Go to step (2) for 40 cycles
(5) 72 °C for 5 min
(6) hold at 10 °C

5.1.8 Agarose gel electrophoresis

Agarose gel electrophoresis was used to verify cassette amplification, confirm restriction digestion and determine the size of cPCR products. The DNA samples were mixed in a 1:5 ratio with DNA loading buffer (0.5 % SDS, 0.25% orange G, 25 % glycerol, 25 mM EDTA pH 8.0) and loaded on a 1 % agarose gel containing ethidium bromide (0.5 µL / 10 mL gel) in TAE buffer (40 mM Tris-HCl pH 7.6, 20 mM acetic acid, 1 mM EDTA pH 8.0). The gel was run at 100 V for 20 min in TAE buffer and the separated bands were visualised using a ChemiDoc MP imaging system (BioRad).

5.1.9 Mating, sporulation and tetrad dissection

For mating, 100 µL of two overnight cultures of strains with opposite mating types were added to 5 mL YPD and incubated for 4 h at 30 °C. Zygotes were spotted on warm YPD plates, picked using the micromanipulator of a tetrad microscope (Singer MSM 300 system) and incubated at 30 °C for 3-4 days until they formed visible colonies. Sporulation was performed by streaking diploids on sporulation plates (0.2 % yeast extract, 1.2 % potassium acetate, 0.08 % glucose, 1.6 % agar, 1000 mg/L Phe, 400 mg/L Ade, Ura, 200 mg/L His, Leu, Lys, Trp, Met, Arg, 80 mg/L Tyr) and incubation at 30 °C for 3 days. For tetrad dissection, the asci from the sporulation plates were resuspended in water, mixed 1:1 with a zymolyase solution (0.5 mg/mL zymolyase, 0.9 M sorbitol, 100 mM EDTA pH 8.0, 100 mM Tris-HCl pH 8.0, 50 mM dithiothreitol) and incubated for 10 min at room temperature to release the tetrads. Tetrad dissection was performed using the micromanipulator of a tetrad microscope on YPD plates and followed by an incubation at 30 °C. Genotype and mating type of each spore were determined by replica-plating on selective and mating type tester plates.

The mating type tester plates were freshly prepared by resuspending one big colony of RH448 (MAT A) or RC757 (MAT α) in 1 mL sterile H_2O. This cell suspension was added to 50 mL of a 1 % agar solution and a thin layer poured onto a YPD plate. When dry, replica plating was performed and after incubation for 1-2 days the mating type was determined through formation of a halo.

5.2 Growth assays

Saturated yeast cultures, grown at 23 °C due to the *cdc13-1* mutation, were diluted to 1 OD600 and six five-fold serial dilutions were spotted onto YPD plates (2 % glucose). Photographs were taken after 48 h incubation at the indicated temperatures. To test the influence of degradation of mIAA7-tagged proteins, YPD plates containing 1 mM IAA (Sigma, I3750) were used in addition to YPD control plates. For each experiment, two biological replicates were performed each including two technical repetitions for each condition.

5.3 Flow cytometry

Yeast cells were pelleted and resuspended in fixation buffer (70 % ethanol, 50 mM Tris-HCl, pH 8.0) to be stored at 4 °C for at least overnight. Fixed cells were washed with 50 mM Tris-HCl, pH 8.0 and then treated with 520 µL RNase A solution consisting of 500 µL 50 mM Tris-HCl, pH 8.0 and 20 µL RNase A (Sigma, R4875; 10 mg/mL in 10 mM Tris-HCl, pH 8.0, 10 mM $MgCl_2$) for at least 4 h at 37 °C. Cells were pelleted and treated with 220 µL Proteinase K solution consisting of 200 µL 50 mM Tris-HCl, pH 8.0 and 20 µL Proteinase K (Sigma, P2308; 20 mg/mL in 10 mM Tris-HCl, pH 8.0) for 30 min at 50 °C. Finally, cells were resuspended in 500 µL 50 mM Tris-HCl, pH 8.0 and sonicated. The final cell suspensions were diluted 1:20 with SYTOX Green solution (Invitrogen, S7020, 1 µM in 50 mM Tris-HCl, pH 8.0) and measured using a MACSQuant Analyzer 10 Flow Cytometer (Milteny Biotec). Data containing 30 000 events per sample were analysed and plotted using FlowJo as previously described (Reusswig et al. 2016) (version 10.10.0) (FlowJo LLC).

5.4 SDS-PAGE and western blot

2×10^7 yeast cells (corresponding to 1 mL of cell suspension at OD600 = 1) were harvested at the indicated timepoints and snap-frozen in liquid nitrogen. For alkaline lysis, yeast pellets were resuspended in 1 mL of ice-cold water, 150 µL 1.85 M NaOH and 7.5 % β-mercaptoethanol and incubated on ice for 15 min. 150 µL of 55 % trichloroacetic acid (TCA, Roth, 8789.2) were added and samples were incubated for 10 min on ice before centrifugation. Pellets were resuspended in 50 µL HU buffer (8 M urea, 5 % SDS, 200 mM Tris-HCl pH 6.8, 1.5 % DTT, traces of bromophenol blue) and heated for 10 min at 65 °C.

Samples were run on NuPAGE 3-8 % Tris-Acetate acrylamide gels (Invitrogen, 30131968) with MOPS buffer (50 mM MOPS, 50 mM Tris base, 0.1 % SDS, 1 mM EDTA) for 1.5 h at 180 V. To resolve Rad53 phospho-shifts, samples were run on 10 % acrylamide gels in SDS buffer (25 mM Tris base, 192 mM glycine, 0.1 % SDS) for 2.5 h at 150 V at 4 °C. The 10 % acrylamide gels were poured using the BioRad mini gel system with 0.75 mm spacers. The separating gel mix was filled to approximately 80 % of the gel and covered with H_2O until polymerized. After discarding the H_2O layer, stacking gel was filled on top and a 15-fold comb inserted. Gel mixes were prepared as follows:

Separating gel mix for 4 BioRad mini gels (10 %):

40 % acrylamide	5 mL
2 % bis-acrylamide	1.32 mL
1.5 M Tris-HCl pH 8.8	5 mL
10 % SDS	200 µL
H_2O	8.7 mL
TEMED	25 µL
10 % APS	100 µL

Stacking gel for 4 BioRad mini gels:

40 % acrylamide	640 µL
2 % bis-acrylamide	350 µL
1.0 M Tris-HCl pH 6.8	625 µL
10 % SDS	50 µL
H_2O	3.35 mL
TEMED	20 µL
10 % APS	40 µL

For western blotting, proteins were transferred to a nitrocellulose membrane using transfer buffer (48 mM Tris base, 39 mM glycine, 0.0375 % SDS, 20 % methanol) at 4 °C for 90 min at 90 V. Incubation with the primary antibody was performed overnight at 4 °C while shaking. Membranes were washed three times for 5 min with western wash buffer (0.2 % NP-40 in TBS). Secondary HRP-coupled antibodies were incubated for 2 h at room temperature. Membranes were washed three times for 10 min and chemiluminescence was detected using Pierce ECL reagents (Thermo Fisher Scientific, 32106) and ChemiDoc MP imaging system (BioRad). All dilutions were performed in Superblotto solution (2.5 % skim milk powder, 0.5 % BSA, 0.5 % NP-40, 0.1 % Tween in TBS).

For semi-quantitative western blot analysis three 2-fold serial dilutions were blotted. Background subtracted signal intensities of the protein of interest (AsiSI-3HA) and the loading control (Cdc48) were quantified using Fiji (ImageJ 1.54p) and their ratio plotted.

Table 4: List of antibodies.

Number	Antibody name	Company	Host	Dilution
a0047	anti-Rad53	abcam: ab104232	Rabbit	1:2000
a0030	anti-PGK1 (22C5D8)	abcam: ab113687, LOT:GR3286258-2	Mouse	1:5000
a0008	anti-FLAG	Sigma: F1804	Mouse	1:1000
a0005	anti-HA	Covance (clone 16B12)	Mouse	1:2000
a0052	anti-Cdc48	from Jentsch lab	Rabbit	1:10000

5.5 Quantitative amplification of ssDNA (QAOS)

Telomere deprotection of *cdc13-1* strains was induced by temperature shift to 30 °C. With the exception of the long-time course experiment of Figure 33C and D, samples were taken 30, 60 and 120 min after temperature shift. For Figure 33C and D, samples were taken 2, 4 and 6 h after temperature shift. Approximately 1.6×10^9 yeast cells (corresponding to 80 mL of cell suspension at OD600 = 1) were harvested, washed in TE20 buffer (10 mM Tris pH 8.0, 20 mM EDTA) and frozen in liquid nitrogen to be stored at -80 °C until further processing. The pellets were resuspended in 1.8 mL freshly prepared Buffer Y1 (1 M Sorbitol, 0.1 M EDTA, 14 mM β-mercaptoethanol) supplemented with 40 µL Zymolyase 20T (100 mg/mL in n2 buffer (1.2 M Sorbitol, 50 mM EDTA, 50 mM Sodium citrate phosphate buffer pH = 5.6 (2.68 % (w/v) Na_2HPO_4, 0.92 % (w/v) citric acid))). After incubation for 40 min at 37 °C with regular inversion, effective spheroplasting (>90 %) was monitored by microscopic examination and samples were centrifuged at 4 °C. Spheroplasts were resuspended in 200 µL breaking buffer (2 % Triton X-100, 1 % SDS, 100 mM NaCl, 10 mM Tris Cl pH 8.0, 1 mM EDTA) and transferred to a phase-lock-tube. 200 µL phenol/chloroform/isoamyl alcohol was added and samples were incubated for 15 min with regular inversion. 200 µL TE buffer (10 mM Tris pH 8.0, 1 mM EDTA) was added, samples mixed by inversion and centrifuged (5 min, 1400 rpm). Aqueous layer was transferred to a clean tube and 1 mL of 100 % ethanol added. After inversion, samples were centrifuged (3 min, 1400 rpm) and pellets were resuspended in 400 µL TE buffer. 30 µL DNase-free RNase A (1 mg/mL) was added and samples were incubated for 5 min at 37 °C. 5 µL Proteinase K (1 mg/mL) was added and samples incubated for 1 h at 37 °C. gDNA was precipitated by adding 10 µL ammonium acetate (4 M) and 1 mL ethanol (100 %). The DNA pellet was dried and resuspended in 40 µL TE20 buffer for 1 h at RT.

For QAOS ssDNA tagging reaction, 25 ng of gDNA (0.5 ng/µL final concentration) were treated with 25 µL Q5 High-Fidelity 2X Master Mix (NEB, M0942), 2.5 µL of the corresponding tagging oligo (final concentration 500 nM) and 17.5 µL sterile water. *PAC2* locus is used as a control and does not require tagging, therefore a mock tagging reaction was performed with sterile water instead of tagging oligos. Tagging reactions were performed at 40 °C for 5 min and 72 °C for 5 min. After tagging, qPCR was performed to determine ssDNA signal at telomeres by adding 2.5 µL forward oligo (10 µM), 2.5 µL reverse oligo (10 µM), 0.2 µL Blue Dye (100x, 172555 BioRad) and 0.5 µL dsGreen (100 x, 11010 Lumiprobe). Each sample was divided in 3 technical replicates (10 µL) in a 384 multiwell plate and run in a LightCycler480 (Roche) with the following settings: activation at 98 °C for 3 min and 40 amplification cycles of 98°C for 10 s, 64 °C for 5 s and 72 °C for 10 s. To ensure specific amplification, melting curve analysis was performed (65 °C – 97 °C ramp rate 0.11 °C/s).

Table 5: List of oligos used for QAOS.

Number	Name	Sequence
BP8618	PAC2 fwd	AATAACGAATTGAGCTATGACACCAA
BP8619	PAC2 rev	AGCTTACTCATATCGATTTCATACGACTT
BP8620	PDA1 tagging	AACCAGCGCAGCGGCATGtgtgatgatggaa
BP8621	PDA1 fwd	TGGAGATGGCTTGTGACGCCTTG
BP8622	PDA1 rev	AACCAGCGCAGCGGCATGTGT
BP8626	YER186C tagging	GATCTCGAGCTCGATATCGGATCCatttacggcgga
BP8627	YER186C fwd	AATCTCGCCTAACAAAAAAAGGCTTCTTAGTG
BP8628	YER186C rev	GATCTCGAGCTCGATATCGGATCCATT
BP8635	Y´5000 tagging	TGCCCTCGCATCGCTCTCgaaacaaagtcagtga
BP8636	Y´5000 fwd	GTCCTGGAACGTTGTCACGAAAAAGC
BP8637	Y´5000 rev	TGCCCTCGCATCGCTCTCGAA

Ct values were calculated via 2nd derivative analysis and ssDNA/dsDNA standard curves were used to translate the Ct values into the percentage of ssDNA. ssDNA was generated by boiling (4 cycles: 98 °C for 7 min and 25 °C for 30 s) and mixed with different amounts of dsDNA. For *PAC2* locus, the actual DNA amount of the sample was calculated from the measured Ct value and the dilution series to determine the correction factor for normalisation of the ssDNA percentage. The determined ssDNA amount was multiplied by the correction factor and plotted. Using the same strains, a shift in experimental values of the 2 h samples was observed when comparing short and long-time course experiments of Figure 33A and B with Figure 33C

and D, which were conducted with a temporal gap of 4 months and by two different researchers.

Significant differences of tested mutants compared to the *cdc13-1* control strain were determined using a linear mixed-effects model implemented in RStudio using the lme4 package. Specifically, we assumed linear growth of ssDNA over the time course of the experiment and conducted linear regression, as this fitted best to the observed increase in ssDNA. The linear mixed-effects model considers the different timepoints and yeast strains as fixed effects, while variations between biological replicates are considered random effects. The formula: lmer(percentage ~ time0 + time0:yeast_strain + (0 + time0 | replicate)) was used, assuming all strains have the same amount ssDNA at the 0 h timepoints, but then accumulate ssDNA with different speeds. The calculated mean slope values for each strain are listed in Table S1. The significances between the *cdc13-1* control strain and the mutants are indicated with * in the figures: p-value < 0.05 corresponds to *, p-value < 0.01 corresponds to ** and p-value < 0.001 corresponds to ***.

5.6 Analysis of DSB resection by strand-specific sequencing

Exponentially growing cells containing *pGAL1-10 AsiSI* grown in YP-Raffinose were treated with nocodazole (5 µg/mL) for 3 h to induce mitotic cell cycle arrest. After taking samples for the 0 h timepoint, galactose was added to 2 % final concentration to induce AsiSI expression and DSB induction. Samples for flow cytometry, western blotting and nanopore sequencing were collected for each timepoint in addition to the samples for strand-specific sequencing. Cells were processed as previously described (Peritore et al. 2021). Briefly, 100 mL samples were crosslinked with para-formaldehyde (1 % final concentration) for 16 min before quenching with glycine. For each timepoint, 1.6×10^9 yeast cells (corresponding to 80 mL of cell suspension at OD600 = 1) were harvested, washed twice in cold PBS and snap-frozen. Cell lysis was performed by resuspension in 800 µl lysis buffer (50 mM HEPES KOH pH 7.5, 150 mM NaCl, 1 mM EDTA, 1 % Triton X-100, 0.1 % Na-deoxycolate, 0.1 % SDS) supplemented with protease inhibitors (10 mM Pefabloc SC (Sigma-Aldrich) and 1 cOmplete protease inhibitor tablet (Roche) per 50 mL lysis buffer). Silica beads were added and lysis was performed using a beat beater (MM301, Retsch GmbH) for 6 cycles of 3 min ON / 3 minutes OFF. After centrifugation, the insoluble chromatin fraction was resuspended in 1 mL cold lysis buffer

containing protease inhibitors and sonicated using Diagenode Bioruptor UCD-200 to shear the DNA in 200-500 bp fragments. After centrifugation, the cleared lysate was diluted with 1 mL (1:1) lysis buffer containing protease inhibitors. 20 µL (1 %) was taken as input sample and 800 µL (40 %) for chromatin immunoprecipitation. 2 µg of antibody (anti-H3 Abcam ab195277 or anti-H2A.Z Active Motif 39647) was added to each ChIP sample and rotated for 2 h at 4 °C. After antibody incubation, 20 µL of Protein A Dynabeads (Invitrogen) were added to each sample and incubated for 30 min at 4 °C with rotation. For washing 1 mL of buffer was added to the samples and soaked off using a magnetic rack. Three washes with lysis buffer (50 mM HEPES KOH pH 7.5, 150 mM NaCl, 1 mM EDTA, 1 % Triton X-100, 0.1 % Na-deoxycolate, 0.1 % SDS), one with high salt lysis buffer (50 mM HEPES KOH pH 7.5, 500 mM NaCl, 1 mM EDTA, 1 % Triton X-100, 0.1 % Na-deoxycolate, 0.1 % SDS), one with ChIP wash buffer (10 mM Tris-HCl pH 8.0, 250 mM LiCl, 1 mM EDTA pH 8.0, 0.5 % NP-40, 0.5 % Na-deoxycolate) and one with TE buffer (10 mM Tris-HCl pH 8.0, 1 mM EDTA pH 8.0) were performed. For elution, 110 µL of ChIP elution buffer (50 mM Tris-HCl pH 8.0, 10 mM EDTA pH 8.0, 1 % SDS) was added to the samples and incubated for 10 min at 65 °C while shaking. 60 µL TE buffer was added to the eluates and 100 µL ChIP elution buffer and 80 µL TE buffer were added to each input sample. All samples were incubated for 45 min at 37 °C with 5 µL RNase A (10 mg/mL). To remove proteins, 20 µL Proteinase K (20 mg/mL) was added and samples were incubated for 1 h at 42 °C. Protein crosslinks were reversed by incubation at 65 °C overnight. DNA fragments were purified using the QIAquick PCR purification kit 250 (QIAGEN 28106) and eluted in 25 µL water.

For strand-specific library preparation, the Accel-NGSR 1S Plus Library Kit was used according to the manufacturer's instructions, with 2 ng of DNA and 14 cycles of library amplification. For clean-up, SPRIselect beads were used. Paired-end Illumina sequencing with 75 cycles per read was performed at the sequencing facility of the MPIB (Martinsried, Germany). The experiment was performed twice, showing similar results.

For data analysis, bowtie2 was used to map reads to the *S. cerevisiae* R64 (*sacCer3)* genome and multi-mapping reads were excluded using SAMtools. Using RStudio (version 4.2.3), coverage was adjusted to the same amount for all samples by randomly excluding excessive reads. Forward and reverse coverage was calculated separately, samples were normalised to the 0 h timepoint and the mean coverage around 13 AsiSI sites (Peritore et al. 2021) was plotted in a window over 40 kb.

5.7 Analysis of DSB induction by nanopore sequencing

1.6×10^9 yeast cells (corresponding to 80 mL of cell suspension at OD600 = 1) were harvested, washed in TE20 (10 mM Tris pH 8.0, 20 mM EDTA) and snap frozen in liquid nitrogen to be stored at -80 °C until further processing. gDNA was extracted analogously to QAOS. Before library preparation, an additional purification step using AMPure XP beads (A63881 Beckman Coulter) was performed by adding 1.8-fold bead volume, incubation for 5 min, precipitation with a magnetic rack and two washes with 80 % ethanol before eluting with water for 10 min. Libraries were prepared according to the manufacturer's instructions for the Native Barcoding Kit 24 V14 (SQK-NBD114.24). Briefly, DNA repair and end-prep was performed by treating 800-1000 ng of gDNA with FFPE DNA Repair Mix (NEB: M6630S and E6622A) and Ultra II End-Prep Enzyme Mix (NEB: E7646A and E7647A), 5 min at 20 °C and 5 min at 65 °C. Then, native barcode ligation was performed to allow for multiplexing by ligating End-prepped DNA with Native Barcodes (NB01-24) using Blunt/TA Ligase Master Mix (NEB: M0367S) for 20 min at RT. Finally, barcoded DNA was ligated to Native Adapter using Quick T4 DNA Ligase (NEB: M2200S and B2200S) for 20 min at RT. Nanopore sequencing was performed using R10 Flowcells in a MinION Mk1B sequencer with standard settings. Basecalling was performed using Dorado basecaller (Dorado 7.9.8) integrated in MinKNOW using high-accuracy basecalling model (dna_r10.4.1_e8.2_400bps_5khz). Unaligned bam files were mapped to the *S. cerevisiae* R64 (*sacCer3)* reference genome using Epi2me workflow "*wf alignment*" using default settings. Mean coverage of the 2 bp DNA sequence (AT of the AsiSI cut site) was determined, as this sequence is lost from nanopore reads upon cutting. For total coverage, the mean value of two genomic windows of 5 kb to the left and right of the DSB was determined. To avoid artefacts related to DNA end resection, the windows were displaced 5 kb from the centre of the AsiSI cut site, thus covering the area between 5 and 10 kb from the DSB. The percentage of uncut DNA is given by dividing the mean coverage of the 2 bp AsiSI sequence by the mean coverage of the windows around the DSB. The cutting efficiency is 1 minus the uncut DNA proportion. Both biological replicates of the strand-specific sequencing experiments were analysed via nanopore sequencing to measure the corresponding cutting efficiencies.

5.8 Statistical analysis and coding

All biological replicates were generated by either using a different clone with the same genotype or independent cultivation of the same clone. For QAOS experiments the mean of three technical replicates was calculated for each biological replicate. Means across biological replicates were obtained and a linear mixed-effects model was used to test for significance. Significance is indicated in the respective figures: p-value < 0.05 corresponds to *, p-value < 0.01 corresponds to ** and p-value < 0.001 corresponds to ***.

All code used in this study was written in RStudio R4.2.3 using the packages BSgenome.Scerevisiae.NIH.sacCerW303, readxl, writexl, lme4, pbkrtest, lmerTest, emmeans, ggsignif, GenomicRanges, GenomicAlignments, rtracklayer, Rsamtools, dplyr, tidyr, tidyverse, reshape2, parallel, grid, gridExtra, cowplot, ggplot2 and Cairo.

5.9 Data availability

The sequencing data generated in this study have been deposited in the NCBI GEO database under accession code GSE325557.

5.10 AI usage

The whole text was written by me. Phrasing and clarity were improved with support from an AI-based language model (ChatGPT).

6. Supplementary

Table S1: List of slope values of mixed-effects models

	Slope values at locus:		
Strain	**PDA1**	**YER186C**	**Y´5000**
cdc13-1	0.693	2.253	5.232
cdc13-1 exo1Δ	0.524	1.204	2.616
cdc13-1 sgs1Δ	0.793	2.086	4.664
cdc13-1 exo1Δ sgs1Δ	0.29	0.698	2.208
cdc13-1	0.693	2.253	5.232
cdc13-1 dna2-mIAA7	0.69	1.845	3.205
cdc13-1 dna2-mIAA7 sgs1Δ	0.694	2.09	4.181
cdc13-1 dna2-mIAA7 exo1Δ	0.485	0.744	1.242
cdc13-1 0h	0.415	2.178	6.200
cdc13-1 arp8Δ 0.5h	0.305	1.914	6.030
cdc13-1 swr1Δhtz1Δ 1h	0.471	1.675	5.005
cdc13-1 arp8Δ swr1Δhtz1Δ 2h	0.527	2.062	5.690
cdc13-1 0h	0.497	1.137	2.159
cdc13-1 arp8Δ 2h	0.535	1.126	1.992
cdc13-1 swr1Δhtz1Δ 4h	0.566	0.955	1.639
cdc13-1 arp8Δ swr1Δhtz1Δ 6h	0.543	1.049	2.059
cdc13-1	0.391	1.873	5.938
cdc13-1 sth1-mIAA7	0.241	0.449	0.574
cdc13-1 snf2-mIAA7	0.119	0.294	0.045
cdc13-1 sth1-mIAA7 snf2-mIAA7	0.006	0.442	0.064
cdc13-1 exo1Δ	0.365	1.551	2.687
cdc13-1 exo1Δ dna2-mIAA7	0.326	0.651	1.313
cdc13-1 exo1Δ sgs1Δ	0.131	0.606	2.284

7. References

Adkins, Nicholas L., Hengyao Niu, Patrick Sung, and Craig L. Peterson. 2013. 'Nucleosome Dynamics Regulates DNA Processing'. *Nature Structural & Molecular Biology* 20 (7): 836–42. https://doi.org/10.1038/nsmb.2585.

Alatwi, Hanan E., and Jessica A. Downs. 2015. 'Removal of H2A.Z by INO80 Promotes Homologous Recombination'. *EMBO Reports* 16 (8): 986–94. https://doi.org/10.15252/embr.201540330.

Amiard, Simon, Michel Doudeau, Sébastien Pinte, et al. 2007. 'A Topological Mechanism for TRF2-Enhanced Strand Invasion'. *Nature Structural & Molecular Biology* 14 (2): 147–54. https://doi.org/10.1038/nsmb1192.

Anderson, E. M. 2002. 'Delineation of the High-Affinity Single-Stranded Telomeric DNA-Binding Domain of Saccharomyces Cerevisiae Cdc13'. *Nucleic Acids Research* 30 (19): 4305–13. https://doi.org/10.1093/nar/gkf554.

Aylon, Yael, Batia Liefshitz, and Martin Kupiec. 2004. 'The CDK Regulates Repair of Double-strand Breaks by Homologous Recombination during the Cell Cycle'. *The EMBO Journal* 23 (24): 4868–75. https://doi.org/10.1038/sj.emboj.7600469.

Balajee, Adayabalam S., and Charles R. Geard. 2004. 'Replication Protein A and γ-H2AX Foci Assembly Is Triggered by Cellular Response to DNA Double-Strand Breaks'. *Experimental Cell Research* 300 (2): 320–34. https://doi.org/10.1016/j.yexcr.2004.07.022.

Baldi, Sandro, Philipp Korber, and Peter B. Becker. 2020. 'Beads on a String—Nucleosome Array Arrangements and Folding of the Chromatin Fiber'. *Nature Structural & Molecular Biology* 27 (2): 109–18. https://doi.org/10.1038/s41594-019-0368-x.

Bantele, Susanne C. S., Pedro Ferreira, Dalia Gritenaite, Dominik Boos, and Boris Pfander. 2017. 'Targeting of the Fun30 Nucleosome Remodeller by the Dpb11 Scaffold Facilitates Cell Cycle-Regulated DNA End Resection'. *eLife* 6 (January): e21687. https://doi.org/10.7554/eLife.21687.

Bantele, Susanne C. S., Michael Lisby, and Boris Pfander. 2019. 'Quantitative Sensing and Signalling of Single-Stranded DNA during the DNA Damage Response'. *Nature Communications* 10 (1): 944. https://doi.org/10.1038/s41467-019-08889-5.

Bantele, Susanne C. S., and Boris Pfander. 2019. 'Nucleosome Remodeling by Fun30 SMARCAD1 in the DNA Damage Response'. *Frontiers in Molecular Biosciences* 6 (September): 78. https://doi.org/10.3389/fmolb.2019.00078.

Barisic, Darko, Michael B. Stadler, Mario Iurlaro, and Dirk Schübeler. 2019. 'Mammalian ISWI and SWI/SNF Selectively Mediate Binding of Distinct Transcription Factors'. *Nature* 569 (7754): 136–40. https://doi.org/10.1038/s41586-019-1115-5.

Barrientos, Katharine S., Megan F. Kendellen, Brian D. Freibaum, Blaine N. Armbruster, Katherine T. Etheridge, and Christopher M. Counter. 2008. 'Distinct Functions of POT1 at Telomeres'. *Molecular and Cellular Biology* 28 (17): 5251–64. https://doi.org/10.1128/MCB.00048-08.

Bartocci, Cristina, Jolene K. Diedrich, Iliana Ouzounov, et al. 2014. 'Isolation of Chromatin from Dysfunctional Telomeres Reveals an Important Role for Ring1b in NHEJ-Mediated Chromosome Fusions'. *Cell Reports* 7 (4): 1320–32. https://doi.org/10.1016/j.celrep.2014.04.002.

Baskar, Rajamanickam, Jiawen Dai, Nei Wenlong, Richard Yeo, and Kheng-Wei Yeoh. 2014. 'Biological Response of Cancer Cells to Radiation Treatment'. *Frontiers in Molecular Biosciences* 1 (November). https://doi.org/10.3389/fmolb.2014.00024.

Baumann, Peter, and Thomas R. Cech. 2001. 'Pot1, the Putative Telomere End-Binding Protein in Fission Yeast and Humans'. *Science* 292 (5519): 1171–75. https://doi.org/10.1126/science.1060036.

Belton, Jon-Matthew, Bryan R. Lajoie, Sylvain Audibert, et al. 2015. 'The Conformation of Yeast Chromosome III Is Mating Type Dependent and Controlled by the Recombination Enhancer'. *Cell Reports* 13 (9): 1855–67. https://doi.org/10.1016/j.celrep.2015.10.063.

Bennett, Gwendolyn, Manolis Papamichos-Chronakis, and Craig L. Peterson. 2013. 'DNA Repair Choice Defines a Common Pathway for Recruitment of Chromatin Regulators'. *Nature Communications* 4 (1): 2084. https://doi.org/10.1038/ncomms3084.

Bennett, Gwendolyn, and Craig L. Peterson. 2015. 'SWI/SNF Recruitment to a DNA Double-Strand Break by the NuA4 and Gcn5 Histone Acetyltransferases'. *DNA Repair* 30 (June): 38–45. https://doi.org/10.1016/j.dnarep.2015.03.006.

Benson, Fiona E., Peter Baumann, and Stephen C. West. 1998. 'Synergistic Actions of Rad51 and Rad52 in Recombination and DNA Repair'. *Nature* 391 (6665): 401–4. https://doi.org/10.1038/34937.

Berkovich, Elijahu, Raymond J. Monnat, and Michael B. Kastan. 2007. 'Roles of ATM and NBS1 in Chromatin Structure Modulation and DNA Double-Strand Break Repair'. *Nature Cell Biology* 9 (6): 683–90. https://doi.org/10.1038/ncb1599.

Berzsenyi, Ivett, Vasiliki Pantazi, Barbara N. Borsos, and Tibor Pankotai. 2021. 'Systematic Overview on the Most Widespread Techniques for Inducing and Visualizing the DNA Double-Strand Breaks'. *Mutation Research/Reviews in Mutation Research* 788 (July): 108397. https://doi.org/10.1016/j.mrrev.2021.108397.

Billon, Pierre, and Jacques Côté. 2012. 'Precise Deposition of Histone H2A.Z in Chromatin for Genome Expression and Maintenance'. *Biochimica et Biophysica Acta (BBA) - Gene Regulatory Mechanisms* 1819 (3–4): 290–302. https://doi.org/10.1016/j.bbagrm.2011.10.004.

Blackburn, Elizabeth H., Carol W. Greider, and Jack W. Szostak. 2006. 'Telomeres and Telomerase: The Path from Maize, Tetrahymena and Yeast to Human Cancer and Aging'. *Nature Medicine* 12 (10): 1133–38. https://doi.org/10.1038/nm1006-1133.

Bonetti, Diego, Michela Clerici, Savani Anbalagan, Marina Martina, Giovanna Lucchini, and Maria Pia Longhese. 2010. 'Shelterin-Like Proteins and Yku Inhibit Nucleolytic Processing of Saccharomyces Cerevisiae Telomeres'. *PLoS Genetics* 6 (5): e1000966. https://doi.org/10.1371/journal.pgen.1000966.

Bonetti, Diego, Michela Clerici, Nicola Manfrini, Giovanna Lucchini, and Maria Pia Longhese. 2010. 'The MRX Complex Plays Multiple Functions in Resection of Yku- and Rif2-Protected DNA Ends'. *PLOS One* 5 (11): e14142. https://doi.org/10.1371/journal.pone.0014142.

Booth, C. 2001. 'Quantitative Amplification of Single-Stranded DNA (QAOS) Demonstrates That Cdc13-1 Mutants Generate ssDNA in a Telomere to Centromere Direction'. *Nucleic Acids Research* 29 (21): 4414–22. https://doi.org/10.1093/nar/29.21.4414.

Bothmer, Anne, Davide F. Robbiani, Michela Di Virgilio, et al. 2011. 'Regulation of DNA End Joining, Resection, and Immunoglobulin Class Switch Recombination by 53BP1'. *Molecular Cell* 42 (3): 319–29. https://doi.org/10.1016/j.molcel.2011.03.019.

Bourns, Brenda D., Mary Kate Alexander, Andrew M. Smith, and Virginia A. Zakian. 1998. 'Sir Proteins, Rif Proteins, and Cdc13p Bind *Saccharomyces* Telomeres In Vivo'. *Molecular and Cellular Biology* 18 (9): 5600–5608. https://doi.org/10.1128/MCB.18.9.5600.

Brahma, Sandipan, Mzwanele Ngubo, Somnath Paul, Maheshi Udugama, and Blaine Bartholomew. 2018. 'The Arp8 and Arp4 Module Acts as a DNA Sensor Controlling INO80 Chromatin Remodeling'. *Nature Communications* 9 (1): 3309. https://doi.org/10.1038/s41467-018-05710-7.

Brahma, Sandipan, Maheshi I. Udugama, Jongseong Kim, et al. 2017. 'INO80 Exchanges H2A.Z for H2A by Translocating on DNA Proximal to Histone Dimers'. *Nature Communications* 8 (1): 15616. https://doi.org/10.1038/ncomms15616.

Branzei, Dana, and Marco Foiani. 2006. 'The Rad53 Signal Transduction Pathway: Replication Fork Stabilization, DNA Repair, and Adaptation'. *Experimental Cell Research* 312 (14): 2654–59. https://doi.org/10.1016/j.yexcr.2006.06.012.

Budd, Martin E., and Judith L. Campbell. 1997. 'A Yeast Replicative Helicase, Dna2 Helicase, Interacts with Yeast FEN-1 Nuclease in Carrying Out Its Essential Function'. *Molecular and Cellular Biology* 17 (4): 2136–42. https://doi.org/10.1128/MCB.17.4.2136.

Cairns, Bradley R., Yahli Lorch, Yang Li, et al. 1996. 'RSC, an Essential, Abundant Chromatin-Remodeling Complex'. *Cell* 87 (7): 1249–60. https://doi.org/10.1016/S0092-8674(00)81820-6.

Cannavo, Elda, Dominic Johnson, Sara N. Andres, et al. 2018. 'Regulatory Control of DNA End Resection by Sae2 Phosphorylation'. *Nature Communications* 9 (1): 4016. https://doi.org/10.1038/s41467-018-06417-5.

Casari, Erika, Marco Gnugnoli, Carlo Rinaldi, et al. 2022. 'To Fix or Not to Fix: Maintenance of Chromosome Ends Versus Repair of DNA Double-Strand Breaks'. *Cells* 11 (20): 3224. https://doi.org/10.3390/cells11203224.

Casari, Erika, Elisa Gobbini, Marco Gnugnoli, Marco Mangiagalli, Michela Clerici, and Maria Pia Longhese. 2021. 'Dpb4 Promotes Resection of DNA Double-Strand Breaks and Checkpoint Activation by Acting in Two Different Protein Complexes'. *Nature Communications* 12 (1): 4750. https://doi.org/10.1038/s41467-021-25090-9.

Cejka, Petr. 2015. 'DNA End Resection: Nucleases Team Up with the Right Partners to Initiate Homologous Recombination'. *Journal of Biological Chemistry* 290 (38): 22931–38. https://doi.org/10.1074/jbc.R115.675942.

Cejka, Petr, Elda Cannavo, Piotr Polaczek, et al. 2010. 'DNA End Resection by Dna2–Sgs1–RPA and Its Stimulation by Top3–Rmi1 and Mre11–Rad50–Xrs2'. *Nature* 467 (7311): 112–16. https://doi.org/10.1038/nature09355.

Cejka, Petr, Jody L. Plank, Csanad Z. Bachrati, Ian D. Hickson, and Stephen C. Kowalczykowski. 2010. 'Rmi1 Stimulates Decatenation of Double Holliday Junctions during Dissolution by Sgs1–Top3'. *Nature Structural & Molecular Biology* 17 (11): 1377–82. https://doi.org/10.1038/nsmb.1919.

Cejka, Petr, and Lorraine S. Symington. 2021. 'DNA End Resection: Mechanism and Control'. *Annual Review of Genetics* 55 (1): 285–307. https://doi.org/10.1146/annurev-genet-071719-020312.

Celli, Giulia B., and Titia De Lange. 2005. 'DNA Processing Is Not Required for ATM-Mediated Telomere Damage Response after TRF2 Deletion'. *Nature Cell Biology* 7 (7): 712–18. https://doi.org/10.1038/ncb1275.

Chai, Bob, Jian Huang, Bradley R. Cairns, and Brehon C. Laurent. 2005. 'Distinct Roles for the RSC and Swi/Snf ATP-Dependent Chromatin Remodelers in DNA Double-Strand Break Repair'. *Genes & Development* 19 (14): 1656–61. https://doi.org/10.1101/gad.1273105.

Chandra, A., T. R. Hughes, C. I. Nugent, and V. Lundblad. 2001. 'Cdc13 Both Positively and Negatively Regulates Telomere Replication'. *Genes & Development* 15 (4): 404–14. https://doi.org/10.1101/gad.861001.

Chang, Howard H. Y., Nicholas R. Pannunzio, Noritaka Adachi, and Michael R. Lieber. 2017. 'Non-Homologous DNA End Joining and Alternative Pathways to Double-Strand Break Repair'. *Nature Reviews Molecular Cell Biology* 18 (8): 495–506. https://doi.org/10.1038/nrm.2017.48.

Chapman, J. Ross, Martin R. G. Taylor, and Simon J. Boulton. 2012. 'Playing the End Game: DNA Double-Strand Break Repair Pathway Choice'. *Molecular Cell* 47 (4): 497–510. https://doi.org/10.1016/j.molcel.2012.07.029.

Chatterjee, Nimrat, and Graham C. Walker. 2017. 'Mechanisms of DNA Damage, Repair, and Mutagenesis'. *Environmental and Molecular Mutagenesis* 58 (5): 235–63. https://doi.org/10.1002/em.22087.

Chen, Xuefeng, Dandan Cui, Alma Papusha, et al. 2012. 'The Fun30 Nucleosome Remodeller Promotes Resection of DNA Double-Strand Break Ends'. *Nature* 489 (7417): 576–80. https://doi.org/10.1038/nature11355.

Chen, Xuefeng, Hengyao Niu, Woo-Hyun Chung, et al. 2011. 'Cell Cycle Regulation of DNA Double-Strand Break End Resection by Cdk1-Dependent Dna2 Phosphorylation'. *Nature Structural & Molecular Biology* 18 (9): 1015–19. https://doi.org/10.1038/nsmb.2105.

Chen, Yinhuai, and Yolanda Sanchez. 2004. 'Chk1 in the DNA Damage Response: Conserved Roles from Yeasts to Mammals'. *DNA Repair* 3 (8–9): 1025–32. https://doi.org/10.1016/j.dnarep.2004.03.003.

Cheung, Annie, L. M. 2008. 'Telomere Dysfunction, Genome Instability and Cancer'. *Frontiers in Bioscience* 13 (13): 2075. https://doi.org/10.2741/2825.

Chiruvella, K. K., Z. Liang, and T. E. Wilson. 2013. 'Repair of Double-Strand Breaks by End Joining'. *Cold Spring Harbor Perspectives in Biology* 5 (5): a012757–a012757. https://doi.org/10.1101/cshperspect.a012757.

Ciccia, Alberto, and Stephen J. Elledge. 2010. 'The DNA Damage Response: Making It Safe to Play with Knives'. *Molecular Cell* 40 (2): 179–204. https://doi.org/10.1016/j.molcel.2010.09.019.

Clapier, Cedric R., and Bradley R. Cairns. 2009. 'The Biology of Chromatin Remodeling Complexes'. *Annual Review of Biochemistry* 78 (1): 273–304. https://doi.org/10.1146/annurev.biochem.77.062706.153223.

Clapier, Cedric R., Janet Iwasa, Bradley R. Cairns, and Craig L. Peterson. 2017. 'Mechanisms of Action and Regulation of ATP-Dependent Chromatin-Remodelling Complexes'. *Nature Reviews Molecular Cell Biology* 18 (7): 407–22. https://doi.org/10.1038/nrm.2017.26.

Clerici, Michela, Davide Mantiero, Ilaria Guerini, Giovanna Lucchini, and Maria Pia Longhese. 2008. 'The Yku70–Yku80 Complex Contributes to Regulate Double-strand Break Processing and Checkpoint Activation during the Cell Cycle'. *EMBO Reports* 9 (8): 810–18. https://doi.org/10.1038/embor.2008.121.

Conrad, Michael N., Jocelyn H. Wright, Alexander J. Wolf, and Virginia A. Zakian. 1990. 'RAP1 Protein Interacts with Yeast Telomeres in Vivo: Overproduction Alters Telomere Structure and Decreases Chromosome Stability'. *Cell* 63 (4): 739–50. https://doi.org/10.1016/0092-8674(90)90140-A.

Corneo, Barbara, Rebecca L. Wendland, Ludovic Deriano, et al. 2007. 'Rag Mutations Reveal Robust Alternative End Joining'. *Nature* 449 (7161): 483–86. https://doi.org/10.1038/nature06168.

Corona, Davide F. V., and John W. Tamkun. 2004. 'Multiple Roles for ISWI in Transcription, Chromosome Organization and DNA Replication'. *Biochimica et Biophysica Acta (BBA) - Gene Structure and Expression* 1677 (1–3): 113–19. https://doi.org/10.1016/j.bbaexp.2003.09.018.

Costelloe, Thomas, Raphaël Louge, Nozomi Tomimatsu, et al. 2012. 'The Yeast Fun30 and Human SMARCAD1 Chromatin Remodellers Promote DNA End Resection'. *Nature* 489 (7417): 581–84. https://doi.org/10.1038/nature11353.

Courilleau, Céline, Catherine Chailleux, Alain Jauneau, et al. 2012. 'The Chromatin Remodeler P400 ATPase Facilitates Rad51-Mediated Repair of DNA Double-Strand Breaks'. *The Journal of Cell Biology* 199 (7): 1067–81. https://doi.org/10.1083/jcb.201205059.

Crabbe, Laure, Ramiro E. Verdun, Candy I. Haggblom, and Jan Karlseder. 2004. 'Defective Telomere Lagging Strand Synthesis in Cells Lacking WRN Helicase Activity'. *Science* 306 (5703): 1951–53. https://doi.org/10.1126/science.1103619.

D'Andrea, Alan D. 2008. 'DNA Repair Pathways and Human Cancer'. In *The Molecular Basis of Cancer*. Elsevier. https://doi.org/10.1016/B978-141603703-3.10004-4.

De Bruin, Derik, Zafar Zaman, Rachel A. Liberatore, and Mark Ptashne. 2001. 'Telomere Looping Permits Gene Activation by a Downstream UAS in Yeast'. *Nature* 409 (6816): 109–13. https://doi.org/10.1038/35051119.

De Lange, Titia. 2009. 'How Telomeres Solve the End-Protection Problem'. *Science* 326 (5955): 948–52. https://doi.org/10.1126/science.1170633.

Deiser, Anja M., Caitlyn Agar, Juan De Dios Barba Tena, and Boris Pfander. 2026. 'A Role for Nucleosome Remodellers during Resection of Deprotected Telomeres in Yeast'. *PLOS One* 21 (7): e0352656. https://doi.org/10.1371/journal.pone.0352656.

Denchi, Eros Lazzerini, and Titia De Lange. 2007. 'Protection of Telomeres through Independent Control of ATM and ATR by TRF2 and POT1'. *Nature* 448 (7157): 1068–71. https://doi.org/10.1038/nature06065.

Deng, Dong, Chuangye Yan, Xiaojing Pan, et al. 2012. 'Structural Basis for Sequence-Specific Recognition of DNA by TAL Effectors'. *Science* 335 (6069): 720–23. https://doi.org/10.1126/science.1215670.

Densham, Ruth M., Alexander J. Garvin, Helen R. Stone, et al. 2016. 'Human BRCA1–BARD1 Ubiquitin Ligase Activity Counteracts Chromatin Barriers to DNA Resection'. *Nature Structural & Molecular Biology* 23 (7): 647–55. https://doi.org/10.1038/nsmb.3236.

Deshpande, Ishan, Andrew Seeber, Kenji Shimada, Jeremy J. Keusch, Heinz Gut, and Susan M. Gasser. 2017. 'Structural Basis of Mec1-Ddc2-RPA Assembly and Activation on Single-Stranded DNA at Sites of Damage'. *Molecular Cell* 68 (2): 431-445.e5. https://doi.org/10.1016/j.molcel.2017.09.019.

Dewar, James M., and David Lydall. 2012. 'Similarities and Differences between "Uncapped" Telomeres and DNA Double-Strand Breaks'. *Chromosoma* 121 (2): 117–30. https://doi.org/10.1007/s00412-011-0357-2.

Dhillon, Namrita, Masaya Oki, Shawn J. Szyjka, Oscar M. Aparicio, and Rohinton T. Kamakaka. 2006. 'H2A.Z Functions To Regulate Progression through the Cell Cycle'. *Molecular and Cellular Biology* 26 (2): 489–501. https://doi.org/10.1128/MCB.26.2.489-501.2006.

Dilley, Robert L., and Roger A. Greenberg. 2015. 'ALTernative Telomere Maintenance and Cancer'. *Trends in Cancer* 1 (2): 145–56. https://doi.org/10.1016/j.trecan.2015.07.007.

Dimitrova, Nadya, Yi-Chun M. Chen, David L. Spector, and Titia De Lange. 2008. '53BP1 Promotes Non-Homologous End Joining of Telomeres by Increasing Chromatin Mobility'. *Nature* 456 (7221): 524–28. https://doi.org/10.1038/nature07433.

Doksani, Ylli, John Y. Wu, Titia de Lange, and Xiaowei Zhuang. 2013. 'Super-Resolution Fluorescence Imaging of Telomeres Reveals TRF2-Dependent T-Loop Formation'. *Cell* 155 (2): 345–56. https://doi.org/10.1016/j.cell.2013.09.048.

Downs, Jessica A., Stéphane Allard, Olivier Jobin-Robitaille, et al. 2004. 'Binding of Chromatin-Modifying Activities to Phosphorylated Histone H2A at DNA Damage Sites'. *Molecular Cell* 16 (6): 979–90. https://doi.org/10.1016/j.molcel.2004.12.003.

Downs, Jessica A., Noel F. Lowndes, and Stephen P. Jackson. 2000. 'A Role for Saccharomyces Cerevisiae Histone H2A in DNA Repair'. *Nature* 408 (6815): 1001–4. https://doi.org/10.1038/35050000.

Dutta, Arnob, Mihaela Sardiu, Madelaine Gogol, et al. 2017. 'Composition and Function of Mutant Swi/Snf Complexes'. *Cell Reports* 18 (9): 2124–34. https://doi.org/10.1016/j.celrep.2017.01.058.

Eapen, Vinay V., Neal Sugawara, Michael Tsabar, Wei-Hua Wu, and James E. Haber. 2012. 'The *Saccharomyces Cerevisiae* Chromatin Remodeler Fun30 Regulates DNA End Resection and Checkpoint Deactivation'. *Molecular and Cellular Biology* 32 (22): 4727–40. https://doi.org/10.1128/MCB.00566-12.

Ellahi, Aisha, Deborah M. Thurtle, and Jasper Rine. 2015. 'The Chromatin and Transcriptional Landscape of Native *Saccharomyces Cerevisiae* Telomeres and Subtelomeric Domains'. *Genetics* 200 (2): 505–21. https://doi.org/10.1534/genetics.115.175711.

Eustermann, Sebastian, Kevin Schall, Dirk Kostrewa, et al. 2018. 'Structural Basis for ATP-Dependent Chromatin Remodelling by the INO80 Complex'. *Nature* 556 (7701): 386–90. https://doi.org/10.1038/s41586-018-0029-y.

Falck, Jacob, Julia Coates, and Stephen P. Jackson. 2005. 'Conserved Modes of Recruitment of ATM, ATR and DNA-PKcs to Sites of DNA Damage'. *Nature* 434 (7033): 605–11. https://doi.org/10.1038/nature03442.

Faure, Virginie, Stéphane Coulon, Julien Hardy, and Vincent Géli. 2010. 'Cdc13 and Telomerase Bind through Different Mechanisms at the Lagging- and Leading-Strand Telomeres'. *Molecular Cell* 38 (6): 842–52. https://doi.org/10.1016/j.molcel.2010.05.016.

Finn, Karen, Noel Francis Lowndes, and Muriel Grenon. 2012. 'Eukaryotic DNA Damage Checkpoint Activation in Response to Double-Strand Breaks'. *Cellular and Molecular Life Sciences* 69 (9): 1447–73. https://doi.org/10.1007/s00018-011-0875-3.

Fisher, Timothy S., Andrew K. P. Taggart, and Virginia A. Zakian. 2004. 'Cell Cycle-Dependent Regulation of Yeast Telomerase by Ku'. *Nature Structural & Molecular Biology* 11 (12): 1198–205. https://doi.org/10.1038/nsmb854.

Flaus, A. 2006. 'Identification of Multiple Distinct Snf2 Subfamilies with Conserved Structural Motifs'. *Nucleic Acids Research* 34 (10): 2887–905. https://doi.org/10.1093/nar/gkl295.

Foster, Steven S., Alessia Balestrini, and John H. J. Petrini. 2011. 'Functional Interplay of the Mre11 Nuclease and Ku in the Response to Replication-Associated DNA Damage'. *Molecular and Cellular Biology* 31 (21): 4379–89. https://doi.org/10.1128/MCB.05854-11.

Foster, Steven S., Mikhajlo K. Zubko, Sandrine Guillard, and David Lydall. 2006. 'MRX Protects Telomeric DNA at Uncapped Telomeres of Budding Yeast Cdc13-1 Mutants'. *DNA Repair* 5 (7): 840–51. https://doi.org/10.1016/j.dnarep.2006.04.005.

Galanti, Lorenzo, Martina Peritore, Robert Gnügge, et al. 2024. 'Dbf4-Dependent Kinase Promotes Cell Cycle Controlled Resection of DNA Double-Strand Breaks and Repair by Homologous Recombination'. *Nature Communications* 15 (1): 2890. https://doi.org/10.1038/s41467-024-46951-z.

Gao, Hua, Rachel B. Cervantes, Edward K. Mandell, Joel H. Otero, and Victoria Lundblad. 2007. 'RPA-like Proteins Mediate Yeast Telomere Function'. *Nature Structural & Molecular Biology* 14 (3): 208–14. https://doi.org/10.1038/nsmb1205.

Gardner, R. 1999. 'RAD53, DUN1 and PDS1 Define Two Parallel G2/M Checkpoint Pathways in Budding Yeast'. *The EMBO Journal* 18 (11): 3173–85. https://doi.org/10.1093/emboj/18.11.3173.

Garvik, Barbara, Michael Carson, and Leland Hartwell. 1995. 'Single-Stranded DNA Arising at Telomeres in *Cdc13* Mutants May Constitute a Specific Signal for the *RAD9* Checkpoint'. *Molecular and Cellular Biology* 15 (11): 6128–38. https://doi.org/10.1128/MCB.15.11.6128.

Giaimo, Benedetto Daniele, Francesca Ferrante, Andreas Herchenröther, Sandra B. Hake, and Tilman Borggrefe. 2019. 'The Histone Variant H2A.Z in Gene Regulation'. *Epigenetics & Chromatin* 12 (1): 37. https://doi.org/10.1186/s13072-019-0274-9.

Gnügge, Robert, and Lorraine S. Symington. 2020. 'Efficient DNA Double-Strand Break Formation at Single or Multiple Defined Sites in the *Saccharomyces Cerevisiae*

Genome'. *Nucleic Acids Research* 48 (20): e115–e115. https://doi.org/10.1093/nar/gkaa833.

Gnugnoli, Marco, Erika Casari, and Maria Pia Longhese. 2021. 'The Chromatin Remodeler Chd1 Supports MRX and Exo1 Functions in Resection of DNA Double-Strand Breaks'. *PLOS Genetics* 17 (9): e1009807. https://doi.org/10.1371/journal.pgen.1009807.

Gospodinov, Anastas, Thomas Vaissiere, Dragomir B. Krastev, Gaëlle Legube, Boyka Anachkova, and Zdenko Herceg. 2011. 'Mammalian Ino80 Mediates Double-Strand Break Repair through Its Role in DNA End Strand Resection'. *Molecular and Cellular Biology* 31 (23): 4735–45. https://doi.org/10.1128/MCB.06182-11.

Govindan, Ganesan, and Sivaprakash Ramalingam. 2016. 'Programmable Site-Specific Nucleases for Targeted Genome Engineering in Higher Eukaryotes: PROGRAMMABLE SITE-SPECIFIC NUCLEASES'. *Journal of Cellular Physiology* 231 (11): 2380–92. https://doi.org/10.1002/jcp.25367.

Granata, Magda, Davide Panigada, Elena Galati, et al. 2013. 'To Trim or Not to Trim: Progression and Control of DSB End Resection'. *Cell Cycle* 12 (12): 1848–60. https://doi.org/10.4161/cc.25042.

Grandin, N. 2001. 'Ten1 Functions in Telomere End Protection and Length Regulation in Association with Stn1 and Cdc13'. *The EMBO Journal* 20 (5): 1173–83. https://doi.org/10.1093/emboj/20.5.1173.

Grandin, N, S. I. Reed, and M. Charbonneau. 1997. 'Stn1, a New Saccharomyces Cerevisiae Protein, Is Implicated in Telomere Size Regulation in Association with Cdc13.' *Genes & Development* 11 (4): 512–27. https://doi.org/10.1101/gad.11.4.512.

Grandin, Nathalie, Christelle Damon, and Michel Charbonneau. 2000. 'Cdc13 Cooperates with the Yeast Ku Proteins and Stn1 To Regulate Telomerase Recruitment'. *Molecular and Cellular Biology* 20 (22): 8397–408. https://doi.org/10.1128/MCB.20.22.8397-8408.2000.

Gravel, Serge, J. Ross Chapman, Christine Magill, and Stephen P. Jackson. 2008. 'DNA Helicases Sgs1 and BLM Promote DNA Double-Strand Break Resection'. *Genes & Development* 22 (20): 2767–72. https://doi.org/10.1101/gad.503108.

Gravel, Serge, Michel Larrivée, Pascale Labrecque, and Raymund J. Wellinger. 1998. 'Yeast Ku as a Regulator of Chromosomal DNA End Structure'. *Science* 280 (5364): 741–44. https://doi.org/10.1126/science.280.5364.741.

Griffith, Jack D., Laurey Comeau, Soraya Rosenfield, et al. 1999. 'Mammalian Telomeres End in a Large Duplex Loop'. *Cell* 97 (4): 503–14. https://doi.org/10.1016/S0092-8674(00)80760-6.

Grolimund, Larissa, Eric Aeby, Romain Hamelin, et al. 2013. 'A Quantitative Telomeric Chromatin Isolation Protocol Identifies Different Telomeric States'. *Nature Communications* 4 (1): 2848. https://doi.org/10.1038/ncomms3848.

Grossi, Simona, Andrea Puglisi, Petr V. Dmitriev, Massimo Lopes, and David Shore. 2004. 'Pol12, the B Subunit of DNA Polymerase α, Functions in Both Telomere Capping and Length Regulation'. *Genes & Development* 18 (9): 992–1006. https://doi.org/10.1101/gad.300004.

Gursoy-Yuzugullu, Ozge, Marina K. Ayrapetov, and Brendan D. Price. 2015. 'Histone Chaperone Anp32e Removes H2A.Z from DNA Double-Strand Breaks and Promotes Nucleosome Reorganization and DNA Repair'. *Proceedings of the National Academy of Sciences* 112 (24): 7507–12. https://doi.org/10.1073/pnas.1504868112.

Halley, Jeffrey E., Tommy Kaplan, Alice Y. Wang, Michael S. Kobor, and Jasper Rine. 2010. 'Roles for H2A.Z and Its Acetylation in GAL1 Transcription and Gene Induction, but Not GAL1-Transcriptional Memory'. *PLoS Biology* 8 (6): e1000401. https://doi.org/10.1371/journal.pbio.1000401.

Hammet, Andrew, Christine Magill, Jörg Heierhorst, and Stephen P. Jackson. 2007. 'Rad9 BRCT Domain Interaction with Phosphorylated H2AX Regulates the G1 Checkpoint in Budding Yeast'. *The EMBO Reports* 8 (9): 851–57. https://doi.org/10.1038/sj.embor.7401036.

Happel, Nicole, and Detlef Doenecke. 2009. 'Histone H1 and Its Isoforms: Contribution to Chromatin Structure and Function'. *Gene* 431 (1–2): 1–12. https://doi.org/10.1016/j.gene.2008.11.003.

Harrison, Jacob C., and James E. Haber. 2006. 'Surviving the Breakup: The DNA Damage Checkpoint'. *Annual Review of Genetics* 40 (1): 209–35. https://doi.org/10.1146/annurev.genet.40.051206.105231.

Hartwell, Leland H., Robert K. Mortimer, Joseph Culotti, and Marilyn Culotti. 1973. 'GENETIC CONTROL OF THE CELL DIVISION CYCLE IN YEAST: V. GENETIC ANALYSIS OF *Cdc* MUTANTS'. *Genetics* 74 (2): 267–86. https://doi.org/10.1093/genetics/74.2.267.

Hays, Emily, Elizabeth Nettleton, Caitlin Carter, et al. 2020. 'The SWI/SNF ATPase BRG1 Stimulates DNA End Resection and Homologous Recombination by Reducing Nucleosome Density at DNA Double Strand Breaks and by Promoting the Recruitment of the CtIP Nuclease'. *Cell Cycle* 19 (22): 3096–114. https://doi.org/10.1080/15384101.2020.1831256.

Hicks, Wade M., Minlee Kim, and James E. Haber. 2010. 'Increased Mutagenesis and Unique Mutation Signature Associated with Mitotic Gene Conversion'. *Science* 329 (5987): 82–85. https://doi.org/10.1126/science.1191125.

Hills, Stephanie A., and John F. X. Diffley. 2014. 'DNA Replication and Oncogene-Induced Replicative Stress'. *Current Biology* 24 (10): R435–44. https://doi.org/10.1016/j.cub.2014.04.012.

Horigome, Chihiro, Yukako Oma, Tatsunori Konishi, et al. 2014. 'SWR1 and INO80 Chromatin Remodelers Contribute to DNA Double-Strand Break Perinuclear Anchorage Site Choice'. *Molecular Cell* 55 (4): 626–39. https://doi.org/10.1016/j.molcel.2014.06.027.

Hubbe, Petra, Charu Sharma, Oliver Pajonk, et al. 2026. 'Systematic Evaluation of Tools for Auxin-Inducible Protein Degradation in Budding Yeast'. *Molecular Biology of the Cell* 37 (2): mr2. https://doi.org/10.1091/mbc.E25-12-0571.

Huertas, Pablo, Felipe Cortés-Ledesma, Alessandro A. Sartori, Andrés Aguilera, and Stephen P. Jackson. 2008. 'CDK Targets Sae2 to Control DNA-End Resection and Homologous Recombination'. *Nature* 455 (7213): 689–92. https://doi.org/10.1038/nature07215.

Huertas, Pablo, and Stephen P. Jackson. 2009. 'Human CtIP Mediates Cell Cycle Control of DNA End Resection and Double Strand Break Repair'. *Journal of Biological Chemistry* 284 (14): 9558–65. https://doi.org/10.1074/jbc.M808906200.

Hughes, Timothy R., Rodney G. Weilbaecher, Monika Walterscheid, and Victoria Lundblad. 2000. 'Identification of the Single-Strand Telomeric DNA Binding Domain of the *Saccharomyces Cerevisiae* Cdc13 Protein'. *Proceedings of the National Academy of Sciences* 97 (12): 6457–62. https://doi.org/10.1073/pnas.97.12.6457.

Iacovoni, Jason S., Pierre Caron, Imen Lassadi, et al. 2010. 'High-resolution Profiling of γH2AX around DNA Double Strand Breaks in the Mammalian Genome'. *The EMBO Journal* 29 (8): 1446–57. https://doi.org/10.1038/emboj.2010.38.

Inoue, Hiroaki, Hiroshi Nojima, and Hiroto Okayama. 1990. 'High Efficiency Transformation of Escherichia Coli with Plasmids'. *Gene* 96 (1): 23–28. https://doi.org/10.1016/0378-1119(90)90336-P.

Ira, Grzegorz, Achille Pellicioli, Alitukiriza Balijja, et al. 2004. 'DNA End Resection, Homologous Recombination and DNA Damage Checkpoint Activation Require CDK1'. *Nature* 431 (7011): 1011–17. https://doi.org/10.1038/nature02964.

Iskandar, Mina, Miguel Xiao Barbero, Muhamed Jaber, et al. 2025. 'A Review of Telomere Attrition in Cancer and Aging: Current Molecular Insights and Future Therapeutic Approaches'. *Cancers* 17 (2): 257. https://doi.org/10.3390/cancers17020257.

Jackson, Stephen P., and Jiri Bartek. 2009. 'The DNA-Damage Response in Human Biology and Disease'. *Nature* 461 (7267): 1071–78. https://doi.org/10.1038/nature08467.

Janke, Carsten, Maria M. Magiera, Nicole Rathfelder, et al. 2004. 'A Versatile Toolbox for PCR-based Tagging of Yeast Genes: New Fluorescent Proteins, More Markers and Promoter Substitution Cassettes'. *Yeast* 21 (11): 947–62. https://doi.org/10.1002/yea.1142.

Jazayeri, Ali, Jacob Falck, Claudia Lukas, et al. 2006. 'ATM- and Cell Cycle-Dependent Regulation of ATR in Response to DNA Double-Strand Breaks'. *Nature Cell Biology* 8 (1): 37–45. https://doi.org/10.1038/ncb1337.

Jinek, Martin, Krzysztof Chylinski, Ines Fonfara, Michael Hauer, Jennifer A. Doudna, and Emmanuelle Charpentier. 2012. 'A Programmable Dual-RNA–Guided DNA Endonuclease in Adaptive Bacterial Immunity'. *Science* 337 (6096): 816–21. https://doi.org/10.1126/science.1225829.

Jones, Morgan, Kamlesh Bisht, Sharon A. Savage, Jayakrishnan Nandakumar, Catherine E. Keegan, and Ivan Maillard. 2016. 'The Shelterin Complex and Hematopoiesis'. *Journal of Clinical Investigation* 126 (5): 1621–29. https://doi.org/10.1172/JCI84547.

Kalocsay, Marian, Natalie Jasmin Hiller, and Stefan Jentsch. 2009. 'Chromosome-Wide Rad51 Spreading and SUMO-H2A.Z-Dependent Chromosome Fixation in Response to a Persistent DNA Double-Strand Break'. *Molecular Cell* 33 (3): 335–43. https://doi.org/10.1016/j.molcel.2009.01.016.

Kao, Hui-I., Judith L. Campbell, and Robert A. Bambara. 2004. 'Dna2p Helicase/Nuclease Is a Tracking Protein, Like FEN1, for Flap Cleavage during Okazaki Fragment Maturation'. *Journal of Biological Chemistry* 279 (49): 50840–49. https://doi.org/10.1074/jbc.M409231200.

Kapoor, Prabodh, Yunhe Bao, Jing Xiao, et al. 2015. 'Regulation of Mec1 Kinase Activity by the SWI/SNF Chromatin Remodeling Complex'. *Genes & Development* 29 (6): 591–602. https://doi.org/10.1101/gad.257626.114.

Kari, Vijayalakshmi, Wael Yassin Mansour, Sanjay Kumar Raul, et al. 2016. 'Loss of *CHD1* Causes DNA Repair Defects and Enhances Prostate Cancer Therapeutic Responsiveness'. *EMBO Reports* 17 (11): 1609–23. https://doi.org/10.15252/embr.201642352.

Karl, Leonhard Andreas, Martina Peritore, Lorenzo Galanti, and Boris Pfander. 2022. 'DNA Double Strand Break Repair and Its Control by Nucleosome Remodeling'. *Frontiers in Genetics* 12 (January): 821543. https://doi.org/10.3389/fgene.2021.821543.

Karlseder, Jan, Dominique Broccoli, Yumin Dai, Stephen Hardy, and Titia De Lange. 1999. 'P53- and ATM-Dependent Apoptosis Induced by Telomeres Lacking TRF2'. *Science* 283 (5406): 1321–25. https://doi.org/10.1126/science.283.5406.1321.

Kent, Nicholas A., Anna L. Chambers, and Jessica A. Downs. 2007. 'Dual Chromatin Remodeling Roles for RSC during DNA Double Strand Break Induction and Repair at the Yeast MAT Locus'. *Journal of Biological Chemistry* 282 (38): 27693–701. https://doi.org/10.1074/jbc.M704707200.

Kim, Y. G., J. Cha, and S. Chandrasegaran. 1996. 'Hybrid Restriction Enzymes: Zinc Finger Fusions to Fok I Cleavage Domain.' *Proceedings of the National Academy of Sciences* 93 (3): 1156–60. https://doi.org/10.1073/pnas.93.3.1156.

Klein-Brill, Avital, Daphna Joseph-Strauss, Alon Appleboim, and Nir Friedman. 2019. 'Dynamics of Chromatin and Transcription during Transient Depletion of the RSC Chromatin Remodeling Complex'. *Cell Reports* 26 (1): 279-292.e5. https://doi.org/10.1016/j.celrep.2018.12.020.

Knoll, Kilian R., Sebastian Eustermann, Vanessa Niebauer, et al. 2018. 'The Nuclear Actin-Containing Arp8 Module Is a Linker DNA Sensor Driving INO80 Chromatin Remodeling'. *Nature Structural & Molecular Biology* 25 (9): 823–32. https://doi.org/10.1038/s41594-018-0115-8.

Konishi, Akimitsu, and Titia De Lange. 2008. 'Cell Cycle Control of Telomere Protection and NHEJ Revealed by a Ts Mutation in the DNA-Binding Domain of TRF2'. *Genes & Development* 22 (9): 1221–30. https://doi.org/10.1101/gad.1634008.

Krietenstein, Nils, Megha Wal, Shinya Watanabe, et al. 2016. 'Genomic Nucleosome Organization Reconstituted with Pure Proteins'. *Cell* 167 (3): 709-721.e12. https://doi.org/10.1016/j.cell.2016.09.045.

Kumar, Namrata, Natália C. Moreno, Bruno C. Feltes, Carlos Fm Menck, and Bennett Van Houten. 2020. 'Cooperation and Interplay between Base and Nucleotide Excision Repair Pathways: From DNA Lesions to Proteins'. *Genetics and Molecular Biology* 43 (1 suppl 1): e20190104. https://doi.org/10.1590/1678-4685-gmb-2019-0104.

Kunert, Franziska, Felix J. Metzner, James Jung, et al. 2022. 'Structural Mechanism of Extranucleosomal DNA Readout by the INO80 Complex'. *Science Advances* 8 (49): eadd3189. https://doi.org/10.1126/sciadv.add3189.

Kunkel, Thomas A., and Dorothy A. Erie. 2015. 'Eukaryotic Mismatch Repair in Relation to DNA Replication'. *Annual Review of Genetics* 49 (1): 291–313. https://doi.org/10.1146/annurev-genet-112414-054722.

Lademann, Claudio A., Jörg Renkawitz, Boris Pfander, and Stefan Jentsch. 2017. 'The INO80 Complex Removes H2A.Z to Promote Presynaptic Filament Formation during Homologous Recombination'. *Cell Reports* 19 (7): 1294–303. https://doi.org/10.1016/j.celrep.2017.04.051.

Lam, Isabel, and Scott Keeney. 2015. 'Mechanism and Regulation of Meiotic Recombination Initiation'. *Cold Spring Harbor Perspectives in Biology* 7 (1): a016634. https://doi.org/10.1101/cshperspect.a016634.

Längst, Gernot, and Laura Manelyte. 2015. 'Chromatin Remodelers: From Function to Dysfunction'. *Genes* 6 (2): 299–324. https://doi.org/10.3390/genes6020299.

Larrivée, Michel, Catherine LeBel, and Raymund J. Wellinger. 2004. 'The Generation of Proper Constitutive G-Tails on Yeast Telomeres Is Dependent on the MRX Complex'. *Genes & Development* 18 (12): 1391–96. https://doi.org/10.1101/gad.1199404.

Lazzaro, Federico, Vasileia Sapountzi, Magda Granata, et al. 2008. 'Histone Methyltransferase Dot1 and Rad9 Inhibit Single-Stranded DNA Accumulation at DSBs and Uncapped Telomeres'. *The EMBO Journal*, ahead of print, April 17. https://doi.org/10.1038/emboj.2008.81.

Lazzerini-Denchi, Eros, and Agnel Sfeir. 2016. 'Stop Pulling My Strings — What Telomeres Taught Us about the DNA Damage Response'. *Nature Reviews Molecular Cell Biology* 17 (6): 364–78. https://doi.org/10.1038/nrm.2016.43.

Lee, Julia Y., Marina Kozak, Joel D. Martin, Erin Pennock, and F. Brad Johnson. 2007. 'Evidence That a RecQ Helicase Slows Senescence by Resolving Recombining Telomeres'. *PLoS Biology* 5 (6): e160. https://doi.org/10.1371/journal.pbio.0050160.

Lee, Sang Eun, J. Kent Moore, Allyson Holmes, Keiko Umezu, Richard D. Kolodner, and James E. Haber. 1998. 'Saccharomyces Ku70, Mre11/Rad50, and RPA Proteins Regulate Adaptation to G2/M Arrest after DNA Damage'. *Cell* 94 (3): 399–409. https://doi.org/10.1016/S0092-8674(00)81482-8.

Levikova, Maryna, Cosimo Pinto, and Petr Cejka. 2017. 'The Motor Activity of DNA2 Functions as an ssDNA Translocase to Promote DNA End Resection'. *Genes & Development* 31 (5): 493–502. https://doi.org/10.1101/gad.295196.116.

Levy, Daniel L., and Elizabeth H. Blackburn. 2004. 'Counting of Rif1p and Rif2p on Saccharomyces Cerevisiae Telomeres Regulates Telomere Length'. *Molecular and Cellular Biology* 24 (24): 10857–67. https://doi.org/10.1128/MCB.24.24.10857-10867.2004.

Li, Bibo, Stephanie Oestreich, and Titia De Lange. 2000. 'Identification of Human Rap1'. *Cell* 101 (5): 471–83. https://doi.org/10.1016/S0092-8674(00)80858-2.

Li, Kevin, Gabriel Bronk, Jane Kondev, and James E. Haber. 2020. 'Yeast ATM and ATR Kinases Use Different Mechanisms to Spread Histone H2A Phosphorylation around a DNA Double-Strand Break'. *Proceedings of the National Academy of Sciences* 117 (35): 21354–63. https://doi.org/10.1073/pnas.2002126117.

Li, L., L. P. Wu, and S. Chandrasegaran. 1992. 'Functional Domains in Fok I Restriction Endonuclease.' *Proceedings of the National Academy of Sciences* 89 (10): 4275–79. https://doi.org/10.1073/pnas.89.10.4275.

Li, Shuxiang, Tiejun Wei, and Anna R. Panchenko. 2023. 'Histone Variant H2A.Z Modulates Nucleosome Dynamics to Promote DNA Accessibility'. *Nature Communications* 14 (1): 769. https://doi.org/10.1038/s41467-023-36465-5.

Liang, Bing, Jiajing Qiu, Kajan Ratnakumar, and Brehon C. Laurent. 2007. 'RSC Functions as an Early Double-Strand-Break Sensor in the Cell's Response to DNA Damage'. *Current Biology* 17 (16): 1432–37. https://doi.org/10.1016/j.cub.2007.07.035.

Lieb, Jason D., Xiaole Liu, David Botstein, and Patrick O. Brown. 2001. 'Promoter-Specific Binding of Rap1 Revealed by Genome-Wide Maps of Protein–DNA Association'. *Nature Genetics* 28 (4): 327–34. https://doi.org/10.1038/ng569.

Little, John B. 2000. 'Radiation Carcinogenesis'. *Carcinogenesis* 21 (3): 397–404. https://doi.org/10.1093/carcin/21.3.397.

Longtine, Mark S., Nancy Maxfield Wilson, Marie E. Petracek, and Judith Berman. 1989. 'A Yeast Telomere Binding Activity Binds to Two Related Telomere Sequence Motifs and Is Indistinguishable from RAPT'. *Current Genetics* 16 (4): 225–39. https://doi.org/10.1007/BF00422108.

Lopez-Mosqueda, Jaime, Genevieve M. Vidanes, and David P. Toczyski. 2010. 'Cdc5 Blocks in Vivo Rad53 Activity, but Not in Situ Activity (ISA)'. *Cell Cycle* (Georgetown, Tex.) 9 (21): 4266–68. https://doi.org/10.4161/cc.9.21.13637.

Lottersberger, Francisca, Anne Bothmer, Davide F. Robbiani, Michel C. Nussenzweig, and Titia De Lange. 2013. 'Role of 53BP1 Oligomerization in Regulating Double-Strand Break Repair'. *Proceedings of the National Academy of Sciences* 110 (6): 2146–51. https://doi.org/10.1073/pnas.1222617110.

Luger, Karolin, Armin W. Mäder, Robin K. Richmond, David F. Sargent, and Timothy J. Richmond. 1997. 'Crystal Structure of the Nucleosome Core Particle at 2.8 Å Resolution'. *Nature* 389 (6648): 251–60. https://doi.org/10.1038/38444.

Luijsterburg, Martijn S., and Haico Van Attikum. 2011. 'Chromatin and the DNA Damage Response: The Cancer Connection'. *Molecular Oncology* 5 (4): 349–67. https://doi.org/10.1016/j.molonc.2011.06.001.

Lustig, Arthur J. 2019. 'Towards the Mechanism of Yeast Telomere Dynamics'. *Trends in Cell Biology* 29 (5): 361–70. https://doi.org/10.1016/j.tcb.2019.01.005.

Lustig, Arthur J., Stephen Kurtz, and David Shore. 1990. 'Involvement of the Silencer and UAS Binding Protein RAP1 in Regulation of Telomere Length'. *Science* 250 (4980): 549–53. https://doi.org/10.1126/science.2237406.

Maeder, Morgan L., and Charles A. Gersbach. 2016. 'Genome-Editing Technologies for Gene and Cell Therapy'. *Molecular Therapy* 24 (3): 430–46. https://doi.org/10.1038/mt.2016.10.

Malik, Deepshikha, Ashish Deshmukh, Silvija Bilokapic, and Mario Halic. 2025. 'Mechanisms of Chromatin Remodeling by the Human Snf2-Type ATPase SNF2H'. *Cell Research* 35 (6): 465–68. https://doi.org/10.1038/s41422-025-01103-w.

Malone, Jim. 2020. 'X-Rays for Medical Imaging: Radiation Protection, Governance and Ethics over 125 Years'. *Physica Medica* 79 (November): 47–64. https://doi.org/10.1016/j.ejmp.2020.09.012.

Manning, Benjamin J., and Craig L. Peterson. 2014. 'Direct Interactions Promote Eviction of the Sir3 Heterochromatin Protein by the SWI/SNF Chromatin Remodeling Enzyme'. *Proceedings of the National Academy of Sciences* 111 (50): 17827–32. https://doi.org/10.1073/pnas.1420096111.

Mantiero, Davide, Michela Clerici, Giovanna Lucchini, and Maria Pia Longhese. 2007. 'Dual Role for Saccharomyces Cerevisiae Tel1 in the Checkpoint Response to Double-strand Breaks'. *The EMBO Reports* 8 (4): 380–87. https://doi.org/10.1038/sj.embor.7400911.

Marsella, Antonio, Elisa Gobbini, Corinne Cassani, et al. 2021. 'Sae2 and Rif2 Regulate MRX Endonuclease Activity at DNA Double-Strand Breaks in Opposite Manners'. *Cell Reports* 34 (13): 108906. https://doi.org/10.1016/j.celrep.2021.108906.

Martina, Marina, Michela Clerici, Veronica Baldo, Diego Bonetti, Giovanna Lucchini, and Maria Pia Longhese. 2012. 'A Balance between Tel1 and Rif2 Activities Regulates Nucleolytic Processing and Elongation at Telomeres'. *Molecular and Cellular Biology* 32 (9): 1604–17. https://doi.org/10.1128/MCB.06547-11.

Martins-Taylor, Kristen, Upasna Sharma, Tania Rozario, and Scott G. Holmes. 2011. 'H2A.Z (Htz1) Controls the Cell-Cycle-Dependent Establishment of Transcriptional Silencing at *Saccharomyces Cerevisiae* Telomeres'. *Genetics* 187 (1): 89–104. https://doi.org/10.1534/genetics.110.123844.

Mason, Mark, Jennifer J. Wanat, Sandy Harper, et al. 2013. 'Cdc13 OB2 Dimerization Required for Productive Stn1 Binding and Efficient Telomere Maintenance'. *Structure* 21 (1): 109–20. https://doi.org/10.1016/j.str.2012.10.012.

Mattarocci, Stefano, Giordano Reginato, Elda Cannavo, et al. 2026. 'Rap1-Mediated Steric Hindrance Protects Telomeres from MRX Sensing'. *Nature Structural & Molecular Biology* 33 (6): 915–27. https://doi.org/10.1038/s41594-026-01810-x.

Meena, Jitendra, K. Lenhard Rudolph, and Cagatay Günes. 2015. 'Telomere Dysfunction, Chromosomal Instability and Cancer'. In *Chromosomal Instability in Cancer Cells*, edited by B. Michael Ghadimi and Thomas Ried, vol. 200. Recent Results in Cancer Research. Springer International Publishing. https://doi.org/10.1007/978-3-319-20291-4_3.

Mehta, A., and J. E. Haber. 2014. 'Sources of DNA Double-Strand Breaks and Models of Recombinational DNA Repair'. *Cold Spring Harbor Perspectives in Biology* 6 (9): a016428–a016428. https://doi.org/10.1101/cshperspect.a016428.

Mersaoui, Sofiane Y., Erin Bonnell, and Raymund J. Wellinger. 2018. 'Nuclear Import of Cdc13 Limits Chromosomal Capping'. *Nucleic Acids Research* 46 (6): 2975–89. https://doi.org/10.1093/nar/gky085.

Mimitou, Eleni P., and Lorraine S. Symington. 2008. 'Sae2, Exo1 and Sgs1 Collaborate in DNA Double-Strand Break Processing'. *Nature* 455 (7214): 770–74. https://doi.org/10.1038/nature07312.

Mimitou, Eleni P., and Lorraine S. Symington. 2010. 'Ku Prevents Exo1 and Sgs1-dependent Resection of DNA Ends in the Absence of a Functional MRX Complex or Sae2'. *The EMBO Journal* 29 (19): 3358–69. https://doi.org/10.1038/emboj.2010.193.

Mizuguchi, Gaku, Xuetong Shen, Joe Landry, Wei-Hua Wu, Subhojit Sen, and Carl Wu. 2004. 'ATP-Driven Exchange of Histone H2AZ Variant Catalyzed by SWR1 Chromatin Remodeling Complex'. *Science* 303 (5656): 343–48. https://doi.org/10.1126/science.1090701.

Morillo-Huesca, Macarena, Marta Clemente-Ruiz, Eloísa Andújar, and Félix Prado. 2010. 'The SWR1 Histone Replacement Complex Causes Genetic Instability and Genome-Wide Transcription Misregulation in the Absence of H2A.Z'. *PLOS One* 5 (8): e12143. https://doi.org/10.1371/journal.pone.0012143.

Morrison, Ashby J., Jessica Highland, Nevan J. Krogan, et al. 2004. 'INO80 and γ-H2AX Interaction Links ATP-Dependent Chromatin Remodeling to DNA Damage Repair'. *Cell* 119 (6): 767–75. https://doi.org/10.1016/j.cell.2004.11.037.

Muoio, Daniela, and Elise Fouquerel. 2025. 'The Alternative Lengthening of Telomeres Pathway through a DNA Repair Lens: Mechanism and Therapeutic Opportunities'. *NAR Cancer* 7 (4): zcaf056. https://doi.org/10.1093/narcan/zcaf056.

Nakada, Daisuke, Kunihiro Matsumoto, and Katsunori Sugimoto. 2003. 'ATM-Related Tel1 Associates with Double-Strand Breaks through an Xrs2-Dependent Mechanism'. *Genes & Development* 17 (16): 1957–62. https://doi.org/10.1101/gad.1099003.

Nandakumar, Jayakrishnan, Caitlin F. Bell, Ina Weidenfeld, Arthur J. Zaug, Leslie A. Leinwand, and Thomas R. Cech. 2012. 'The TEL Patch of Telomere Protein TPP1 Mediates Telomerase Recruitment and Processivity'. *Nature* 492 (7428): 285–89. https://doi.org/10.1038/nature11648.

Ng, Huck Hui, François Robert, Richard A. Young, and Kevin Struhl. 2002. 'Genome-Wide Location and Regulated Recruitment of the RSC Nucleosome-Remodeling Complex'. *Genes & Development* 16 (7): 806–19. https://doi.org/10.1101/gad.978902.

Ngo, Hien-Ping, and David Lydall. 2010. 'Survival and Growth of Yeast without Telomere Capping by Cdc13 in the Absence of Sgs1, Exo1, and Rad9'. *PLoS Genetics* 6 (8): e1001072. https://doi.org/10.1371/journal.pgen.1001072.

Nguyen, Vu Q., Anand Ranjan, Florian Stengel, et al. 2013. 'Molecular Architecture of the ATP-Dependent Chromatin-Remodeling Complex SWR1'. *Cell* 154 (6): 1220–31. https://doi.org/10.1016/j.cell.2013.08.018.

Nickoloff, J. A., E. Y. Chen, and F. Heffron. 1986. 'A 24-Base-Pair DNA Sequence from the MAT Locus Stimulates Intergenic Recombination in Yeast.' *Proceedings of the National Academy of Sciences* 83 (20): 7831–35. https://doi.org/10.1073/pnas.83.20.7831.

Nicolás, Andrea L., Patricia L. Munz, Erik Falck-Pedersen, and C. S. H. Young. 2000. 'Creation and Repair of Specific DNA Double-Strand Breaks in Vivo Following Infection with Adenovirus Vectors Expressing Saccharomyces Cerevisiae HO Endonuclease'. *Virology* 266 (1): 211–24. https://doi.org/10.1006/viro.1999.0062.

Nimonkar, Amitabh V., Jochen Genschel, Eri Kinoshita, et al. 2011. 'BLM–DNA2–RPA–MRN and EXO1–BLM–RPA–MRN Constitute Two DNA End Resection Machineries for Human DNA Break Repair'. *Genes & Development* 25 (4): 350–62. https://doi.org/10.1101/gad.2003811.

Nishibuchi, Ikuno, Hidekazu Suzuki, Aiko Kinomura, et al. 2014. 'Reorganization of Damaged Chromatin by the Exchange of Histone Variant H2A.Z-2'. *International Journal of Radiation Oncology*Biology*Physics* 89 (4): 736–44. https://doi.org/10.1016/j.ijrobp.2014.03.031.

Niu, Hengyao, Woo-Hyun Chung, Zhu Zhu, et al. 2010. 'Mechanism of the ATP-Dependent DNA End-Resection Machinery from Saccharomyces Cerevisiae'. *Nature* 467 (7311): 108–11. https://doi.org/10.1038/nature09318.

Norbury, Chris J., and Ian D. Hickson. 2001. 'Cellular Responses to DNA Damage'. *Annual Review of Pharmacology and Toxicology* 41 (1): 367–401. https://doi.org/10.1146/annurev.pharmtox.41.1.367.

Nugent, Constance I., Timothy R. Hughes, Neal F. Lue, and Victoria Lundblad. 1996. 'Cdc13p: A Single-Strand Telomeric DNA-Binding Protein with a Dual Role in Yeast Telomere Maintenance'. *Science* 274 (5285): 249–52. https://doi.org/10.1126/science.274.5285.249.

Oberbeckmann, Elisa, Nils Krietenstein, Vanessa Niebauer, et al. 2021. 'Genome Information Processing by the INO80 Chromatin Remodeler Positions Nucleosomes'. *Nature Communications* 12 (1): 3231. https://doi.org/10.1038/s41467-021-23016-z.

Oberbeckmann, Elisa, Vanessa Niebauer, Shinya Watanabe, et al. 2021. 'Ruler Elements in Chromatin Remodelers Set Nucleosome Array Spacing and Phasing'. *Nature Communications* 12 (1): 3232. https://doi.org/10.1038/s41467-021-23015-0.

Oberbeckmann, Elisa, Michael Wolff, Nils Krietenstein, et al. 2019. 'Absolute Nucleosome Occupancy Map for the *Saccharomyces Cerevisiae* Genome'. *Genome Research* 29 (12): 1996–2009. https://doi.org/10.1101/gr.253419.119.

Ocampo, Josefina, Răzvan V. Chereji, Peter R. Eriksson, and David J. Clark. 2016. 'The ISW1 and CHD1 ATP-Dependent Chromatin Remodelers Compete to Set Nucleosome Spacing *in Vivo*'. *Nucleic Acids Research* 44 (10): 4625–35. https://doi.org/10.1093/nar/gkw068.

O'Connor, Mark J. 2015. 'Targeting the DNA Damage Response in Cancer'. *Molecular Cell* 60 (4): 547–60. https://doi.org/10.1016/j.molcel.2015.10.040.

O'Driscoll, M. 2012. 'Diseases Associated with Defective Responses to DNA Damage'. *Cold Spring Harbor Perspectives in Biology* 4 (12): a012773–a012773. https://doi.org/10.1101/cshperspect.a012773.

Olins, Ada L., and Donald E. Olins. 1974. 'Spheroid Chromatin Units (ν Bodies)'. *Science* 183 (4122): 330–32. https://doi.org/10.1126/science.183.4122.330.

Oudet, P., M. Gross-Bellard, and P. Chambon. 1975. 'Electron Microscopic and Biochemical Evidence That Chromatin Structure Is a Repeating Unit'. *Cell* 4 (4): 281–300. https://doi.org/10.1016/0092-8674(75)90149-X.

Palm, Wilhelm, and Titia De Lange. 2008. 'How Shelterin Protects Mammalian Telomeres'. *Annual Review of Genetics* 42 (1): 301–34. https://doi.org/10.1146/annurev.genet.41.110306.130350.

Palm, Wilhelm, Dirk Hockemeyer, Tatsuya Kibe, and Titia De Lange. 2009. 'Functional Dissection of Human and Mouse POT1 Proteins'. *Molecular and Cellular Biology* 29 (2): 471–82. https://doi.org/10.1128/MCB.01352-08.

Panier, Stephanie, and Simon J. Boulton. 2014. 'Double-Strand Break Repair: 53BP1 Comes into Focus'. *Nature Reviews Molecular Cell Biology* 15 (1): 7–18. https://doi.org/10.1038/nrm3719.

Pannunzio, Nicholas R., Go Watanabe, and Michael R. Lieber. 2018. 'Nonhomologous DNA End-Joining for Repair of DNA Double-Strand Breaks'. *Journal of Biological Chemistry* 293 (27): 10512–23. https://doi.org/10.1074/jbc.TM117.000374.

Papamichos-Chronakis, Manolis, Jocelyn E. Krebs, and Craig L. Peterson. 2006. 'Interplay between Ino80 and Swr1 Chromatin Remodeling Enzymes Regulates Cell Cycle Checkpoint Adaptation in Response to DNA Damage'. *Genes & Development* 20 (17): 2437–49. https://doi.org/10.1101/gad.1440206.

Papamichos-Chronakis, Manolis, Shinya Watanabe, Oliver J. Rando, and Craig L. Peterson. 2011. 'Global Regulation of H2A.Z Localization by the INO80 Chromatin-Remodeling Enzyme Is Essential for Genome Integrity'. *Cell* 144 (2): 200–213. https://doi.org/10.1016/j.cell.2010.12.021.

Pardo, Benjamin, and Stéphane Marcand. 2005. 'Rap1 Prevents Telomere Fusions by Nonhomologous End Joining'. *The EMBO Journal* 24 (17): 3117–27. https://doi.org/10.1038/sj.emboj.7600778.

Park, Ji-Hye, Eun-Jung Park, Han-Sae Lee, et al. 2006. 'Mammalian SWI/SNF Complexes Facilitate DNA Double-strand Break Repair by Promoting γ-H2AX Induction'. *The EMBO Journal* 25 (17): 3986–97. https://doi.org/10.1038/sj.emboj.7601291.

Parmar, Jyotsana J., Maxime Woringer, and Christophe Zimmer. 2019. 'How the Genome Folds: The Biophysics of Four-Dimensional Chromatin Organization'. *Annual Review of Biophysics* 48 (1): 231–53. https://doi.org/10.1146/annurev-biophys-052118-115638.

Paull, Tanya T., Emmy P. Rogakou, Vikky Yamazaki, Cordula U. Kirchgessner, Martin Gellert, and William M. Bonner. 2000. 'A Critical Role for Histone H2AX in Recruitment of Repair Factors to Nuclear Foci after DNA Damage'. *Current Biology* 10 (15): 886–95. https://doi.org/10.1016/S0960-9822(00)00610-2.

Pellicioli, Achille, Sang Eun Lee, Chiara Lucca, Marco Foiani, and James E. Haber. 2001. 'Regulation of Saccharomyces Rad53 Checkpoint Kinase during Adaptation from DNA Damage–Induced G2/M Arrest'. *Molecular Cell* 7 (2): 293–300. https://doi.org/10.1016/S1097-2765(01)00177-0.

Peritore, Martina, Karl-Uwe Reusswig, Susanne C. S. Bantele, Tobias Straub, and Boris Pfander. 2021. 'Strand-Specific ChIP-Seq at DNA Breaks Distinguishes ssDNA versus dsDNA Binding and Refutes Single-Stranded Nucleosomes'. *Molecular Cell* 81 (8): 1841-1853.e4. https://doi.org/10.1016/j.molcel.2021.02.005.

Peterson, Craig L., and Ira Herskowitz. 1992. 'Characterization of the Yeast SWI1, SWI2, and SWI3 Genes, Which Encode a Global Activator of Transcription'. *Cell* 68 (3): 573–83. https://doi.org/10.1016/0092-8674(92)90192-F.

Petty, Emily, and Lorraine Pillus. 2013. 'Balancing Chromatin Remodeling and Histone Modifications in Transcription'. *Trends in Genetics: TIG* 29 (11): 621–29. https://doi.org/10.1016/j.tig.2013.06.006.

Pfeifer, Gerd P. 2020. 'Mechanisms of UV-Induced Mutations and Skin Cancer'. *Genome Instability & Disease* 1 (3): 99–113. https://doi.org/10.1007/s42764-020-00009-8.

Phanindhar, Kundurthi, and Rakesh K. Mishra. 2023. 'Auxin-Inducible Degron System: An Efficient Protein Degradation Tool to Study Protein Function'. *BioTechniques* 74 (4): 186–98. https://doi.org/10.2144/btn-2022-0108.

Pinto, Cosimo, Kristina Kasaciunaite, Ralf Seidel, and Petr Cejka. 2016. 'Human DNA2 Possesses a Cryptic DNA Unwinding Activity That Functionally Integrates with BLM or WRN Helicases'. *eLife* 5 (September): e18574. https://doi.org/10.7554/eLife.18574.

Pires, Vanessa Borges, Nina Lohner, Tina Wagner, et al. 2023. 'RNA-DNA Hybrids Prevent Resection at Dysfunctional Telomeres'. *Cell Reports* 42 (2): 112077. https://doi.org/10.1016/j.celrep.2023.112077.

Poulet, Anaïs, Rémi Buisson, Cendrine Faivre-Moskalenko, et al. 2009. 'TRF2 Promotes, Remodels and Protects Telomeric Holliday Junctions'. *The EMBO Journal* 28 (6): 641–51. https://doi.org/10.1038/emboj.2009.11.

Povirk, Lawrence F. 1996. 'DNA Damage and Mutagenesis by Radiomimetic DNA-Cleaving Agents: Bleomycin, Neocarzinostatin and Other Enediynes'. *Mutation Research - Fundamental and Molecular Mechanisms of Mutagenesis* 355 (1–2): 71–89. https://doi.org/10.1016/0027-5107(96)00023-1.

Qi, H., and V. A. Zakian. 2000. 'The Saccharomyces Telomere-Binding Protein Cdc13p Interacts with Both the Catalytic Subunit of DNA Polymerase Alpha and the Telomerase-Associated Est1 Protein'. *Genes & Development* 14 (14): 1777–88.

Rajavel, Malligarjunan, Michael R. Mullins, and Derek J. Taylor. 2014. 'Multiple Facets of TPP1 in Telomere Maintenance'. *Biochimica Et Biophysica Acta* 1844 (9): 1550–59. https://doi.org/10.1016/j.bbapap.2014.04.014.

Ranjha, Lepakshi, Sean M. Howard, and Petr Cejka. 2018. 'Main Steps in DNA Double-Strand Break Repair: An Introduction to Homologous Recombination and Related Processes'. *Chromosoma* 127 (2): 187–214. https://doi.org/10.1007/s00412-017-0658-1.

Rawal, Yashpal, Răzvan V. Chereji, Hongfang Qiu, et al. 2018. 'SWI/SNF and RSC Cooperate to Reposition and Evict Promoter Nucleosomes at Highly Expressed Genes in Yeast'. *Genes & Development* 32 (9–10): 695–710. https://doi.org/10.1101/gad.312850.118.

Reginato, Giordano, Elda Cannavo, and Petr Cejka. 2017. 'Physiological Protein Blocks Direct the Mre11–Rad50–Xrs2 and Sae2 Nuclease Complex to Initiate DNA End Resection'. *Genes & Development* 31 (23–24): 2325–30. https://doi.org/10.1101/gad.308254.117.

Reusswig, Karl-Uwe, Fabian Zimmermann, Lorenzo Galanti, and Boris Pfander. 2016. 'Robust Replication Control Is Generated by Temporal Gaps between Licensing and Firing Phases and Depends on Degradation of Firing Factor Sld2'. *Cell Reports* 17 (2): 556–69. https://doi.org/10.1016/j.celrep.2016.09.013.

Rice, Cory, and Emmanuel Skordalakes. 2016. 'Structure and Function of the Telomeric CST Complex'. *Computational and Structural Biotechnology Journal* 14 (January): 161–67. https://doi.org/10.1016/j.csbj.2016.04.002.

Robert, Isabelle, Françoise Dantzer, and Bernardo Reina-San-Martin. 2009. 'Parp1 Facilitates Alternative NHEJ, Whereas Parp2 Suppresses IgH/c-Myc Translocations during Immunoglobulin Class Switch Recombination'. *Journal of Experimental Medicine* 206 (5): 1047–56. https://doi.org/10.1084/jem.20082468.

Rogakou, Emmy P., Duane R. Pilch, Ann H. Orr, Vessela S. Ivanova, and William M. Bonner. 1998. 'DNA Double-Stranded Breaks Induce Histone H2AX Phosphorylation on Serine 139'. *Journal of Biological Chemistry* 273 (10): 5858–68. https://doi.org/10.1074/jbc.273.10.5858.

Rouet, P., F. Smih, and M. Jasin. 1994. 'Expression of a Site-Specific Endonuclease Stimulates Homologous Recombination in Mammalian Cells.' *Proceedings of the National Academy of Sciences* 91 (13): 6064–68. https://doi.org/10.1073/pnas.91.13.6064.

Sahu, Rakesh Kumar, Sakshi Singh, and Raghuvir Singh Tomar. 2021. 'The ATP-Dependent SWI/SNF and RSC Chromatin Remodelers Cooperatively Induce Unfolded Protein Response Genes during Endoplasmic Reticulum Stress'. *Biochimica et Biophysica Acta (BBA) - Gene Regulatory Mechanisms* 1864 (11–12): 194748. https://doi.org/10.1016/j.bbagrm.2021.194748.

Saini, Saurabh, and Prajwal Gurung. 2025. 'A Comprehensive Review of Sensors of Radiation-induced Damage, Radiation-induced Proximal Events, and Cell Death'. *Immunological Reviews* 329 (1): e13409. https://doi.org/10.1111/imr.13409.

Sakofsky, Cynthia J., and Anna Malkova. 2017. 'Break Induced Replication in Eukaryotes: Mechanisms, Functions, and Consequences'. *Critical Reviews in Biochemistry and Molecular Biology* 52 (4): 395–413. https://doi.org/10.1080/10409238.2017.1314444.

Sanchez, Yolanda, Brian A. Desany, William J. Jones, Qinghua Liu, Bin Wang, and Stephen J. Elledge. 1996. 'Regulation of *RAD53* by the *ATM* -Like Kinases *MEC1* and *TEL1* in Yeast Cell Cycle Checkpoint Pathways'. *Science* 271 (5247): 357–60. https://doi.org/10.1126/science.271.5247.357.

Sartori, Alessandro A., Claudia Lukas, Julia Coates, et al. 2007. 'Human CtIP Promotes DNA End Resection'. *Nature* 450 (7169): 509–14. https://doi.org/10.1038/nature06337.

Schaetzlein, Sonja, N. R. Kodandaramireddy, Zhenyu Ju, et al. 2007. 'Exonuclease-1 Deletion Impairs DNA Damage Signaling and Prolongs Lifespan of Telomere-Dysfunctional Mice'. *Cell* 130 (5): 863–77. https://doi.org/10.1016/j.cell.2007.08.029.

Schlichter, Alisha, Margaret M. Kasten, Timothy J. Parnell, and Bradley R. Cairns. 2020. 'Specialization of the Chromatin Remodeler RSC to Mobilize Partially-Unwrapped Nucleosomes'. *eLife* 9 (June): e58130. https://doi.org/10.7554/eLife.58130.

Sepers, Jorian J., Noud H. M. Verstappen, An A. Vo, et al. 2022. 'The mIAA7 Degron Improves Auxin-Mediated Degradation in *Caenorhabditis Elegans*'. *G3 Genes|Genomes|Genetics* 12 (10): jkac222. https://doi.org/10.1093/g3journal/jkac222.

Sfeir, Agnel, and Titia De Lange. 2012. 'Removal of Shelterin Reveals the Telomere End-Protection Problem'. *Science* 336 (6081): 593–97. https://doi.org/10.1126/science.1218498.

Sfeir, Agnel, Settapong T. Kosiyatrakul, Dirk Hockemeyer, et al. 2009. 'Mammalian Telomeres Resemble Fragile Sites and Require TRF1 for Efficient Replication'. *Cell* 138 (1): 90–103. https://doi.org/10.1016/j.cell.2009.06.021.

Sfeir, Agnel, and Lorraine S. Symington. 2015. 'Microhomology-Mediated End Joining: A Back-up Survival Mechanism or Dedicated Pathway?' *Trends in Biochemical Sciences* 40 (11): 701–14. https://doi.org/10.1016/j.tibs.2015.08.006.

Shampay, Janis, Jack W. Szostak, and Elizabeth H. Blackburn. 1984. 'DNA Sequences of Telomeres Maintained in Yeast'. *Nature* 310 (5973): 154–57. https://doi.org/10.1038/310154a0.

Shen, X., G. Mizuguchi, A. Hamiche, and C. Wu. 2000. 'A Chromatin Remodelling Complex Involved in Transcription and DNA Processing'. *Nature* 406 (6795): 541–44. https://doi.org/10.1038/35020123.

Shen, Xuetong, Ryan Ranallo, Eugene Choi, and Carl Wu. 2003. 'Involvement of Actin-Related Proteins in ATP-Dependent Chromatin Remodeling'. *Molecular Cell* 12 (1): 147–55. https://doi.org/10.1016/S1097-2765(03)00264-8.

Shi, Tianlai, Richard D. Bunker, Stefano Mattarocci, et al. 2013. 'Rif1 and Rif2 Shape Telomere Function and Architecture through Multivalent Rap1 Interactions'. *Cell* 153 (6): 1340–53. https://doi.org/10.1016/j.cell.2013.05.007.

Shim, Eun Yong, Woo-Hyun Chung, Matthew L. Nicolette, et al. 2010. 'Saccharomyces Cerevisiae Mre11/Rad50/Xrs2 and Ku Proteins Regulate Association of Exo1 and Dna2 with DNA Breaks'. *The EMBO Journal* 29 (19): 3370–80. https://doi.org/10.1038/emboj.2010.219.

Shim, Eun Yong, Soo Jin Hong, Ji-Hyun Oum, Yvonne Yanez, Yu Zhang, and Sang Eun Lee. 2007. 'RSC Mobilizes Nucleosomes To Improve Accessibility of Repair Machinery to the Damaged Chromatin'. *Molecular and Cellular Biology* 27 (5): 1602–13. https://doi.org/10.1128/MCB.01956-06.

Shim, Eun Yong, Jia-Lin Ma, Ji-Hyun Oum, Yvonne Yanez, and Sang Eun Lee. 2005. 'The Yeast Chromatin Remodeler RSC Complex Facilitates End Joining Repair of DNA Double-

Strand Breaks'. *Molecular and Cellular Biology* 25 (10): 3934–44. https://doi.org/10.1128/MCB.25.10.3934-3944.2005.

Shimada, Kenji, Cleo V. D. Tarashev, Stephanie Bregenhorn, et al. 2024. 'TORC2 Inhibition Triggers Yeast Chromosome Fragmentation through Misregulated Base Excision Repair of Clustered Oxidation Events'. *Nature Communications* 15 (1): 9908. https://doi.org/10.1038/s41467-024-54142-z.

Shimizu, Naoto, Kazuki Izawa, Mubasshir Washif, Ryosuke Morozumi, Kouji Hirota, and Masataka Tsuda. 2025. 'Role of TDP2 in the Repair of DNA Damage Induced by the Radiomimetic Drug Bleomycin'. *Genes and Environment: The Official Journal of the Japanese Environmental Mutagen Society* 47 (1): 7. https://doi.org/10.1186/s41021-025-00329-9.

Shiotani, Bunsyo, and Lee Zou. 2009. 'Single-Stranded DNA Orchestrates an ATM-to-ATR Switch at DNA Breaks'. *Molecular Cell* 33 (5): 547–58. https://doi.org/10.1016/j.molcel.2009.01.024.

Silva, George, Laurent Poirot, Roman Galetto, et al. 2011. 'Meganucleases and Other Tools for Targeted Genome Engineering: Perspectives and Challenges for Gene Therapy'. *Current Gene Therapy* 11 (1): 11–27. https://doi.org/10.2174/156652311794520111.

Singh, Raushan K., Jiayl Fan, Nathan Gioacchini, Shinya Watanabe, Osman Bilsel, and Craig L. Peterson. 2019. 'Transient Kinetic Analysis of SWR1C-Catalyzed H2A.Z Deposition Unravels the Impact of Nucleosome Dynamics and the Asymmetry of Histone Exchange'. *Cell Reports* 27 (2): 374-386.e4. https://doi.org/10.1016/j.celrep.2019.03.035.

Sinha, Manisha, Shinya Watanabe, Aaron Johnson, Danesh Moazed, and Craig L. Peterson. 2009. 'Recombinational Repair within Heterochromatin Requires ATP-Dependent Chromatin Remodeling'. *Cell* 138 (6): 1109–21. https://doi.org/10.1016/j.cell.2009.07.013.

Smogorzewska, Agata, Bas Van Steensel, Alessandro Bianchi, et al. 2000. 'Control of Human Telomere Length by TRF1 and TRF2'. *Molecular and Cellular Biology* 20 (5): 1659–68. https://doi.org/10.1128/MCB.20.5.1659-1668.2000.

Soulas-Sprauel, P., P. Rivera-Munoz, L. Malivert, et al. 2007. 'V(D)J and Immunoglobulin Class Switch Recombinations: A Paradigm to Study the Regulation of DNA End-Joining'. *Oncogene* 26 (56): 7780–91. https://doi.org/10.1038/sj.onc.1210875.

Stansel, Rachel M., Titia De Lange, and Jack D. Griffith. 2001. 'T-loop Assembly in Vitro Involves Binding of TRF2 near the 3' Telomeric Overhang'. *The EMBO Journal* 20 (19): 5532–40. https://doi.org/10.1093/emboj/20.19.5532.

Strahl-Bolsinger, S., A. Hecht, K. Luo, and M. Grunstein. 1997. 'SIR2 and SIR4 Interactions Differ in Core and Extended Telomeric Heterochromatin in Yeast.' *Genes & Development* 11 (1): 83–93. https://doi.org/10.1101/gad.11.1.83.

Sudarsanam, Priya, Vishwanath R. Iyer, Patrick O. Brown, and Fred Winston. 2000. 'Whole-Genome Expression Analysis of *Snf/Swi* Mutants of *Saccharomyces Cerevisiae*'. *Proceedings of the National Academy of Sciences* 97 (7): 3364–69. https://doi.org/10.1073/pnas.97.7.3364.

Symington, L. S. 2014. 'End Resection at Double-Strand Breaks: Mechanism and Regulation'. *Cold Spring Harbor Perspectives in Biology* 6 (8): a016436–a016436. https://doi.org/10.1101/cshperspect.a016436.

Symington, Lorraine S., and Jean Gautier. 2011. 'Double-Strand Break End Resection and Repair Pathway Choice'. *Annual Review of Genetics* 45 (1): 247–71. https://doi.org/10.1146/annurev-genet-110410-132435.

Toiber, Debra, Fabian Erdel, Karim Bouazoune, et al. 2013. 'SIRT6 Recruits SNF2H to DNA Break Sites, Preventing Genomic Instability through Chromatin Remodeling'. *Molecular Cell* 51 (4): 454–68. https://doi.org/10.1016/j.molcel.2013.06.018.

Tomimatsu, Nozomi, Bipasha Mukherjee, Molly Catherine Hardebeck, et al. 2014. 'Phosphorylation of EXO1 by CDKs 1 and 2 Regulates DNA End Resection and Repair Pathway Choice'. *Nature Communications* 5 (1): 3561. https://doi.org/10.1038/ncomms4561.

Tosi, Alessandro, Caroline Haas, Franz Herzog, et al. 2013. 'Structure and Subunit Topology of the INO80 Chromatin Remodeler and Its Nucleosome Complex'. *Cell* 154 (6): 1207–19. https://doi.org/10.1016/j.cell.2013.08.016.

Tsukuda, Toyoko, Alastair B. Fleming, Jac A. Nickoloff, and Mary Ann Osley. 2005. 'Chromatin Remodelling at a DNA Double-Strand Break Site in Saccharomyces Cerevisiae'. *Nature* 438 (7066): 379–83. https://doi.org/10.1038/nature04148.

Tsukuda, Toyoko, Yi-Chen Lo, Sanchita Krishna, Rosa Sterk, Mary Ann Osley, and Jac A. Nickoloff. 2009. 'INO80-Dependent Chromatin Remodeling Regulates Early and Late Stages of Mitotic Homologous Recombination'. *DNA Repair* 8 (3): 360–69. https://doi.org/10.1016/j.dnarep.2008.11.014.

Tubbs, Anthony, and André Nussenzweig. 2017. 'Endogenous DNA Damage as a Source of Genomic Instability in Cancer'. *Cell* 168 (4): 644–56. https://doi.org/10.1016/j.cell.2017.01.002.

Van Attikum, Haico, Olivier Fritsch, and Susan M. Gasser. 2007. 'Distinct Roles for SWR1 and INO80 Chromatin Remodeling Complexes at Chromosomal Double-strand Breaks'. *The EMBO Journal* 26 (18): 4113–25. https://doi.org/10.1038/sj.emboj.7601835.

Van Attikum, Haico, Olivier Fritsch, Barbara Hohn, and Susan M. Gasser. 2004. 'Recruitment of the INO80 Complex by H2A Phosphorylation Links ATP-Dependent Chromatin Remodeling with DNA Double-Strand Break Repair'. *Cell* 119 (6): 777–88. https://doi.org/10.1016/j.cell.2004.11.033.

Van Steensel, Bas, and Titia De Lange. 1997. 'Control of Telomere Length by the Human Telomeric Protein TRF1'. *Nature* 385 (6618): 740–43. https://doi.org/10.1038/385740a0.

Vega, Leticia R., Jane A. Phillips, Brian R. Thornton, et al. 2007. 'Sensitivity of Yeast Strains with Long G-Tails to Levels of Telomere-Bound Telomerase'. *PLoS Genetics* 3 (6): e105. https://doi.org/10.1371/journal.pgen.0030105.

Wang, James C. 2002. 'Cellular Roles of DNA Topoisomerases: A Molecular Perspective'. *Nature Reviews Molecular Cell Biology* 3 (6): 430–40. https://doi.org/10.1038/nrm831.

Wang, Mengxue, Jinghua Li, Yong Wang, et al. 2023. 'Single-Molecule Study Reveals Hmo1, Not Hho1, Promotes Chromatin Assembly in Budding Yeast'. *mBio*, July 11, e00993-23. https://doi.org/10.1128/mbio.00993-23.

Ward, Irene M., Kay Minn, Jan Van Deursen, and Junjie Chen. 2003. 'P53 Binding Protein 53BP1 Is Required for DNA Damage Responses and Tumor Suppression in Mice'. *Molecular and Cellular Biology* 23 (7): 2556–63. https://doi.org/10.1128/MCB.23.7.2556-2563.2003.

Ward, J. F. 1995. 'Radiation Mutagenesis: The Initial DNA Lesions Responsible'. *Radiation Research* 142 (3): 362–68.

Watanabe, Shinya, Marta Radman-Livaja, Oliver J. Rando, and Craig L. Peterson. 2013. 'A Histone Acetylation Switch Regulates H2A.Z Deposition by the SWR-C Remodeling Enzyme'. *Science* 340 (6129): 195–99. https://doi.org/10.1126/science.1229758.

Wei, Wei, Yifan Ren, Jinxin Lan, et al. 2026. 'Ionizing Radiation: Molecular Mechanisms, Biological Effects, and Therapeutic Targets'. *Molecular Biomedicine* 7 (1): 3. https://doi.org/10.1186/s43556-025-00358-4.

Weider, M., A. Schröder, F. Klebl, and N. Sauer. 2011. 'A Novel Mechanism for Target Gene-Specific SWI/SNF Recruitment via the Snf2p N-Terminus'. *Nucleic Acids Research* 39 (10): 4088–98. https://doi.org/10.1093/nar/gkr004.

Weiffenbach, B., and J. E. Haber. 1985. 'Homothallic Switching of Saccharomyces Cerevisiae Mating Type Genes by Using a Donor Containing a Large Internal Deletion.' *Molecular and Cellular Biology* 5 (8): 2154–58. https://doi.org/10.1128/MCB.5.8.2154.

Weiner, Assaf, Amanda Hughes, Moran Yassour, Oliver J. Rando, and Nir Friedman. 2010. 'High-Resolution Nucleosome Mapping Reveals Transcription-Dependent Promoter Packaging'. *Genome Research* 20 (1): 90–100. https://doi.org/10.1101/gr.098509.109.

Weinert, T A, and L. H. Hartwell. 1993. 'Cell Cycle Arrest of Cdc Mutants and Specificity of the RAD9 Checkpoint.' *Genetics* 134 (1): 63–80. https://doi.org/10.1093/genetics/134.1.63.

Weinert, T A, G. L. Kiser, and L. H. Hartwell. 1994. 'Mitotic Checkpoint Genes in Budding Yeast and the Dependence of Mitosis on DNA Replication and Repair.' *Genes & Development* 8 (6): 652–65. https://doi.org/10.1101/gad.8.6.652.

Weinert, Ted A., and Leland H. Hartwell. 1988. 'The *RAD9* Gene Controls the Cell Cycle Response to DNA Damage in *Saccharomyces Cerevisiae*'. *Science* 241 (4863): 317–22. https://doi.org/10.1126/science.3291120.

Wellinger, Raymund J., and Virginia A. Zakian. 2012. 'Everything You Ever Wanted to Know About *Saccharomyces Cerevisiae* Telomeres: Beginning to End'. *Genetics* 191 (4): 1073–105. https://doi.org/10.1534/genetics.111.137851.

Widom, J. 1989. 'Toward a Unified Model of Chromatin Folding'. *Annual Review of Biophysics and Biophysical Chemistry* 18 (1): 365–95. https://doi.org/10.1146/annurev.bb.18.060189.002053.

Wiest, Nathaniel E., Scott Houghtaling, Joseph C. Sanchez, Alan E. Tomkinson, and Mary Ann Osley. 2017. 'The SWI/SNF ATP-Dependent Nucleosome Remodeler Promotes Resection Initiation at a DNA Double-Strand Break in Yeast'. *Nucleic Acids Research* 45 (10): 5887–900. https://doi.org/10.1093/nar/gkx221.

Wold, Marc S. 1997. 'REPLICATION PROTEIN A: A Heterotrimeric, Single-Stranded DNA-Binding Protein Required for Eukaryotic DNA Metabolism'. *Annual Review of Biochemistry* 66 (1): 61–92. https://doi.org/10.1146/annurev.biochem.66.1.61.

Woodage, Trevor, Munira A. Basrai, Andreas D. Baxevanis, Philip Hieter, and Francis S. Collins. 1997. 'Characterization of the CHD Family of Proteins'. *Proceedings of the National Academy of Sciences* 94 (21): 11472–77. https://doi.org/10.1073/pnas.94.21.11472.

Wotton, D., and D. Shore. 1997. 'A Novel Rap1p-Interacting Factor, Rif2p, Cooperates with Rif1p to Regulate Telomere Length in Saccharomyces Cerevisiae.' *Genes & Development* 11 (6): 748–60. https://doi.org/10.1101/gad.11.6.748.

Wright, William Douglass, Shanaya Shital Shah, and Wolf-Dietrich Heyer. 2018. 'Homologous Recombination and the Repair of DNA Double-Strand Breaks'. *Journal of Biological Chemistry* 293 (27): 10524–35. https://doi.org/10.1074/jbc.TM118.000372.

Wu, Leonard, and Ian D. Hickson. 2003. 'The Bloom's Syndrome Helicase Suppresses Crossing over during Homologous Recombination'. *Nature* 426 (6968): 870–74. https://doi.org/10.1038/nature02253.

Wu, Xiaohua, and James E. Haber. 1996. 'A 700 Bp Cis-Acting Region Controls Mating-Type Dependent Recombination Along the Entire Left Arm of Yeast Chromosome III'. *Cell* 87 (2): 277–85. https://doi.org/10.1016/S0092-8674(00)81345-8.

Wu, Yun, and Virginia A. Zakian. 2011. 'The Telomeric Cdc13 Protein Interacts Directly with the Telomerase Subunit Est1 to Bring It to Telomeric DNA Ends in Vitro'. *Proceedings of the National Academy of Sciences* 108 (51): 20362–69. https://doi.org/10.1073/pnas.1100281108.

Xu, Ye, Marina K. Ayrapetov, Chang Xu, Ozge Gursoy-Yuzugullu, Yiduo Hu, and Brendan D. Price. 2012. 'Histone H2A.Z Controls a Critical Chromatin Remodeling Step Required for DNA Double-Strand Break Repair'. *Molecular Cell* 48 (5): 723–33. https://doi.org/10.1016/j.molcel.2012.09.026.

Xu, Ye, Yingli Sun, Xiaofeng Jiang, et al. 2010. 'The P400 ATPase Regulates Nucleosome Stability and Chromatin Ubiquitination during DNA Repair'. *Journal of Cell Biology* 191 (1): 31–43. https://doi.org/10.1083/jcb.201001160.

Xue, Chaoyou, and Eric C. Greene. 2021. 'DNA Repair Pathway Choices in CRISPR-Cas9-Mediated Genome Editing'. *Trends in Genetics* 37 (7): 639–56. https://doi.org/10.1016/j.tig.2021.02.008.

Yan, Lijuan, and Zhucheng Chen. 2020. 'A Unifying Mechanism of DNA Translocation Underlying Chromatin Remodeling'. *Trends in Biochemical Sciences* 45 (3): 217–27. https://doi.org/10.1016/j.tibs.2019.09.002.

Yang, Chia-Wei, Shun-Fu Tseng, Chia-Jung Yu, et al. 2017. 'Telomere Shortening Triggers a Feedback Loop to Enhance End Protection'. *Nucleic Acids Research* 45 (14): 8314–28. https://doi.org/10.1093/nar/gkx503.

Yates, Luke A., Xiaodong Zhang, and Peter M. Burgers. 2025. 'DNA Damage and Replication Stress Checkpoints'. *Annual Review of Biochemistry* 94 (1): 195–221. https://doi.org/10.1146/annurev-biochem-072324-031915.

You, Zhongsheng, Linda Z. Shi, Quan Zhu, et al. 2009. 'CtIP Links DNA Double-Strand Break Sensing to Resection'. *Molecular Cell* 36 (6): 954–69. https://doi.org/10.1016/j.molcel.2009.12.002.

Zakian, Virginia A. 1996. 'STRUCTURE, FUNCTION, AND REPLICATION OF *SACCHAROMYCES CEREVISIAE* TELOMERES'. *Annual Review of Genetics* 30 (1): 141–72. https://doi.org/10.1146/annurev.genet.30.1.141.

Zeman, Michelle K., and Karlene A. Cimprich. 2014. 'Causes and Consequences of Replication Stress'. *Nature Cell Biology* 16 (1): 2–9. https://doi.org/10.1038/ncb2897.

Zhang, Haiying, Douglas N. Roberts, and Bradley R. Cairns. 2005. 'Genome-Wide Dynamics of Htz1, a Histone H2A Variant That Poises Repressed/Basal Promoters for Activation through Histone Loss'. *Cell* 123 (2): 219–31. https://doi.org/10.1016/j.cell.2005.08.036.

Zhang, Ming-Liang, Xia-Jing Tong, Xiao-Hong Fu, et al. 2010. 'Yeast Telomerase Subunit Est1p Has Guanine Quadruplex–Promoting Activity That Is Required for Telomere Elongation'. *Nature Structural & Molecular Biology* 17 (2): 202–9. https://doi.org/10.1038/nsmb.1760.

Zhang, Yu, Eun Yong Shim, Melody Davis, and Sang Eun Lee. 2009. 'Regulation of Repair Choice: Cdk1 Suppresses Recruitment of End Joining Factors at DNA Breaks'. *DNA Repair* 8 (10): 1235–41. https://doi.org/10.1016/j.dnarep.2009.07.007.

Zhu, Xuefeng, and Claes M. Gustafsson. 2009. 'Distinct Differences in Chromatin Structure at Subtelomeric X and Y' Elements in Budding Yeast'. *PLOS One* 4 (7): e6363. https://doi.org/10.1371/journal.pone.0006363.

Zhu, Zhu, Woo-Hyun Chung, Eun Yong Shim, Sang Eun Lee, and Grzegorz Ira. 2008. 'Sgs1 Helicase and Two Nucleases Dna2 and Exo1 Resect DNA Double-Strand Break Ends'. *Cell* 134 (6): 981–94. https://doi.org/10.1016/j.cell.2008.08.037.

Zou, Lee, and Stephen J. Elledge. 2003. 'Sensing DNA Damage Through ATRIP Recognition of RPA-ssDNA Complexes'. *Science* 300 (5625): 1542–48. https://doi.org/10.1126/science.1083430.

Zubko, Mikhajlo K., Sandrine Guillard, and David Lydall. 2004. 'Exo1 and Rad24 Differentially Regulate Generation of ssDNA at Telomeres of Saccharomyces Cerevisiae Cdc13-1 Mutants'. *Genetics* 168 (1): 103–15. https://doi.org/10.1534/genetics.104.027904.

Abbreviations

AID	auxin-inducible degron
ATP	adenosine triphosphate
Arp	actin-related protein
BIR	break-induced replication
ChIP	chromatin immunoprecipitation
CtIP	CtBP-interacting protein
dHJ	double Holliday junction
DMSO	dimethyl sulfoxide
DNA	deoxyribonucleic acid
DSB	double-strand break
dsDNA	double-stranded DNA
EDTA	ethylenediaminetetraacetic acid
HEPES	4-(2-hydroxyethyl)-1-piperazineethanesulfonic acid
HR	homologous recombination
IAA	indole-3-acetic acid
INO80	Inositol-requiring mutant 80
IP	immunoprecipitation
ISWI	Imitation SWItch
log	logarithm
MES	2-(N-morpholino)ethanesulfonic acid
MMEJ	microhomology-mediated end joining
MMR	mismatch repair
MOPS	3-(N-morpholino)propanesulfonic acid
MRN	MRE11-RAD50-NBS1
MRX	Mre11-Rad50-Xrs2
NER	nucleotide excision repair
NGS	next-generation sequencing
NHEJ	non-homologous end joining
OD	optical density
PBS	phosphate-buffered saline
PCR	polymerase chain reaction
Pol	polymerase
POT1	protection of telomeres 1
PTM	post-translational modification
QAOS	quantitative amplification of ssDNA
qPCR	quantitative PCR
Rap1	repressor/activator site binding protein
ROS	reactive oxygen species
RPA	replication protein A
RSC	remodeling the structure of chromatin
SDS	sodium dodecyl sulfate
SDSA	synthesis-dependent strand annealing
ssDNA	single-stranded DNA
SUMO	small ubiquitin-like modifier
SWI/SNF	switch/sucrose non-fermentable
SWR1	SWI2/SNF2-related 1

TALEN	transcription activator-like effector nuclease
TBS	Tris-buffered saline
TE	Tris-EDTA
TIN2	TRF1-interacting nuclear factor 2
TPP1	TINT1/PTOP1/PIP1
TRF1/2	telomeric repeat binding factor 1/2
Tris	Tri(hydroxymethyl)aminomethane
UV	ultraviolet
WT	wild type
YP	yeast extract/peptone
ZNF	zinc finger nucleases

Acknowledgements

First of all, I want to thank Prof. Boris Pfander for giving me the opportunity to do my PhD in his group. Thank you for all the advice and supervision scientifically and beyond, I really learned a lot and grew with my project. I appreciate your guidance while still giving me the freedom to come up with and follow my own ideas.

I also want to thank Prof. Hannes Mutschler for being the second examiner of this thesis.

Special thanks go to my thesis advisory committee, Dr. Stephanie Panier and Prof. Philipp Korber for their support and advice. Even though you were in Cologne or Munich, you always made me feel that you were only a phone call away.

I am grateful for the help of the MPI sequencing facility and especially Dr. Rin Ho Kim. He not only supported my project by sequencing my libraries, but also by advising me on the protocol. Thank you for still helping me out, even after our move to Dortmund and all your precious advice on how to set up the sequencing in Dortmund.

A big thank you goes to all members of the Pfander lab whom I got the chance to meet. First of all, thank you Martina for introducing me to the strand-specific sequencing protocol. Lorenzo, you have always been there to help out whenever there was an issue. I really appreciate your knowledge and advice. I am also extremely thankful for Juande and his idea to measure cutting efficiency via nanopore. Thank you for establishing this method with me and measuring my samples. In addition, I want to let you know that your advice has always been precious. Vanessa, the *cdc13-1* project would not have been possible without you. Thanks for getting in contact with the Brian Luke lab and thank you Natali, for providing us with the QAOS protocol and yeast strains. I also want to thank Leif for all the discussions about

the analysis of the QAOS data. Importantly, I really appreciated your work, Caity. Thank you for being my first student and staying with us even after you finished your master´s thesis. It was a pleasure to spend time with you not only in but also outside of the lab. Thank you to Johannes, Chimeg and Julia for creating such a good PhD student environment. Big thanks to Petra, Christiane, Sven, Julian and Sarah for your technical support and organisation!
I also want to thank Dr. Lucia Sironi and Christa Hornemann for coordinating the IMPRS-LM program and allowing me to participate in several workshops as an associate member.

Finally, I want to thank Nick and my family:
Danke Papa und Olga, dass ihr mir beim Umzug nach Dortmund geholfen habt und ich jederzeit zurückkommen konnte. Danke Papa für deine Unterstützung das durchzuziehen! Ohne dich, Mama, wäre ich sportlich wahrscheinlich immer noch eingeschränkt. Danke für deine körperliche und seelische Unterstützung. Nick, ohne dich hätte ich meinen PhD ziemlich sicher abgebrochen. Danke, dass du immer für mich da bist.

Eidesstattliche Versicherung (Affidavit)

_____ _____

Name, Vorname
(Surname, first name)

Matrikel-Nr.
(Enrolment number)

Belehrung:

Wer vorsätzlich gegen eine die Täuschung über Prüfungsleistungen betreffende Regelung einer Hochschulprüfungsordnung verstößt, handelt ordnungswidrig. Die Ordnungswidrigkeit kann mit einer Geldbuße von bis zu 50.000,00 € geahndet werden. Zuständige Verwaltungsbehörde für die Verfolgung und Ahndung von Ordnungswidrigkeiten ist der Kanzler/die Kanzlerin der Technischen Universität Dortmund. Im Falle eines mehrfachen oder sonstigen schwerwiegenden Täuschungsversuches kann der Prüfling zudem exmatrikuliert werden, § 63 Abs. 5 Hochschulgesetz NRW.

Die Abgabe einer falschen Versicherung an Eides statt ist strafbar.

Wer vorsätzlich eine falsche Versicherung an Eides statt abgibt, kann mit einer Freiheitsstrafe bis zu drei Jahren oder mit Geldstrafe bestraft werden, § 156 StGB. Die fahrlässige Abgabe einer falschen Versicherung an Eides statt kann mit einer Freiheitsstrafe bis zu einem Jahr oder Geldstrafe bestraft werden, § 161 StGB.

Die oben stehende Belehrung habe ich zur Kenntnis genommen:

Official notification:

Any person who intentionally breaches any regulation of university examination regulations relating to deception in examination performance is acting improperly. This offence can be punished with a fine of up to EUR 50,000.00. The competent administrative authority for the pursuit and prosecution of offences of this type is the chancellor of the TU Dortmund University. In the case of multiple or other serious attempts at deception, the candidate can also be unenrolled, Section 63, paragraph 5 of the Universities Act of North Rhine-Westphalia.

The submission of a false affidavit is punishable.

Any person who intentionally submits a false affidavit can be punished with a prison sentence of up to three years or a fine, Section 156 of the Criminal Code. The negligent submission of a false affidavit can be punished with a prison sentence of up to one year or a fine, Section 161 of the Criminal Code.

I have taken note of the above official notification.

_____ _____

Ort, Datum
(Place, date)

Unterschrift
(Signature)

Titel der Dissertation:
(Title of the thesis):

_____

_____

_____

Ich versichere hiermit an Eides statt, dass ich die vorliegende Dissertation mit dem Titel selbstständig und ohne unzulässige fremde Hilfe angefertigt habe. Ich habe keine anderen als die angegebenen Quellen und Hilfsmittel benutzt sowie wörtliche und sinngemäße Zitate kenntlich gemacht.
Die Arbeit hat in gegenwärtiger oder in einer anderen Fassung weder der TU Dortmund noch einer anderen Hochschule im Zusammenhang mit einer staatlichen oder akademischen Prüfung vorgelegen.

I hereby swear that I have completed the present dissertation independently and without inadmissible external support. I have not used any sources or tools other than those indicated and have identified literal and analogous quotations.

The thesis in its current version or another version has not been presented to the TU Dortmund University or another university in connection with a state or academic examination.*

*Please be aware that solely the German version of the affidavit ("Eidesstattliche Versicherung") for the PhD thesis is the official and legally binding version.

_____ _____

Ort, Datum
(Place, date)

Unterschrift
(Signature)